SOIL MECHANICS AND BITUMINOUS MATERIALS RESEARCH LABORATORY

DESIGN CONSIDERATIONS

FOR ASPHALT PAVEMENTS

By

C. L. MONISMITH

K. INKABI

D. B. McLEAN

C. R. FREEME

REPORT NO. TE-77-1

to

THE TRANSPORTATION LABORATORY
DIVISION OF HIGHWAYS
STATE OF CALIFORNIA
DEPARTMENT OF TRANSPORTATION
PREPARED IN COOPERATION WITH
THE UNITED STATES DEPARTMENT OF TRANSPORTATION
FEDERAL HIGHWAY ADMINISTRATION

DEPARTMENT OF CIVIL ENGINEERING
INSTITUTE OF TRANSPORTATION AND TRAFFIC ENGINEERING

TE77-1
DND

ClibPDF - www.fastio.com

ClibPDF - www.fastio.com

TECHNICAL REPORT STANDARD TITLE PAGE

1. REPORT NO. FHWA-CA-TL-3153-77-30	2. GOVERNMENT ACCESSION NO.	3. RECIPIENT'S CATALOG NO.
4. TITLE AND SUBTITLE Design Considerations for Asphalt Pavements		5. REPORT DATE March 1977
		6. PERFORMING ORGANIZATION CODE 19301-633153
7. AUTHOR(S) Monismith, C. L., K. Inkabi, D. B. McLean, and C. R. Freeme		8. PERFORMING ORGANIZATION REPORT NO. TE 77-1
9. PERFORMING ORGANIZATION NAME AND ADDRESS Office of Research Services University of California Berkeley, California 94720		10. WORK UNIT NO.
		11. CONTRACT OR GRANT NO. D-6-1
12. SPONSORING AGENCY NAME AND ADDRESS Department of Transportation Division of Highways Sacramento, California 95807		13. TYPE OF REPORT & PERIOD COVERED Final 7-1-70 to 3-31-77
		14. SPONSORING AGENCY CODE RTA 13945-191202 UCB

15. SUPPLEMENTARY NOTES

Conducted in cooperation with the U. S. Department of Transportation, Federal Highway Administration

16. ABSTRACT

This report presents a summary of a series of investigations related to design considerations for asphalt pavements and is divided into three sections.

Section 1 contains a summary of recent research pertaining to the fatigue response of asphalt paving mixtures and includes a discussion of fatigue criteria to be used for design purposes, the effects of air void content and asphalt content on fatigue life, and the cracking of thick asphalt bound layers.

Section 2 contains a summary of studies of three in-service pavements to evaluate the applicability of layered elastic theory to represent pavement response. Results of these studies confirm the validity of the use of elastic theory to represent the response of thick asphalt-bound layers to traffic loading.

In Section 3 is described a subsystem which can be used to predict permanent deformation on asphalt surfaced pavements utilizing laboratory measured permanent deformation characteristics of paving materials and layered elastic theory. Comparison of the observed and predicted deformation in an in-service pavement indicates the potential validity of the procedure.

17. KEY WORDS Asphalt concrete pavements; Fatigue; Fatigue tests; Permanent deformation; Resilient modulus; Layered elastic analysis	18. DISTRIBUTION STATEMENT Unlimited

19. SECURITY CLASSIF. (OF THIS REPORT)	20. SECURITY CLASSIF. (OF THIS PAGE)	21. NO. OF PAGES	22. PRICE
Unclassified	Unclassified		

HMRT - 1242 (ORIG. 9/72)

ClibPDF - www.fastio.com

ClibPDF - www.fastio.com

Soil Mechanics and Bituminous Materials
Research Laboratory

DESIGN CONSIDERATIONS FOR ASPHALT PAVEMENTS

Final Report on an Investigation

by

C. L. Monismith
Professor of Civil Engineering
University of California
and
Research Engineer
Institute of Transportation Studies

K. Inkabi
Research Assistant

D. B. McLean
E. W. Brooker and Associates
Calgary, Alberta, Canada

and

C. R. Freeme
Chief Research Officer
National Institute for Road Research
Pretoria, South Africa

to

The Transportation Laboratory
Division of Highways
State of California
Department of Transportation

under

Research Technical Agreement 13945-191202 UCB
HPR-DR-1(9) D0601
Prepared in cooperation with
The United States Department of Transportation
Federal Highway Administration

Report No. TE 77-1, Office of Research Services
University of California, Berkeley, California
March 1977

ClibPDF - www.fastio.com

ClibPDF - www.fastio.com

TABLE OF CONTENTS

INTRODUCTION 1

PART 1: ADDITIONAL FATIGUE CONSIDERATIONS 3

Introduction 3

Fatigue Criteria for Use in Pavement Design 3

Influence of Asphalt Content and Void Content on Fatigue Life 7

Cracking Development in Thick Asphalt Bound (Some Thoughts) 15

PART 2: ANALYSIS OF IN-SERVICE PAVEMENTS 19

Introduction 19

Indio Project 20

Material Characteristics 20

Structural Section Response 25

Summary 28

Blythe Project 35

Material and Specimen Preparation 35

Fatigue Testing 37

Fatigue Life Determination 39

Willits Project 56

Summary 58

PART 3: PERMANENT DEFORMATION CONSIDERATIONS 60

Introduction 60

Limiting Subgrade Strain Criteria 62

Rutting Estimation from Repeated Traffic Loading 67

Rutting Prediction with Pavement Represented as an Elastic Layered System 67

ClibPDF - www.fastio.com

Summary of Previous Investigations 71

Rutting Prediction with Pavement Represented as a Layered Viscoelastic System 80

Proposed Characterization for Paving Materials 82

Recommended Design (Analysis) Subsystem 85

Rutting Estimate for an In-service Pavement 89

Pavement Section 89

Distortion Characteristics - Asphalt Concrete 89

Rutting Estimate 95

Example of Rut Depth Prediction 98

Effect of Mix Variables on Rutting 98

Summary 100

ACKNOWLEDGMENTS 102

REFERENCES 103

APPENDIX A - Fatigue and Stiffness Tests, Indio Project A-1

APPENDIX B - Influence of Wheel Load Spectrum on Rutting B-1

APPENDIX C - User's Guide: Rut Depth Prediction Program C-1

ClibPDF - www.fastio.com

INTRODUCTION

This report presents a summary of a series of investigations related to design considerations for asphalt pavements and is divided into three sections:

Part 1 - Additional Fatigue Considerations

A summary of recent research pertaining to the fatigue response of asphalt paving mixtures.

Part 2 - Analysis of In-service Pavements

Studies of three in-service pavements to evaluate the applicability of layered elastic theory to represent pavement response.

Part 3 - Permanent Deformation Considerations

Development of a subsystem to predict permanent deformation in asphalt concrete pavements.

The subsystem to predict fatigue developed in an earlier report, Fig. 1, is used as a basis for a portion of the analyses presented in Part 2 and the information contained in Part 1 provides additional data to make the subsystem more useful.

Fig. 2 contains a format for a subsystem to permit estimation of permanent deformation in asphalt concrete pavement structures. Part 3 describes methodology which permits rutting to be estimated within this framework. While this subsystem does not have the extensive research associated with the fatigue subsystem, it does have the potential to assist engineers in achieving the goal of improved design.

Portions of this investigation have been reported in References (20), (56), and (29). Those results will not be included in this final report.

ClibPDF - www.fastio.com

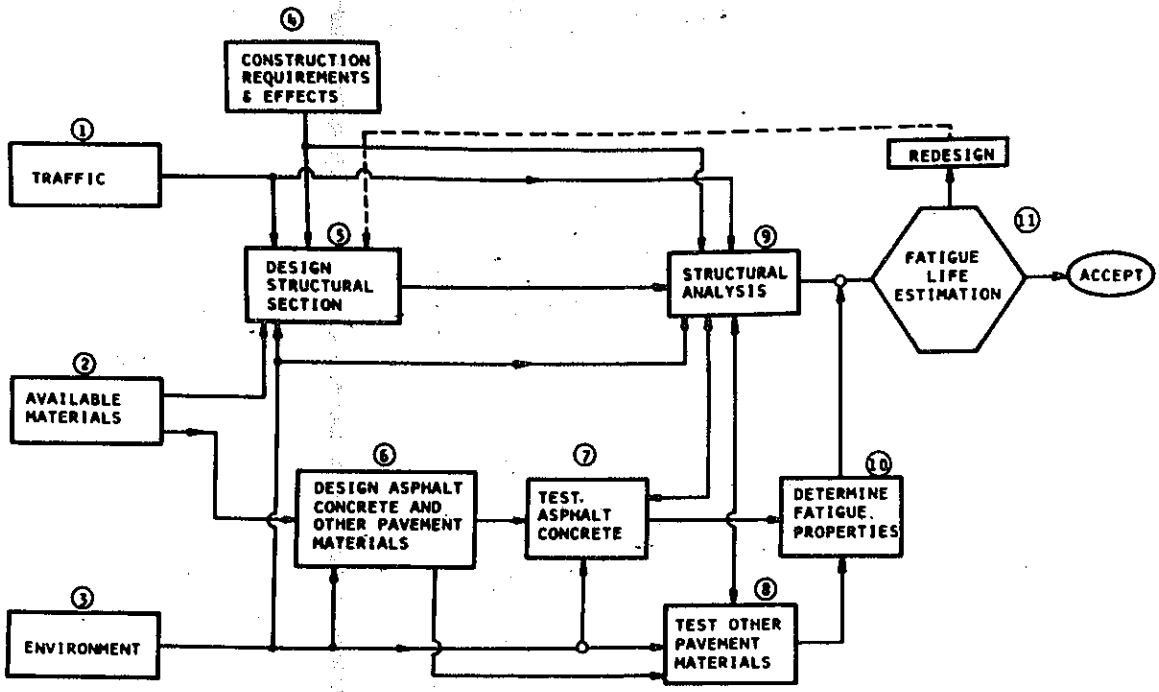

Fig. 1 - Block diagram of a fatigue subsystem.

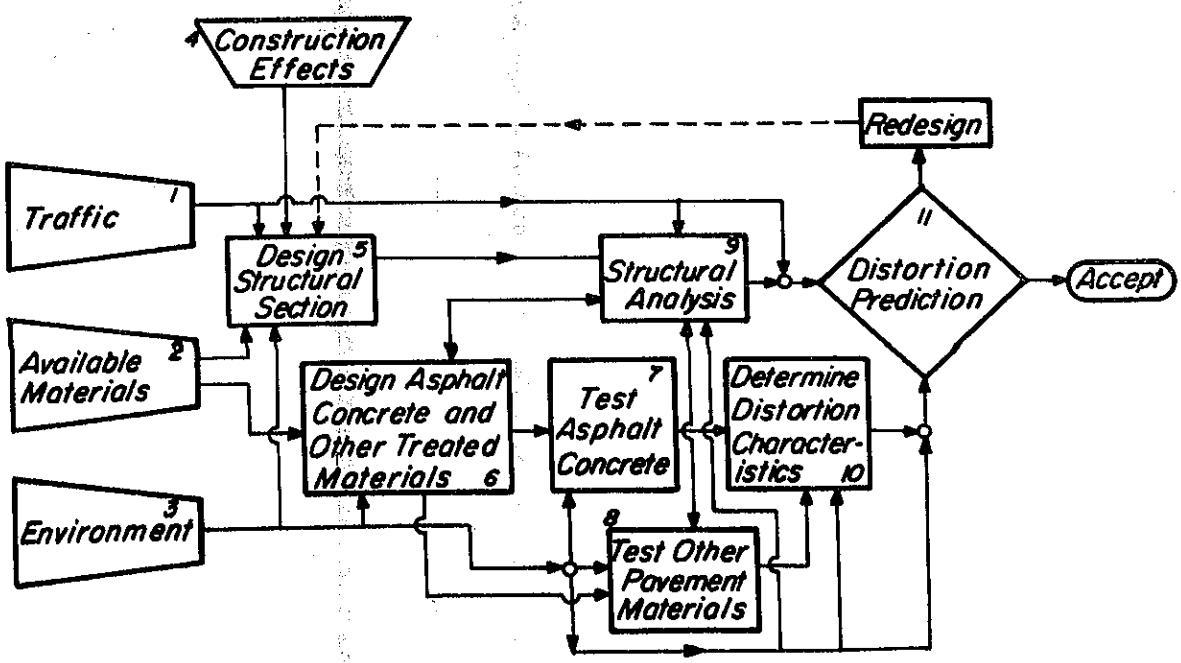

Fig. 2 - Block diagram of a distortion subsystem.

ClibPDF - www.fastio.com

PART 1: ADDITIONAL FATIGUE CONSIDERATIONS

INTRODUCTION

Since the publication of earlier reports (e.g., TE 70-5 (1)), a number of questions have been raised as to which fatigue criteria for asphalt concrete should be used for design purposes (2, 3). In this section some consideration is given to the problem, and alternative solutions are suggested based on a survey of recent literature.

The effects of air void content and asphalt content on fatigue life of asphalt concrete have also been discussed in earlier reports (1). Recent research by Pell has suggested an improved method for considering the effects of both of these variables. Discussion of this approach is also included.

A brief discussion of cracking in thick asphalt-bound layers and its significance relative to design has been incorporated since evidence has been presented to indicate that under some circumstances cracking may be different than that assumed in the fatigue subsystem.

FATIGUE CRITERIA FOR USE IN PAVEMENT DESIGN

Deacon (2) has indicated that a crucial aspect of fatigue life estimation is the development of suitable distress criteria. Such criteria can be established in at least four different ways (2):

(1) from theoretical analyses of existing design curves,

(2) from an analysis of the performance of in-service pavements, particularly road tests operated under rigid control,

(3) from laboratory fatigue testing,

(4) from a combination of two or more of the above procedures.

Finn, et al (3), have shown that care must be exercised in the development

ClibPDF - www.fastio.com

of such criteria since, for example, contradictory results may be obtained for the influence of mix variables on pavement performance. This point is illustrated in Fig. 3 . In this figure, results of analyses show that fatigue damage decreases with increase in asphalt concrete stiffness if either the criteria developed in TE 70-5 (1) or those developed by Heukelom and Klomp (4) are used; on the other hand, if the criteria developed by Kingham (5) are used, damage increases with increase in mixture stiffness. (For information, comparison of these three criteria are shown in Figs. 4 and 5).

Generally, fatigue criteria determined from laboratory controlled stress tests will provide the most conservative results since such tests include relatively few repetitions for crack propagation. In-situ, on the other hand, it is possible that, after initial cracking, the asphalt bound layer will sustain a large number of additional repetitions (associated with a slow rate of crack propagation) before the pavement is considered unserviceable. Such considerations lend support to the suggestion by Deacon (2) that distress criteria derived from the analysis of the performance of in-service pavements would appear most suitable at this time. However, to develop such criteria from analyses, appropriate materials characterization data together with detailed traffic and environmental information are required for the specific projects being analyzed.

Since considerable laboratory fatigue data are available, an alternative approach is to combine methods (2) and (3) above to arrive at interim criteria and to check the reasonableness of pavements designed with these criteria by comparing thicknesses so selected with those obtained using appropriate existing methodology.

In some instances this may involve the shifting of the curves determined from laboratory testing by some reasonable factor (e.g., Pell (6)). Santucci (7) has used this approach in establishing fatigue criteria for full-depth

ClibPDF - www.fastio.com

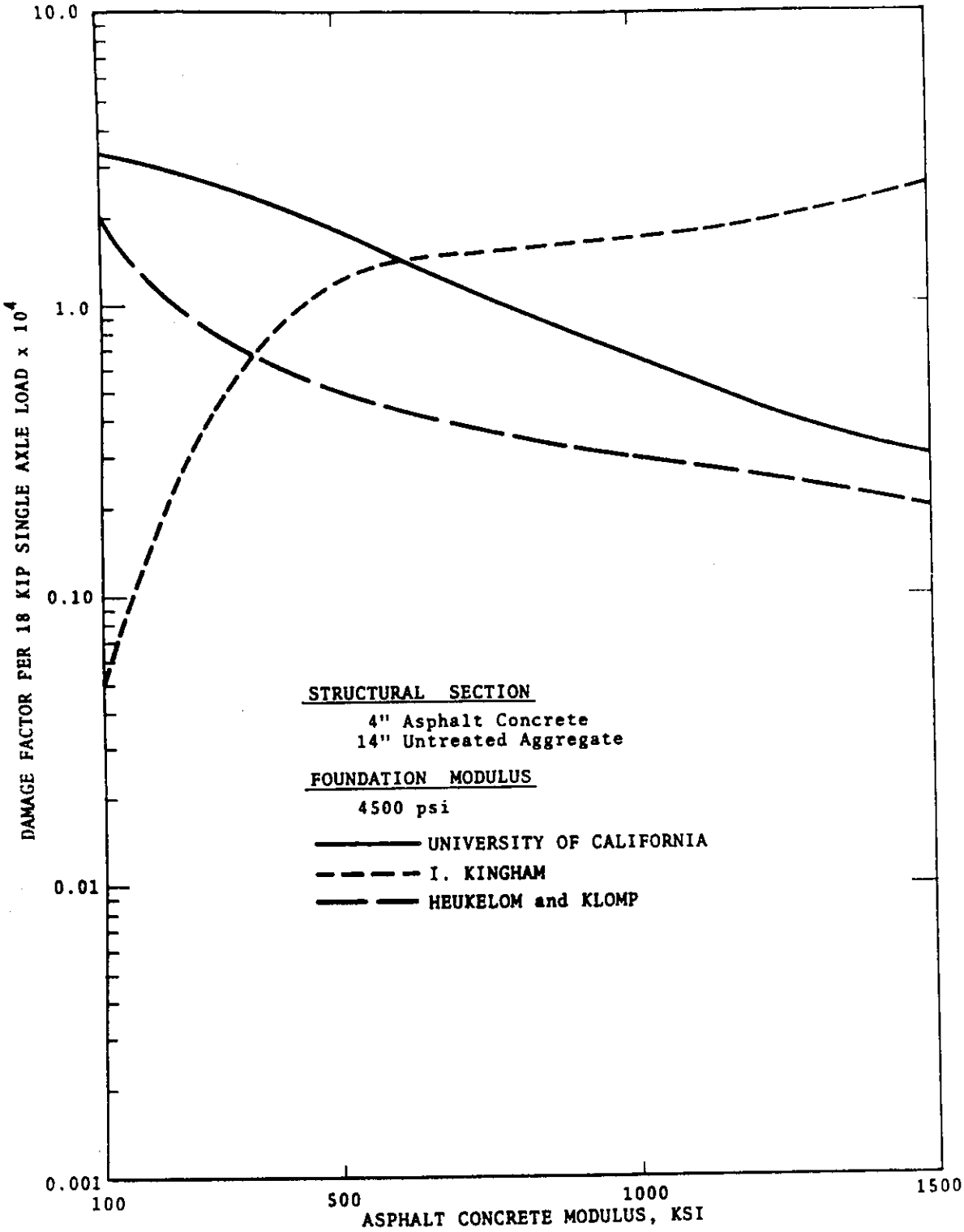

Fig. 3 - Influence of asphalt concrete stiffness on fatigue performance. (after Finn, et al (3)).

ClibPDF - www.fastio.com

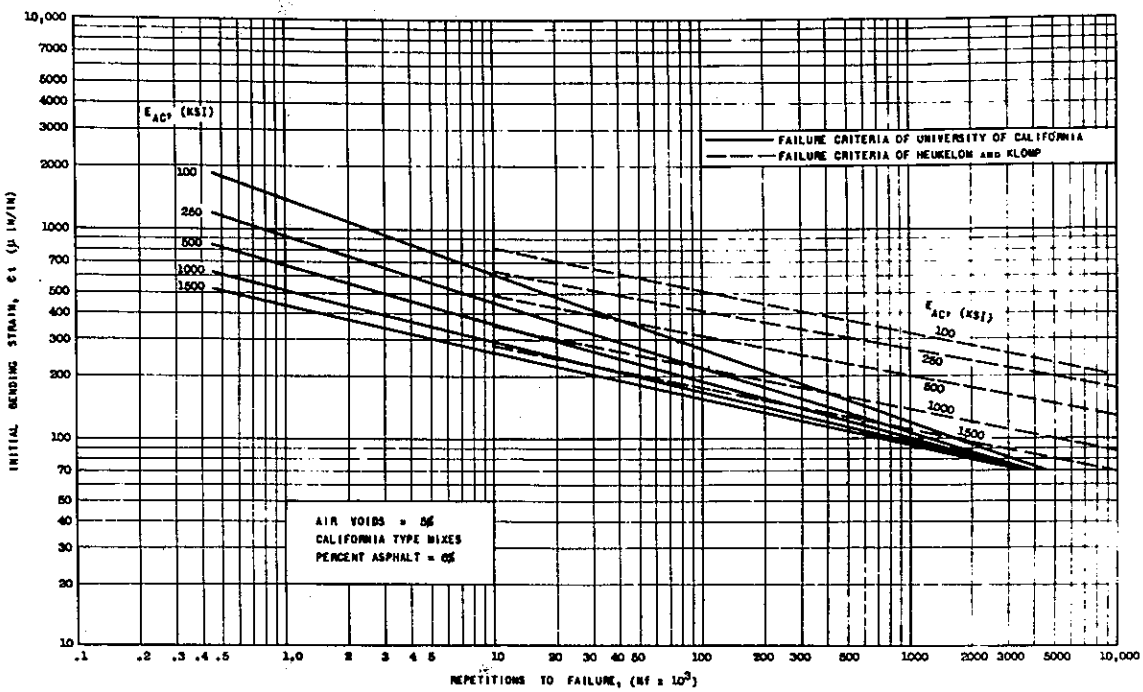

Fig. 4 - Comparison of fatigue criteria developed by Heukelom and Klomp (4) with those suggested in Report TE 70-5 (1). (after Finn et al (3)).

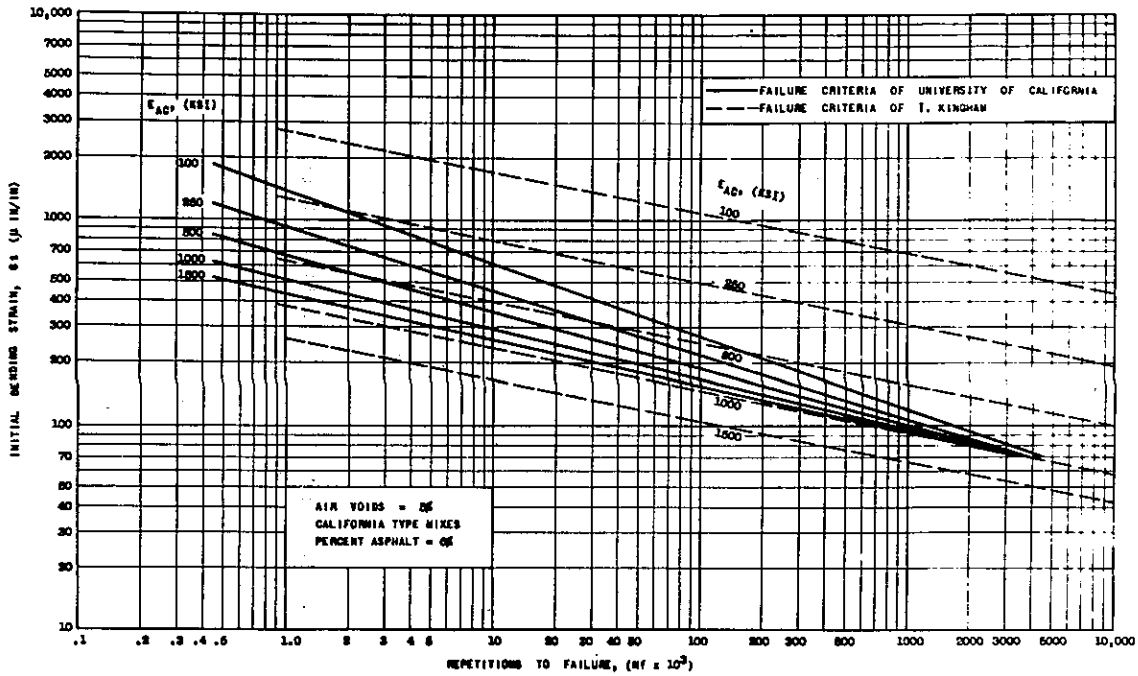

Fig. 5 - Comparison of fatigue criteria developed by Kingham (5) with those suggested in Report TE 70-5 (1). (after Finn et al (5)).

ClibPDF - www.fastio.com

asphalt pavements containing emulsion-treated as well as asphalt concrete base courses. His recommended criteria, shown in Figs. 6 and 7 were obtained by increasing the number of repetitions for the laboratory determined curves by a factor of three.

Recently van Dijk (8) has presented fatigue data obtained from a wheel tracking test. His results indicate that controlled-strain data may be more appropriate to define pavement cracking than controlled-stress data since the former include the influence of crack propagation on the number of repetitions associated with unserviceability. In his tests van Dijk has defined various stages of cracking as shown in Fig. 8 and has compared these results with laboratory tests. If one considers the N_2 stage, shown in the figure, as the damage measure, then the use of criteria less conservative than those based on controlled-stress tests appear reasonable as in Fig. 9 .

The shifting of the laboratory curves obtained from controlled stress testing as done by Santucci thus appears to be a suitable procedure (so long as the resulting designs agree with existing field performance data).

Finally, while still not well documented, it is possible that the use of both controlled-stress and controlled-strain laboratory fatigue data provides an alternative approach to reasonably recognize the influence of crack propagation time on pavement service life. The procedure whereby this might be accomplished is illustrated in a subsequent section describing the Blythe project and involves the concept of the mode factor. Such a procedure has already been described in an earlier report (1) and thus will not be included in this section.

INFLUENCE OF ASPHALT AND VOID CONTENTS ON FATIGUE LIFE

A number of reports (9, 1, 10) have demonstrated the influence of both asphalt content and void content on fatigue life. Recently Pell and Cooper (11)

ClibPDF - www.fastio.com

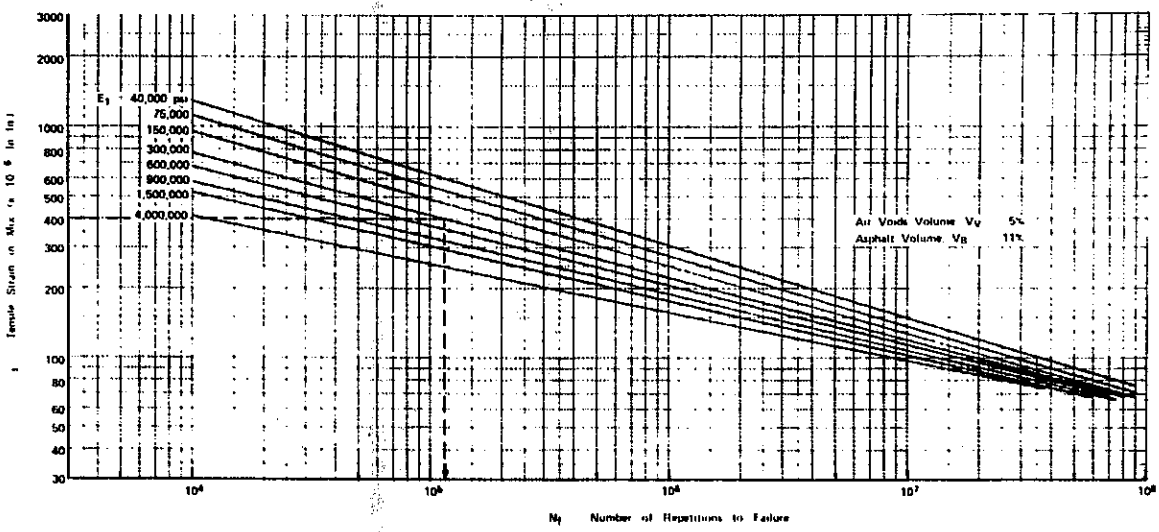

Fig. 6 - Fatigue criteria for asphalt and emulsified asphalt mixes. (after Santucci (7))

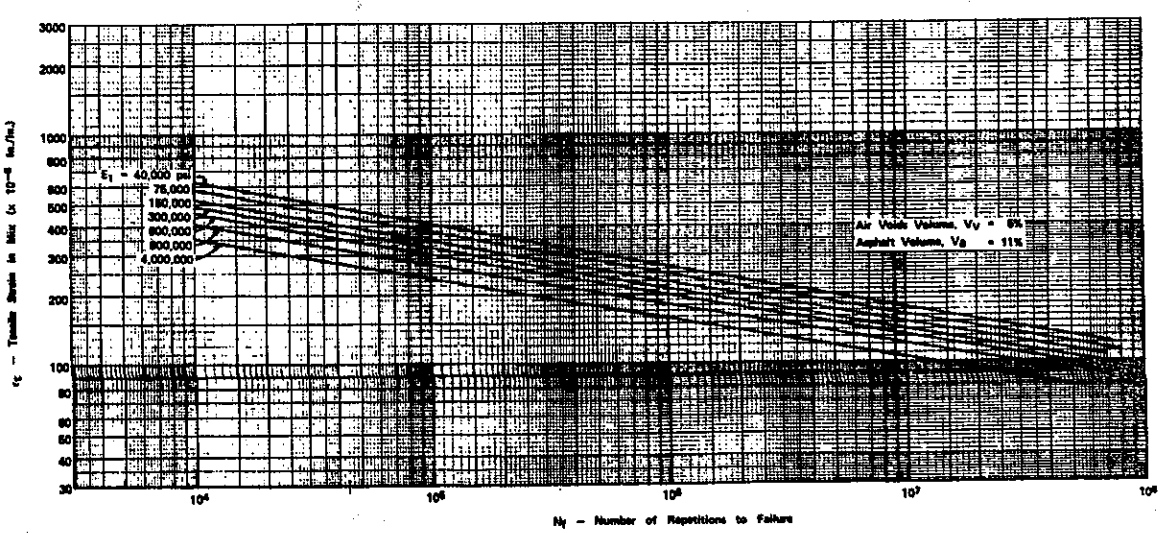

Fig. 7 - Fatigue criteria for cement-modified emulsified asphalt mixes (C-EAM). (after Santucci (7))

ClibPDF - www.fastio.com

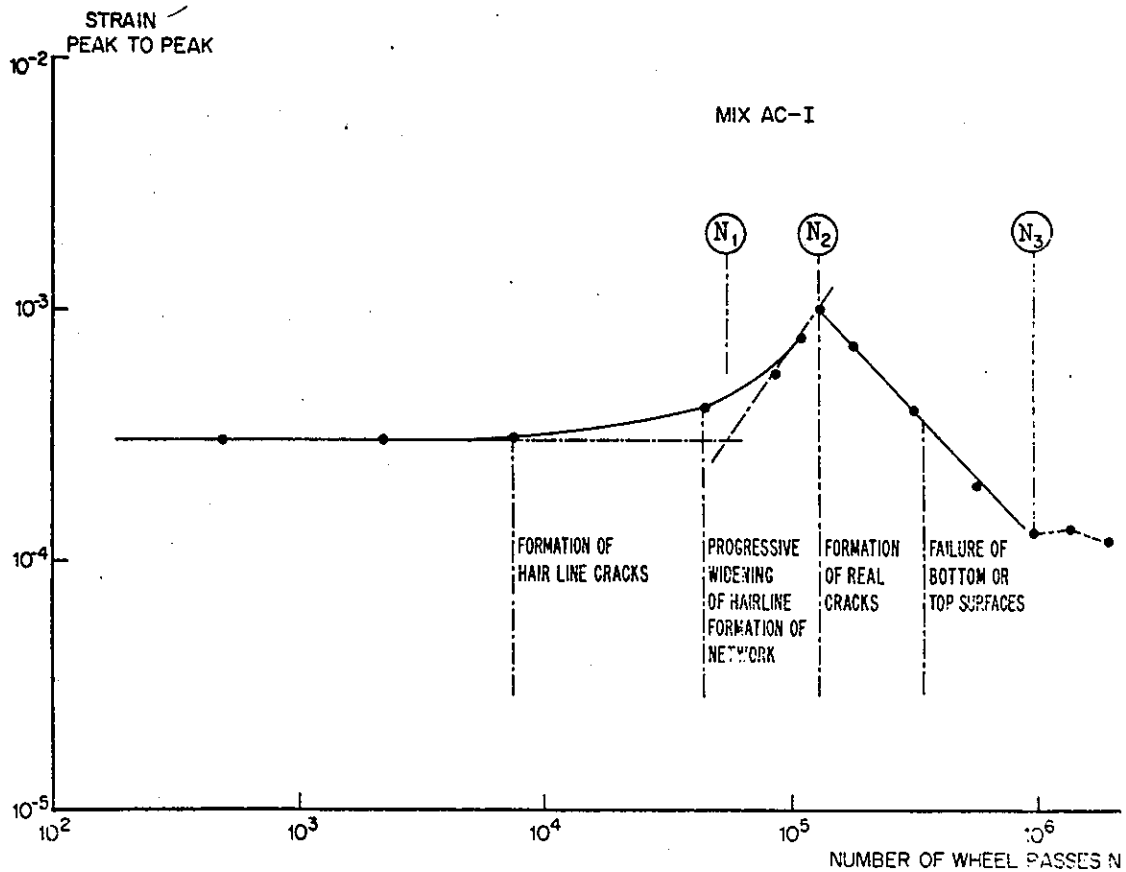

Fig. 8 - Crack development as a function of strain gage readings on underside of slab in wheel tracking tests. (after vanDijk (8))

ClibPDF - www.fastio.com

have suggested that a useful way to incorporate the influence of both of these variables on fatigue life is by means of a correction factor proportional to:

$$\frac{V_B}{V_v + V_B} \qquad (1)$$

where:

V_B = asphalt volume*, percent

V_v = air void volume, percent

Santucci (7) has analyzed the data of Pell and Cooper and developed the regression curve shown in Fig. 10. The data obtained by Epps (12) and reported in TE 70-5 has been analyzed in this manner and the results are shown in Fig. 11. It should be noted that the data of Pell and Cooper are based on fatigue lives associated with strains of 100×10^{-6} in. per in. (mm per mm), while those of Fig. 11 are based on mixture strains in the range of 400 to 600×10^{-6} in. per in. (mm per mm). Interestingly, the slope of the regression line developed from Pell's data appears reasonable for the data developed by Epps.

To use the fatigue data shown in Fig. 11 (California mixes), it is necessary to adjust the fatigue life at a particular strain level for the corresponding stiffness by the ratio:

---

*V_B determined from the expression

$$V_B = \frac{P_{Wasp} G_{agg} (1 - V_v)}{100 \cdot G_{asp} + P_{Wasp} \cdot G_{agg}}$$

where:

P_{Wasp} = percent by weight of asphalt (dry weight of aggregate)

G_{asp} = specific gravity of asphalt

G_{agg} = specific gravity of aggregate

ClibPDF - www.fastio.com

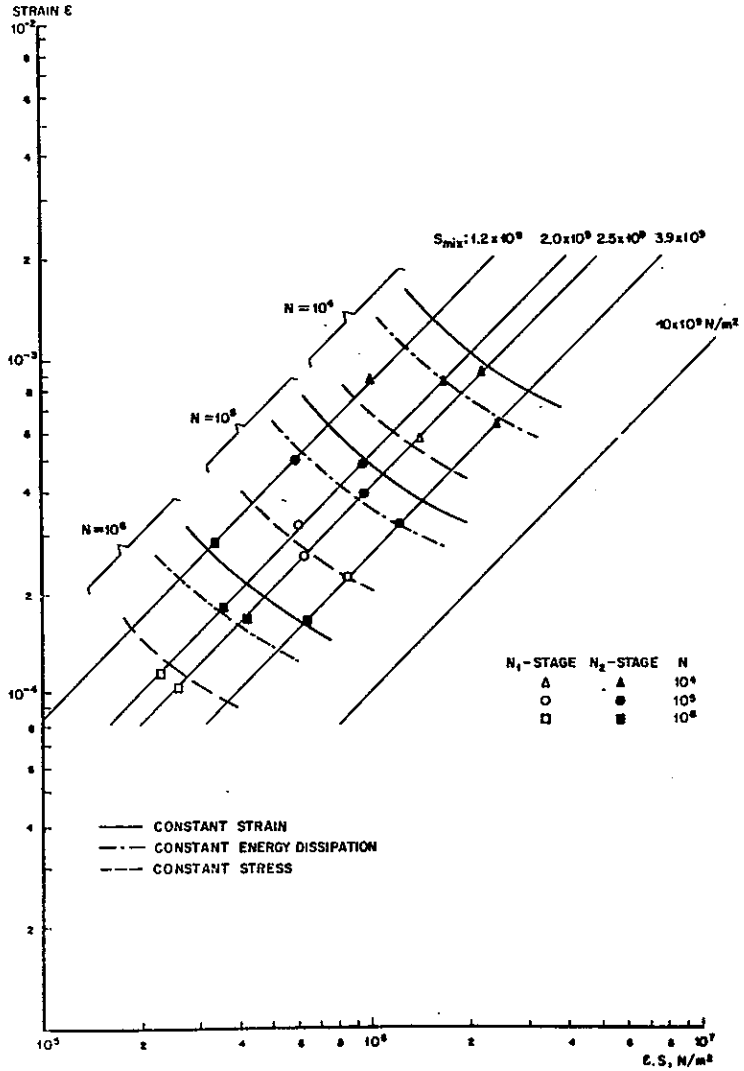

Fig. 9 - Comparison of repetitions to various stages of cracking in wheel tracking test with laboratory determined fatigue lives. (after van Dijk (8))

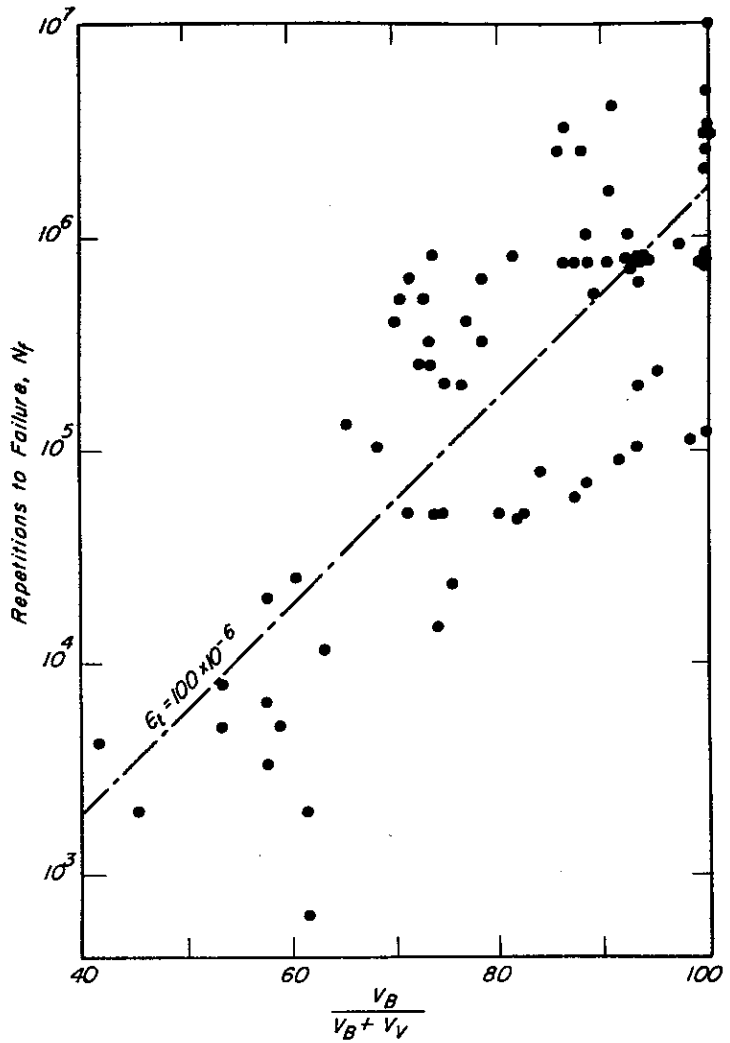

Fig. 10 - Influence of the factor $\frac{V_B}{V_B + V_V}$ on fatigue life on British-type mixes.

ClibPDF - www.fastio.com

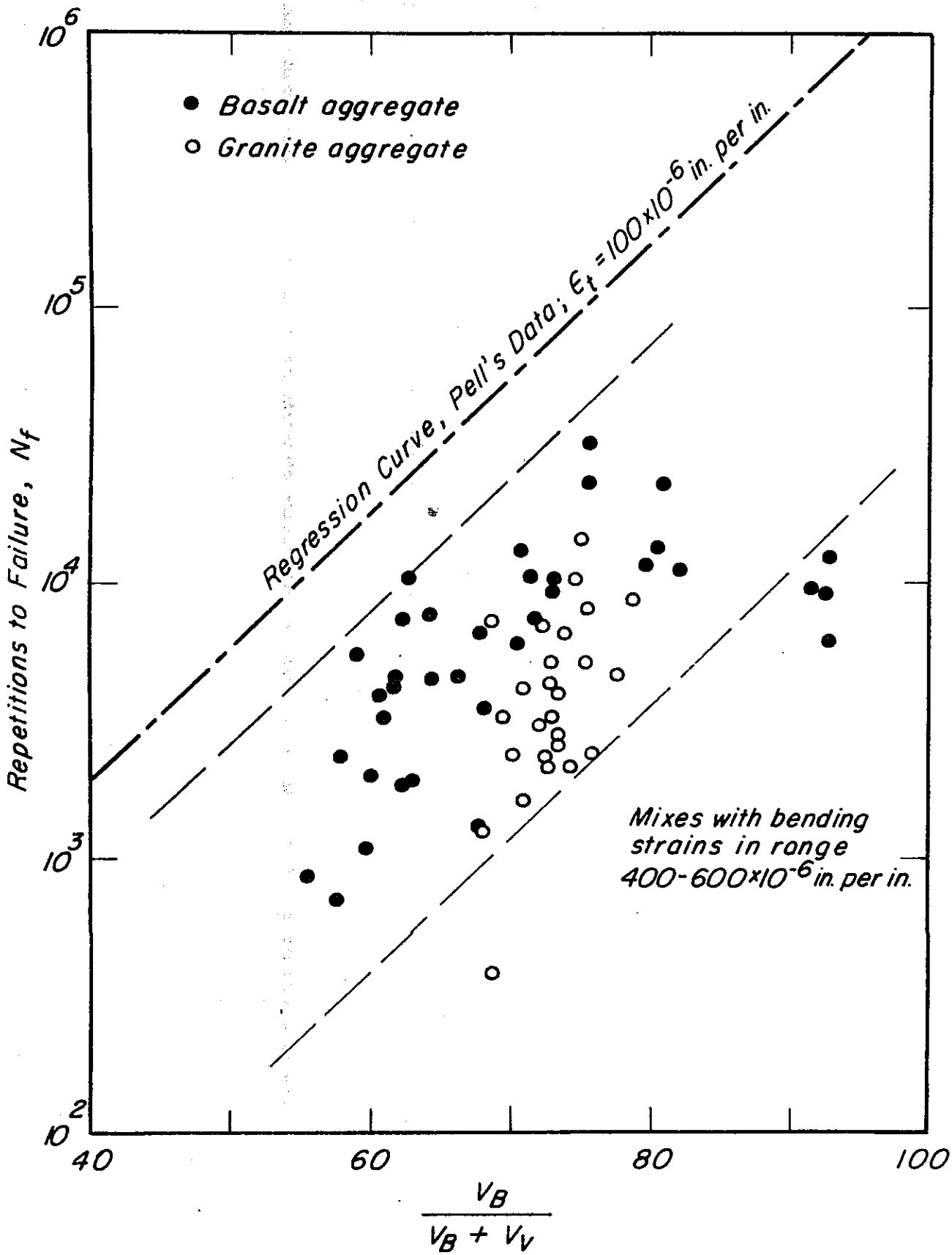

Fig.11 - Influence of the factor $\frac{V_B}{V_B + V_V}$ on fatigue life on California-type mixes.

ClibPDF - www.fastio.com

$$\left\{ \frac{\left[\dfrac{V_B}{V_V + V_B} \right]_1}{\left[\dfrac{V_B}{V_V + V_B} \right]_0} \right\}^{4.84} \qquad (2)$$

where:

condition 1 corresponds to the actual placement of field conditions

and

condition 0 corresponds to the laboratory mix design based on the State of California method with 5 percent air voids.

The exponent 4.84 of equation (2) was determined by a regression analysis (7) of available data.

Recently Pell has demonstrated how such data can be used to assess the influence of field compaction on the fatigue performance of asphalt pavements (13), illustrating again how available data together with theory can assist the engineer in assessing the consequences of design decisions and construction influences. Pell's analyses are shown in Figs. 12 and 13.

Fig. 12 illustrates the results for an analysis of a pavement containing a dense bituminous macadam base (D.B.M.). In the analysis the stiffness of the macadam base was varied according to its variation in both asphalt content and void content (as computed by the Shell procedure (14)). Maximum tensile strains were computed at the underside of the asphalt-bound base layer and the nomograph recently developed by Pell, Fig. 14, used to estimate fatigue life. Pell notes that for this situation the effect of void content is extremely important. However, the influence of asphalt content may be more important than shown since the procedure used to estimate stiffness may overestimate somewhat the effect of void content. The data do, however, stress the

ClibPDF - www.fastio.com

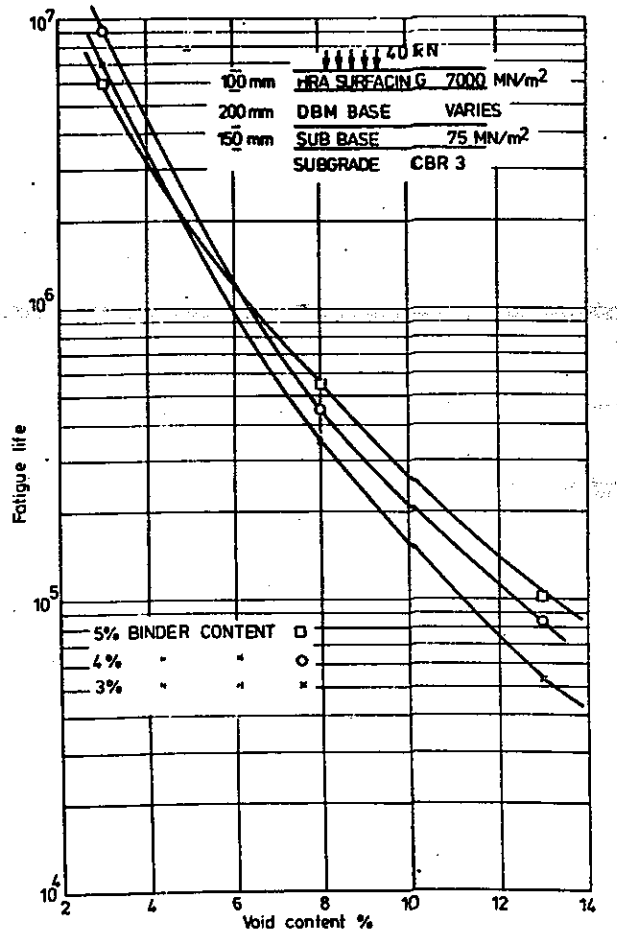

Fig. 12 - Influence of asphalt and void contents on the fatigue behavior of a dense bituminous macadam. (after Pell)

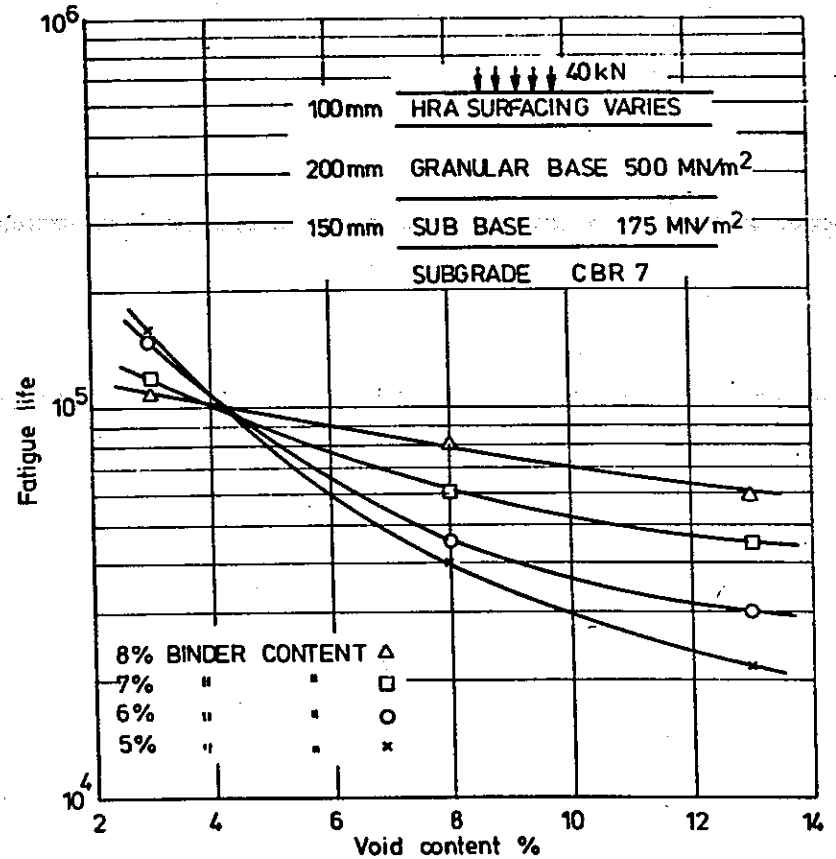

Fig. 13 - Influence of asphalt and void contents on the fatigue behavior of a hot rolled asphalt surfacing. (after Pell)

ClibPDF - www.fastio.com

importance of good compaction.

Fig. 13 illustrates the results for a pavement structure containing a comparatively thin asphalt-bound layer -- termed hot rolled asphalt (H.R.A.). In this case the influence of void content is not as significant since stiffness does not play as predominant a role for the structure of Fig. 12. The importance of higher asphalt contents at higher void contents is emphasized.

In general, as noted earlier, this data indicates how one can analyze the influence of construction variables on performance. Moreover, it emphasizes the point that such variables must be examined in the context of a particular pavement structure!

CRACKING DEVELOPMENT IN THICK ASPHALT-BOUND LAYERS (SOME THOUGHTS)

In the design methodology which has evolved from the research to date in this investigation as well as others (15, 16, 17, 1) to minimize fatigue cracking, it has been assumed that cracking will initiate on the underside of the asphalt-bound layer and is associated with the magnitude of the principal tensile strain repeatedly applied resulting from traffic loading. The Morro Bay project (1), for example, indicated this to be a reasonable assumption. Some recent studies of the performance of thick asphalt-bound layers indicate that cracking may not necessarily start on the underside of the layer and progress upwards (18, 19). Examination by Witczak of crack patterns in some in-situ pavements, e.g., some sections of taxiways at Baltimore-Washington International Airport (18), indicate that cracking may be confined to the upper part of the pavement structure when it is first observed.

As Witczak has noted, cracking near the surface may result from a combination of vertical and horizontal forces associated in the specific instance of the Baltimore-Washington taxiway pavement with turning aircraft. It is also possible that because of temperature gradients in the asphalt concrete, particularly when the surface is warmer than the lower portion, that the

ClibPDF - www.fastio.com

principal strains resulting from combined stresses may be relatively large tensile strains.

Dehlen (19) in his analyses of the San Diego Test Road pavement indicated that such a possibility may exist. Nunn (20) has made a fairly detailed analysis of stresses and strains in thick asphalt pavements for the conditions of (1) constant temperature throughout the layer and (2) temperature gradients representative of those in Great Britain. Fig. 15 illustrates radial strain distributions for constant temperature conditions. At elevated temperatures it will be noted that high tensile strains are obtained. While this may not be a completely realistic situation, it is not difficult to envision circumstances wherein the upper part of the asphalt-bound layer is at a relatively high temperature with the result that such a distribution might be representative of the upper part of the pavement structure. When such conditions occur, it is possible that some fatigue cracking may thus occur in this portion of the pavement. Whether or not this will influence the thickness design procedures is another question.

Witczak has indicated, based on his analysis of the Baltimore-Washington International Airport, that the thickness design procedure which includes consideration of the tensile strain on the underside of the pavement provides a reasonable thickness for this site even though some surface cracking has been observed.

As will be seen in the section containing the analysis of the Indio pavement, when the temperatures are high large tensile strains are computed near the surface.

Thus far, however, there is no indication that the concept of considering the maximum tensile strain in the underside of the asphalt-bound layer as the damage determinant should be revised, e.g., Witczak (18). It is possible, however, that some cracking may occur in thick structures and may have some

ClibPDF - www.fastio.com

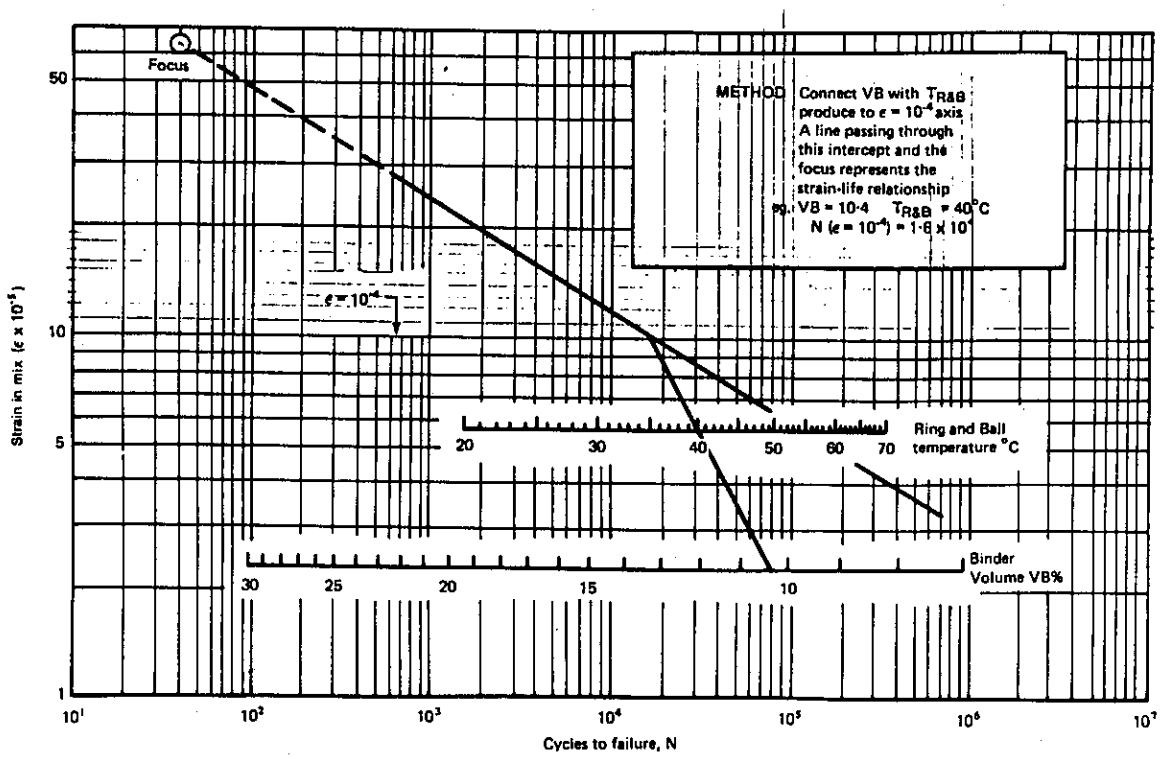

Fig. 14 - Nomograph for prediction of fatigue performance. (after Cooper and Pell (11))

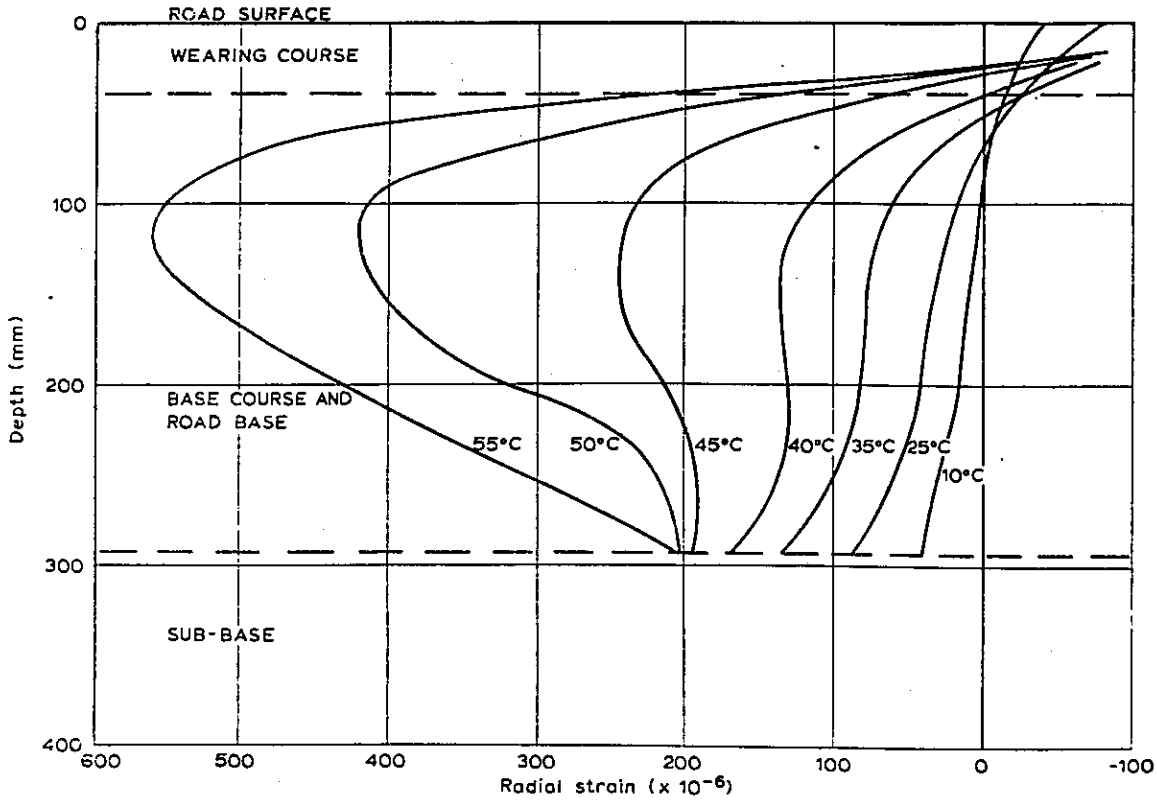

Fig. 15 - Radial strain in asphalt-bound layers at various pavement temperatures. (after Nunn (20))

ClibPDF - www.fastio.com

influence on design thicknesses. Until further evidence becomes available, however, it is recommended that the present concepts used for design, i.e., maximum strain at bottom of layer, be continued.

ClibPDF - www.fastio.com

PART 2: ANALYSIS OF IN-SERVICE PAVEMENTS

INTRODUCTION

As a part of the evaluation program to assess the validity of the use of layered elastic analysis in the design of asphalt concrete pavements, the California Transportation Laboratory selected three "full-depth" pavements for detailed study. These included:

(1) A full depth section of a widening portion of Interstate 10 near Indio, California.

(2) Two 1,000 ft. (305 m) long experimental full depth sections on Interstate 10 near Blythe, California.

(3) A full depth widening project on U. S. 101 in the city of Willits, California.

In this section will be summarized the studies associated with these projects conducted at the Soil Mechanics and Bituminous Materials Laboratory.

ClibPDF - www.fastio.com

INDIO PROJECT

The pavement section for the Indio project consists of a layer of asphalt concrete 1.0 ft. (300 mm) in thickness placed on 0.25 ft. (75 mm) of Class II aggregate base introduced as a working table, both layers, in turn, resting on a sandy subgrade. Fig. 16 illustrates the pavement cross section including the lift thicknesses placed to achieve the 1.0 ft. (300 mm) thick asphalt concrete layer. The surface course* 0.25 ft. (75 mm) in thickness, contains 4.9 percent of a 60-70 penetration asphalt cement while the base course, 0.70 ft. (215 mm) in thickness contains 4.4 percent of an 85-100 penetration asphalt cement.

Instrumentation consisting of strain gages, LVDT's, pressure cells, thermocouples, and moisture movement devices were installed in a section of the project by the staff of the Transportation Laboratory. Fig. 16 also shows locations of the various types of instrumentation.

While the original intent of this phase of the study was to prepare an estimate of the service life of the pavement, studies at the University have been limited to prediction of some of the measured strains and deflections for specified load and environmental conditions.

Material Characteristics

The subgrade soil for the project is a sand. Results of repeated load triaxial compression tests on this material are shown in Figs. 17 and 18 for a condition representative of that in-situ, i.e. water content of 5.1 percent and a dry density of 110 lb per cu ft.

Stiffness results of the usual form (1) were obtained, i.e.:

$$M_R = 3{,}160 \cdot \sigma_3^{0.73} \qquad (3)$$

---

*The open graded mix placed at the surface, 0.05 ft. (15 mm) in thickness was not considered in the structural analyses to be presented herein.

ClibPDF - www.fastio.com

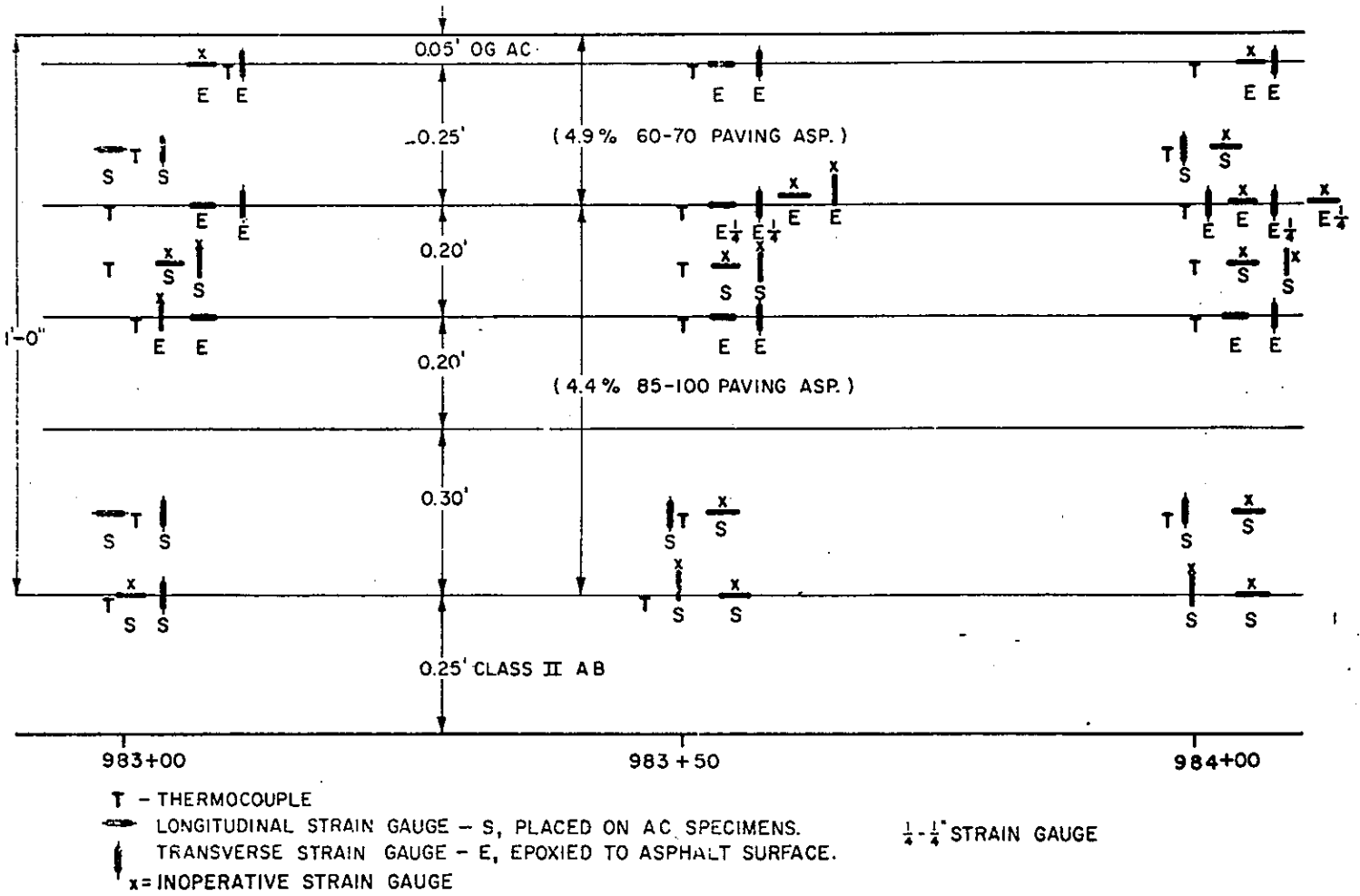

Fig. 16 - Indio pavement section including instrumentation.

ClibPDF - www.fastio.com

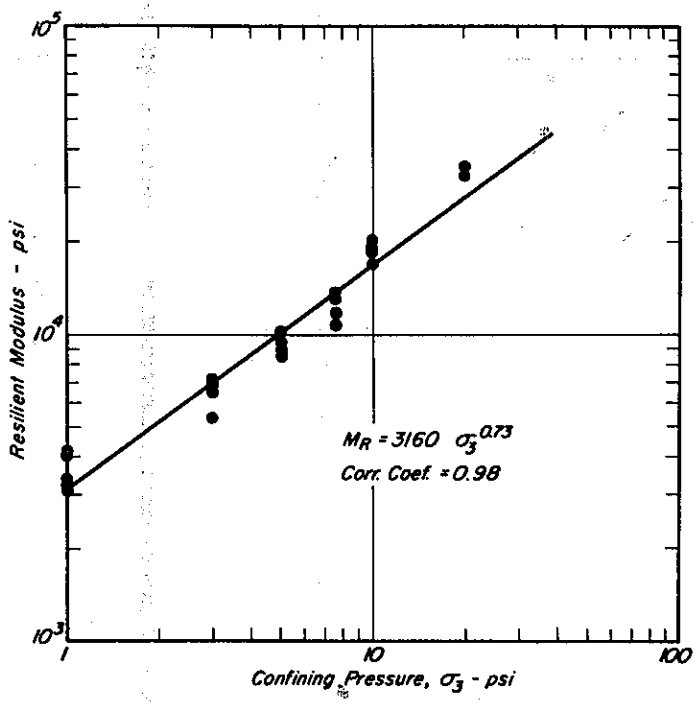

Fig. 17 - Resilient modulus vs. confining pressure - Indio subgrade sand.

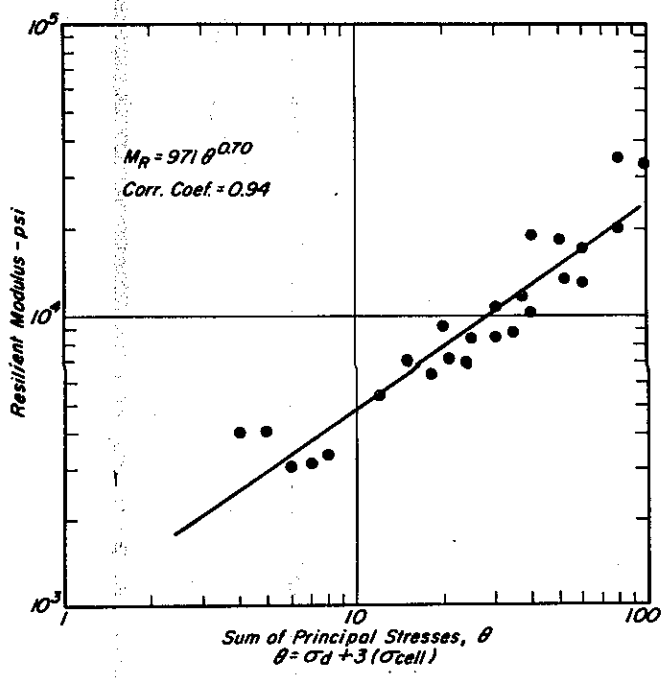

Fig. 18 - Resilient modulus vs. sum of principal stresses - Indio subgrade sand.

ClibPDF - www.fastio.com

where

M_R = resilient modulus, psi

σ_3 = confining pressure, psi

and

$$M_R = 971 \cdot \Theta^{0.70} \tag{4}$$

where:

Θ = sum of principal stresses, $\sigma_d + 3\sigma_3$, psi

σ_d = deviator stress $(\sigma_1 - \sigma_3)$, repeatedly applied, psi

Resilient Poisson's ratios have been plotted as a function of the principal stress ratio, σ_1/σ_3 in Fig. 19 . More recent studies have indicated that the resilient Poisson's ratio may not vary as much with principal stress ratio as shown in Fig. 19 if the confining pressure as well as deviator stress is repeatedly applied. This should permit some simplification in any detailed analysis, e.g., a finite element analysis of a particular section.

Tests were not performed on the Class II aggregate base; rather, this material was assumed to have the same characteristics as the Folsom project base aggregate (1)

Stiffness and fatigue tests were performed on 12 in. (300 mm) diameter cores of the asphalt concrete section obtained by the staff of the Transportation Laboratory. Appendix A contains a summary of the procedures used to obtain the beam specimens as well as a detailed summary of the test results. In the analysis reported herein, only the stiffness measurements have been used. Fatigue data have been included in Appendix A , should additional analyses be desired at some subsequent time.

Tests were also performed on the asphalts recovered from both base and

ClibPDF - www.fastio.com

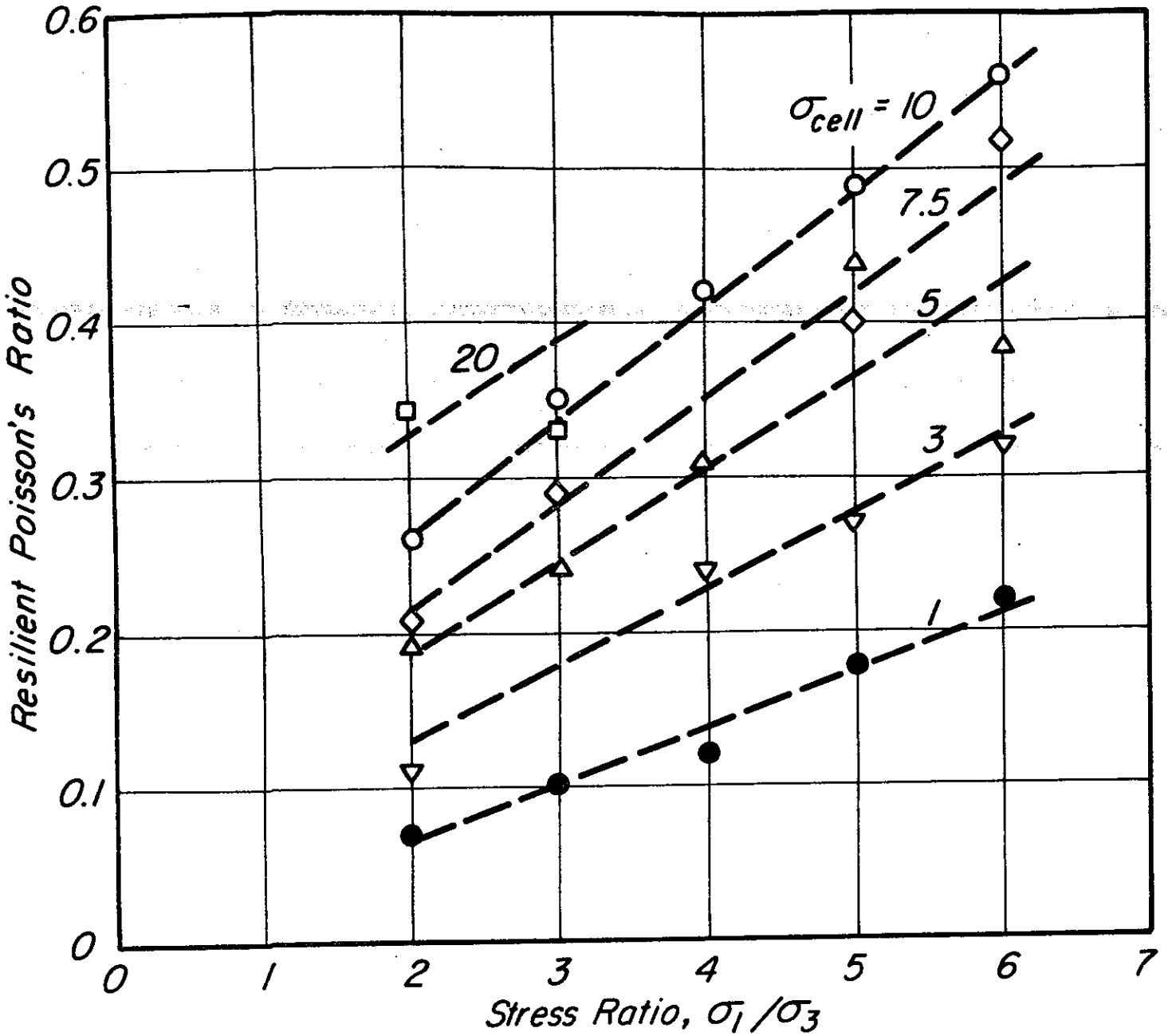

Fig. 19 - Influence of σ_1/σ_3 on resilient Poisson's ratio - Indio subgrade sand.

ClibPDF - www.fastio.com

surface courses. Properties of the recovered materials are shown in Table 1.

To estimate the stiffness using the Shell procedure (15), i.e., in the equation:

$$\frac{S_{mix}}{S_{asp}} = \left[1 + \frac{2.5}{n} \cdot \frac{C_v}{1 - C_v}\right]^n \qquad (5)$$

The quantities shown in Table 2 were determined. In this equation it is necessary to use a modified volume concentration of aggregate, C_v' for air void contents greater than 3 percent. These values are shown in the table. In addition, according to the Shell investigators, this expression is valid so long as the volume concentration of the asphalt, B_v , is greater than $2/3\ (1 - C_v')$. It will be noted that these mixes are within the range; accordingly, estimated stiffnesses were determined and comparisons between computed and measured values are shown in Figs. 20a and b.

These comparisons indicate that the computational procedure can reasonably estimate stiffnesses, although the measured stiffness values at 81°F (27°C) are somewhat less than the estimated values, particularly for the base course. This difference may be due in part to cross section irregularities resulting from sawing. While the irregularities occurred in the specimens tested at the lower temperatures, their influence was more severe at the elevated temperature.

To analyze the pavement under moving traffic, stiffnesses were also estimated at a time of loading of 0.015 sec. These values are shown in Figs. 21a and b. In the high temperature range the computed values may be lower than those which might occur in-situ necessitating some adjustments in the computed values based on comparisons between calculated and measured deflections at these temperatures.

Structural Section Response

As noted earlier, only a few analyses were performed to estimate the pavement response to load for comparison with measured values. For these computations

ClibPDF - www.fastio.com

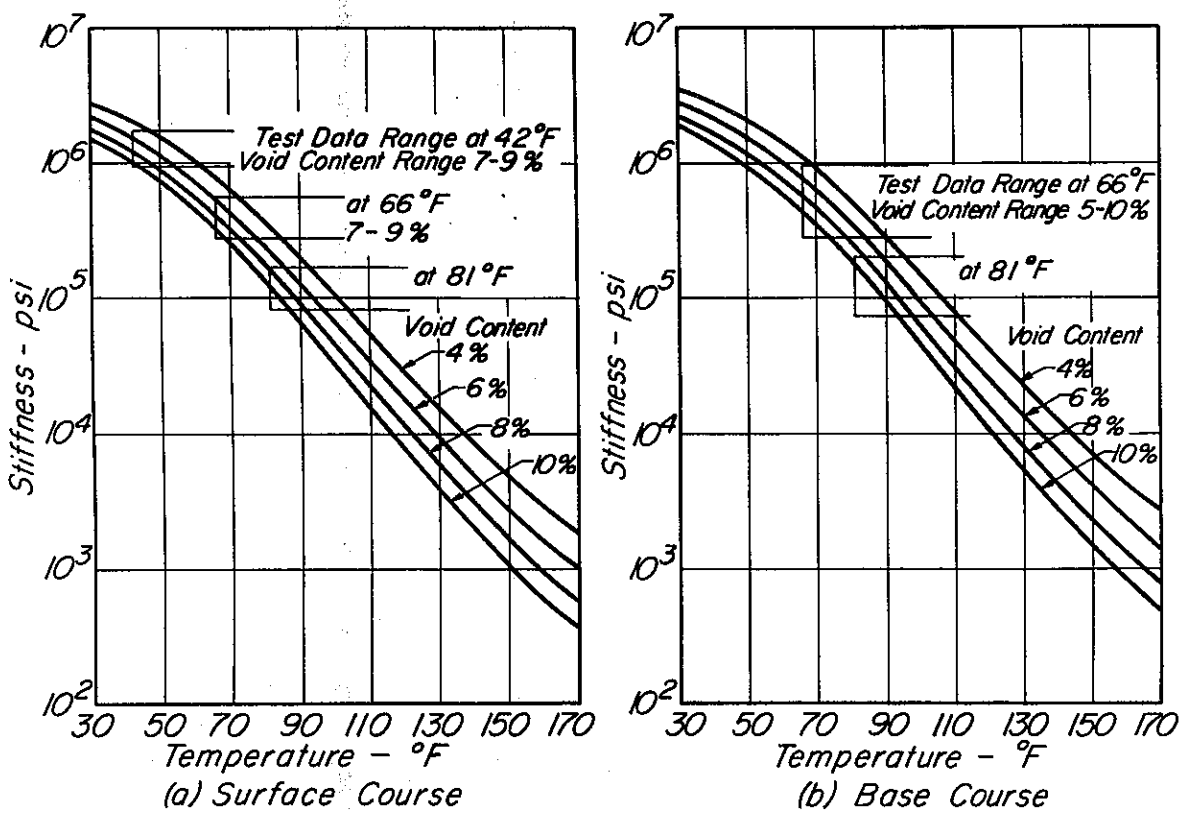

Fig. 20 - Influence of temperature in stiffness of asphalt concrete - Indio mix; time of loading = 0.1 sec.

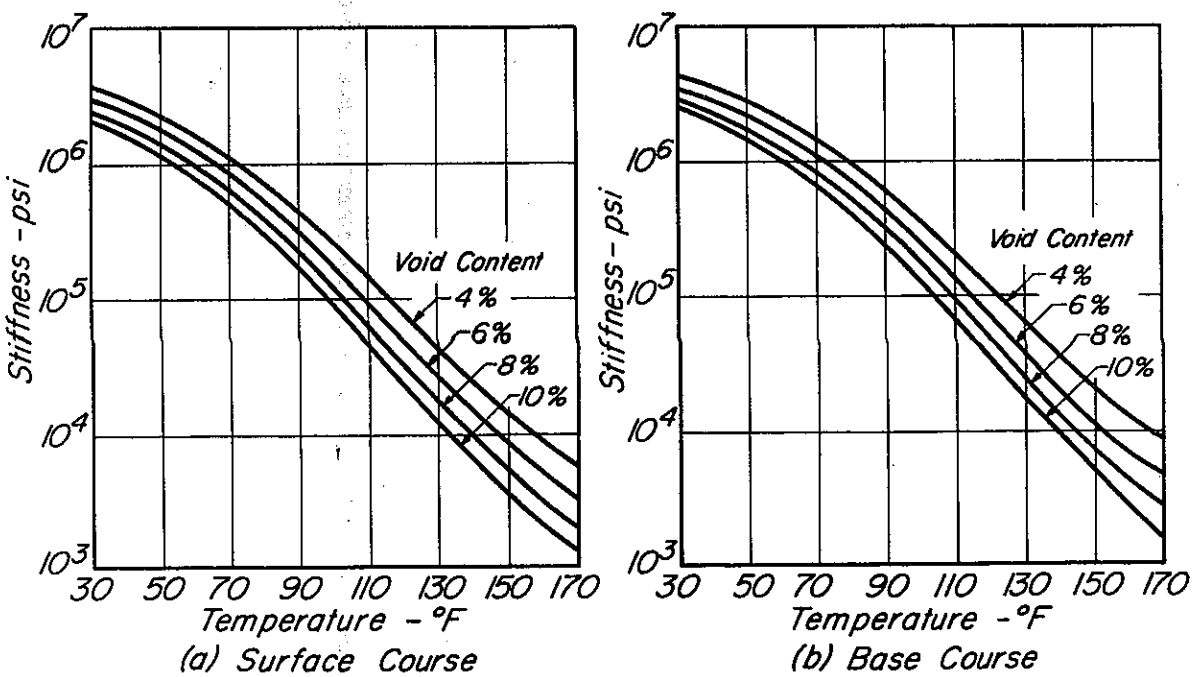

Fig. 21 - Influence of temperature in stiffness of asphalt concrete - Indio mix; time of loading = 0.015 sec.

ClibPDF - www.fastio.com

TABLE 1 - RECOVERED ASPHALT PROPERTIES, INDIO CORE SAMPLES

Test Property	Date Sampled	Base	Surface
Penetration, 77°F, 100 gm, 5 sec. - dmm	July '71 Dec. '71	30 26	36 29
Ring and Ball Softening Point °F	July '71 Dec. '71	128 139.5	127 138

TABLE 2 - PARAMETERS TO PERMIT ESTIMATE OF STIFFNESSES OF INDIO BASE AND SURFACE COURSES BY SHELL PROCEDURE

	Asphalt Content Percent	C_v	Air Void Content Percent	C'_v	B_v	$2/3\ (1 - C'_v)$
Base	4.4	0.893	8.0	0.853	0.107	0.100
Surface	4.9	0.884	8.0	0.841	0.116	0.106

ClibPDF - www.fastio.com

the pavement was represented as a 5-layer elastic system as shown in Fig. 22. Results of the analyses are shown in Tables 3 and 4.

Table 3 summarizes the deflections obtained in December 1971 when the air temperature was estimated to be about 60°F (15°C). Stiffness moduli for the asphalt concrete surface and base were estimated to be in the range 600,000 to 700,000 psi (4,150-4,900 MN/m^2). Comparison of the computed deflections with the measured values indicates that the system can be modeled so long as appropriate stiffness values are selected. Interestingly, the LVDT's show a slight increase in deflection below the pavement surface, the same as that indicated by the computations.

Similar data are contained in Table 4 for measurements taken in June 1972 when the air temperature was estimated to be about 120°F (49°C). Comparisons between measured and computed values indicate the reasonableness of the elastic analysis so long as appropriate stiffness values are used.

A few analyses were also made for strain distributions when the pavement was loaded at an elevated temperature; these results are shown in Figs. 25 and 26. For this analysis the BISTRO program (21) was used to analyze the pavement configuration shown in Fig. 23. This computed program permits examination up to 10 layers; in this case the large number was considered desirable in order to model the stiffness characteristics of the asphalt concrete in the upper portion of the pavement due to a steep temperature gradient, Fig. 24.

For these conditions it will be noted that large tensile strains occur in the upper part of the pavement section. As discussed earlier, strains of this magnitude could lead to cracking at the surface. Unfortunately, strain measurements were not available for comparison with these analyses.

Summary

With the data presented in this section it is possible to develop analyses for the response of the Indio pavement to traffic loading. It must be emphasized that appropriate stiffness values must be used and that if results

ClibPDF - www.fastio.com

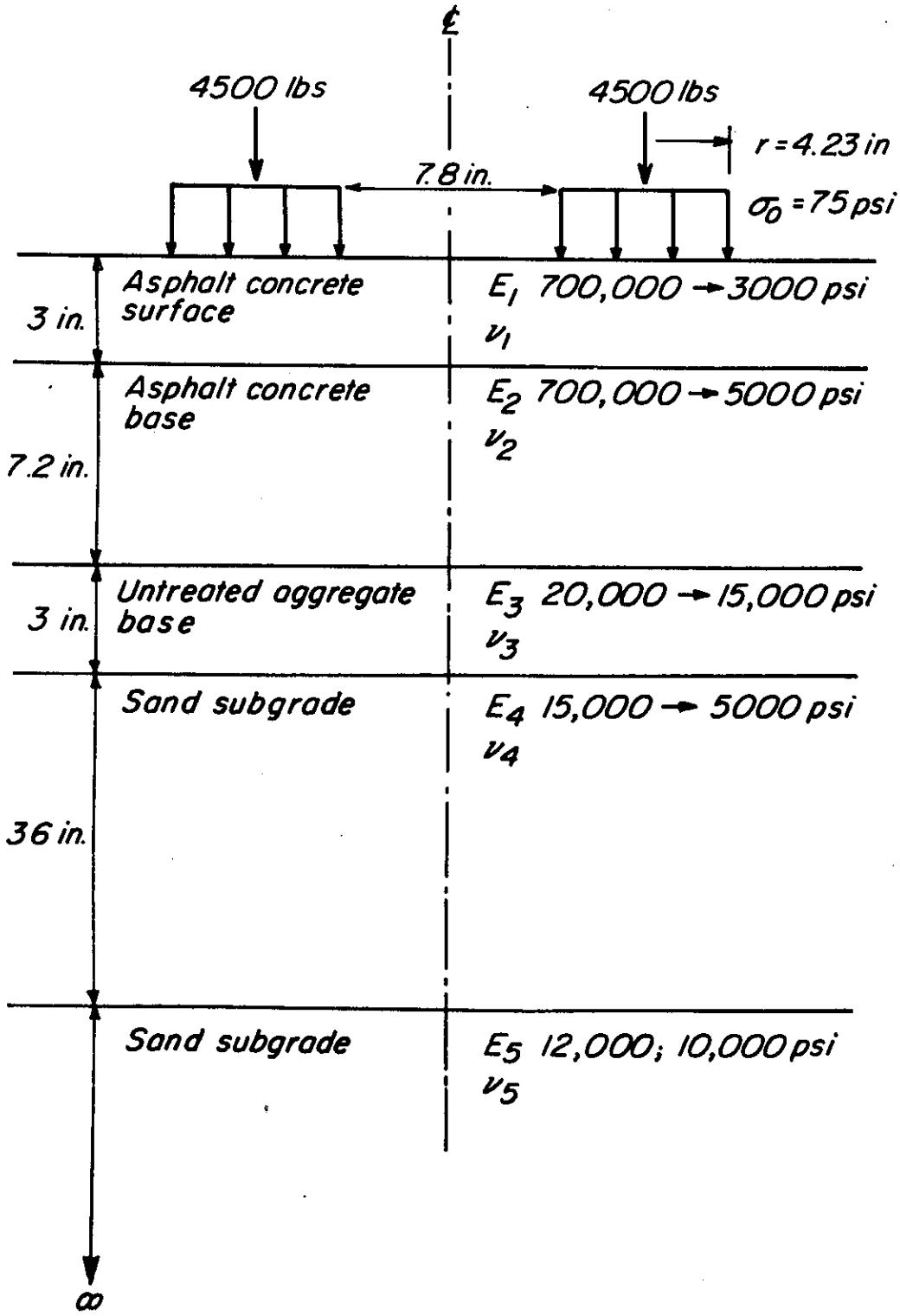

Fig. 22 - Representation of Indio pavement section for pavement analyses.

ClibPDF - www.fastio.com

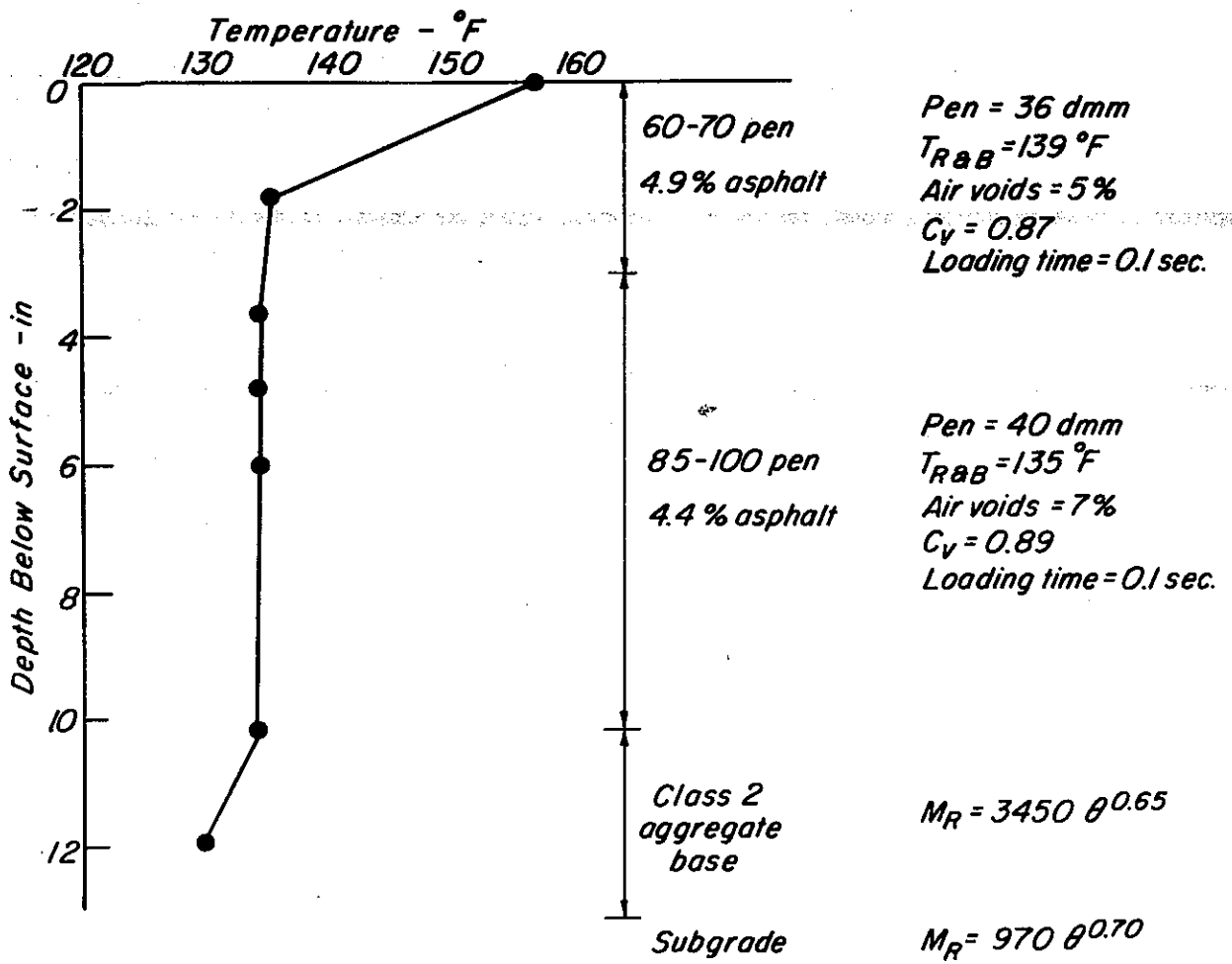

Fig. 23 - Pavement representation for use in BISTRO program.

ClibPDF - www.fastio.com

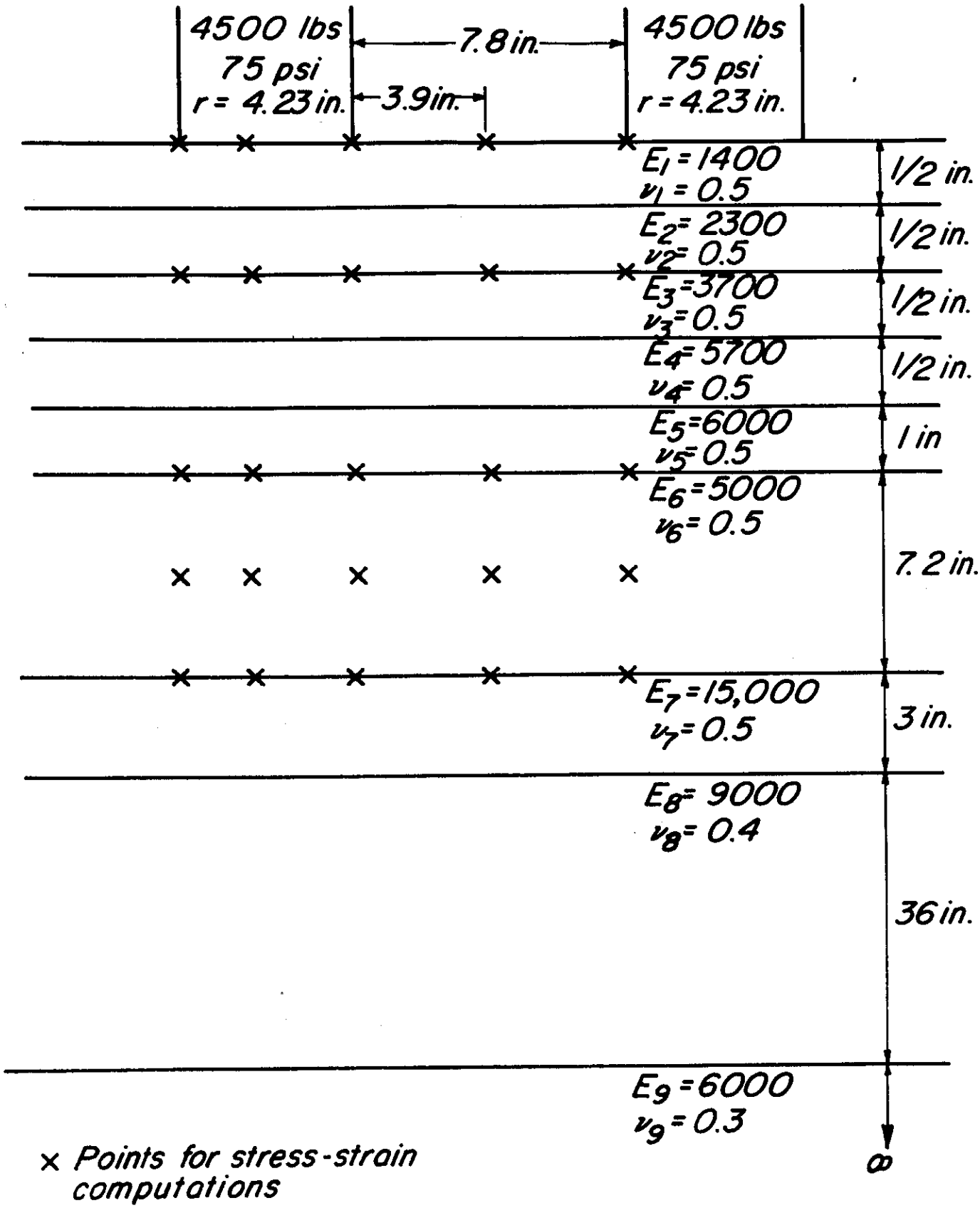

Fig. 24 - Pavement temperature profile and mix characteristics used in analysis.

ClibPDF - www.fastio.com

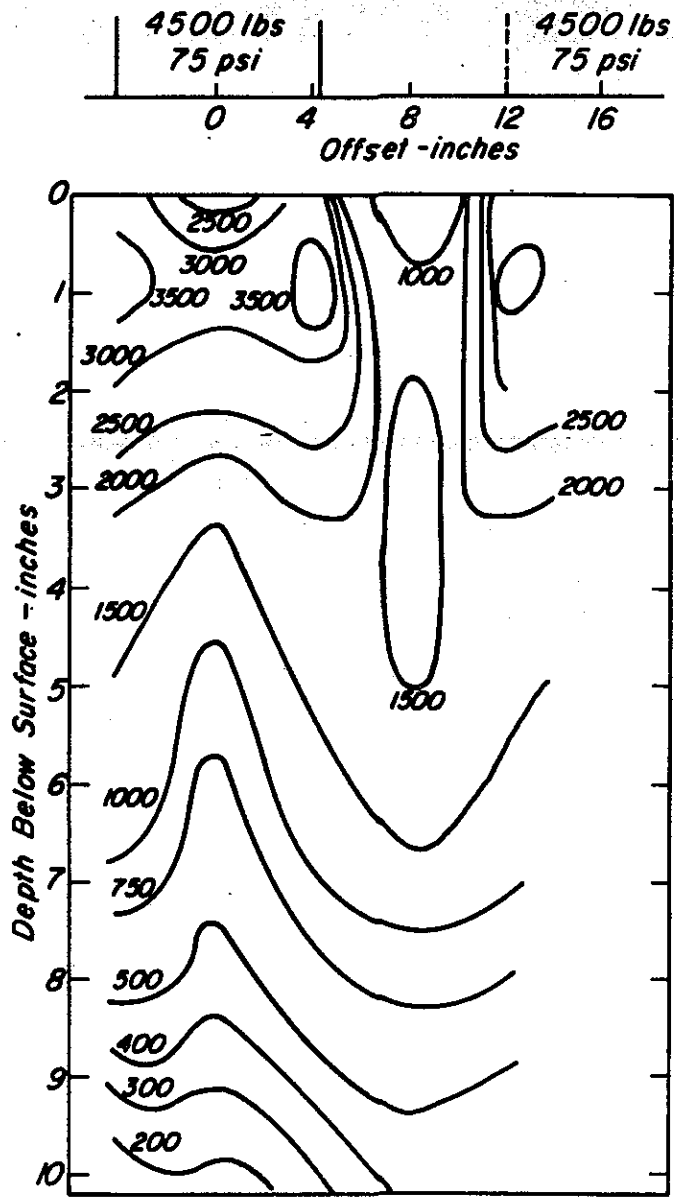

Fig. 25 - Computed strains on horizontal planes - xx direction parallel to traffic. All values are tensile Shell 10 layer program.

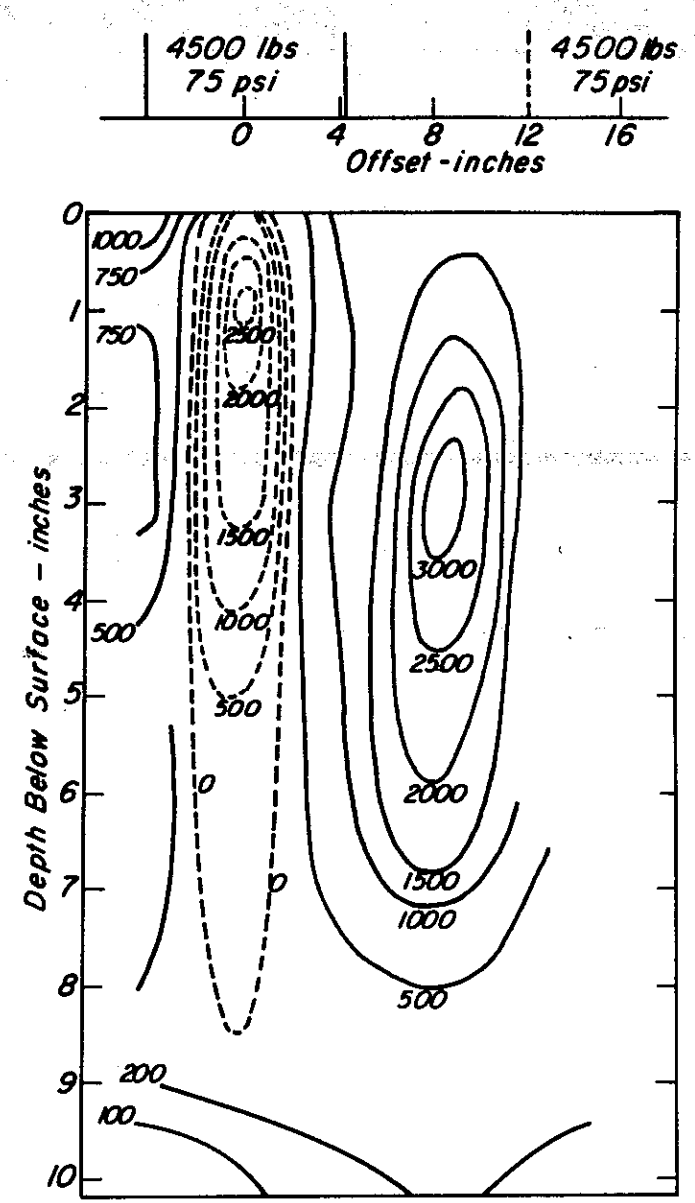

Fig. 26 - Computed strains on horizontal planes - yy direction transverse to traffic solid lines - compressive; dashed lines - tension. Shell 10 layer program.

ClibPDF - www.fastio.com

TABLE 3 - COMPARISON OF MEASURED AND COMPUTED DEFLECTIONS IN DECEMBER*

Depth - in. Measured From Top of Asphalt Concrete	Computed Deflection - in.				Measured Deflection LVDT's - in.	Measured Deflection Traveling Deflectometer - in.
	E_1 = 700,000 psi**	600,000 psi	700,000 psi	700,000 psi		
	E_2 = 700,000 psi	600,000 psi	700,000 psi	700,000 psi		
	E_3 = 20,000 psi	20,000 psi	20,000 psi	20,000 psi		
	E_4 = 15,000 psi	13,000 psi	13,000 psi	15,000 psi		
	E_5 = 12,000 psi	10,000 psi	10,000 psi	10,000 psi**		
0	.0089***	.0105	.0101	.0097	.007	0.009
3.2	.0092	.0107	.0103	.0099	.008	
5.5	.0092	.0108	.0103	.0099	.007	
7.8	.0091	.0107	.0103	.0099	.005	
11.4	.0088	.0104	.0099	.0096		
11.7	.0088	.0103	.0099	.0095		
31.2	.0065	.0076	.0074	.0072		

*Temperature approximately 60°F

** 4,900 to 70 MN/m^2

***To change deflections in inches to deflection in mm, multiply the values shown by 25.4 (e.g. 0.009 in. = 2.29 mm)

ClibPDF - www.fastio.com

TABLE 4 - COMPARISON OF MEASURED AND COMPUTED DEFLECTIONS IN JUNE*

Depth - in. Measured from Top of Asphalt Concrete	Computed Deflection - in.							Measured Deflection LVDT's - in.	Measured Deflection Traveling Deflectometer - in.
	E_1 = 15,000 psi	15,000	15,000	3,000**	15,000	3,000	5,000		
	E_2 = 15,000 psi	13,000	13,000	5,000	13,000	5,000	7,000		
	E_3 = 20,000 psi**	20,000	15,000	20,000	15,000	15,000	15,000		
	E_4 = 13,000 psi	10,000	5,000	10,000	9,000	9,000	9,000		
	E_5 = 10,000 psi	10,000	10,000	10,000	10,000	10,000	10,000		
0	.0209	.0247	.0372	.0232	.0270	.0259	.0268	.021	.011
3.2	.0222	.0260	.0394	.0276	.0285	.0304	.0298	.024	
5.5	.0225	.0264	.0399	.0284	.0289	.0312	.0305	.020	
7.8	.0220	.0258	.0392	.0273	.0281	.0300	.0295	.018	
11.4	.0203	.0239	.0366	.0256	.0259	.0274	.0271		
11.7	.0201	.0238	.0363	.0251	.0256	-	.0268		
31.2	.0110	.0123	.0165	.0126	.0128	-	.0131		

*Temperature approximately 120°F (50°C)

**(140 to 21 MN/m^2)

***To change deflections in inches to deflection in mm, multiply the values shown by 25.4 (e.g. 0.009 in. = 2.29 mm)

ClibPDF - www.fastio.com

such as strains under high temperature conditions are to be examined, care must be given to selection of an appropriate model for the pavement. For the limited data available, the analyses appear to provide "reasonable" estimates of pavement response even at elevated temperatures.

BLYTHE PROJECT

This project is the second of two constructed in the desert area of Southern California by CALTRANS to study the response of thick lift asphalt concrete pavements to traffic loading and to assess the validity of the analysis procedures developed in this program. While analyses were directed primarily to estimations of stress, strain and deflection for the Indio project, an attempt has been for the Blythe project to assess its service life -- in this case as measured by cracking from repetitive traffic loading.

This portion of the report describes the test and analysis program together with service life estimates for the two Blythe pavement sections, cross sections for which are shown in Figs. 27a and 27b. Test Section A consists of 0.80 ft (~ 10 in.) (250 mm) of asphalt concrete resting directly on the sandy subgrade while Test Section B contains 1.5 ft. (455 mm) of asphalt concrete on the sandy subgrade. These figures also illustrated the location of instrumentation; no comparisons between predicted and measured response have been included in the report.

Materials and Specimen Preparation

Laboratory prepared specimens for both the asphalt concrete and subgrade soil were used to define the material response to load.

Asphalt Concrete. The aggregate for the asphalt concrete was obtained from the project stockpiles. This material was separated into individual size fractions and recombined as shown in Fig. 28 to meet the State of California specifications. An 85-100 pen. asphalt cement representative of materials used on the project was supplied by the Chevron Asphalt Company.

ClibPDF - www.fastio.com

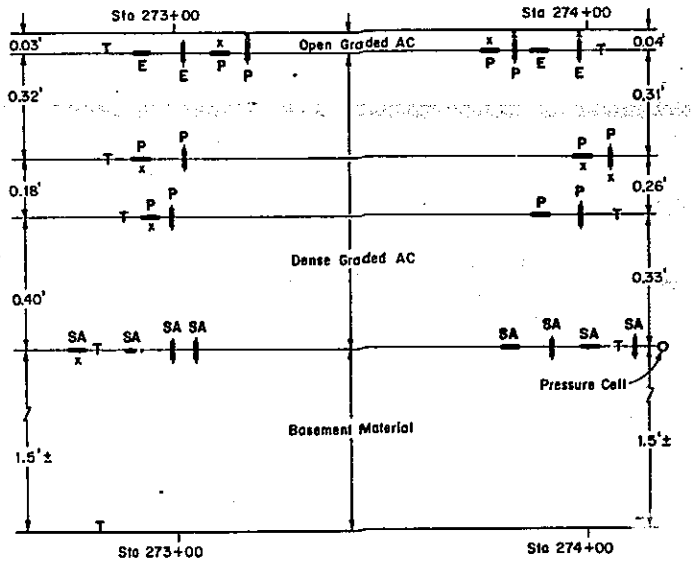

Lift thicknesses shown were determined from cores.
| = Strain gauges placed transversely.
— = Strain gauges placed longitudinally.
T = Thermocouple.
SA = Strain gauge adhered to sand asphalt carriers.
P = Strain gauge adhered to polymide sheets.
E = Strain gauge epoxied to pavement.
x = Inoperative strain gauge

a. Test Section A

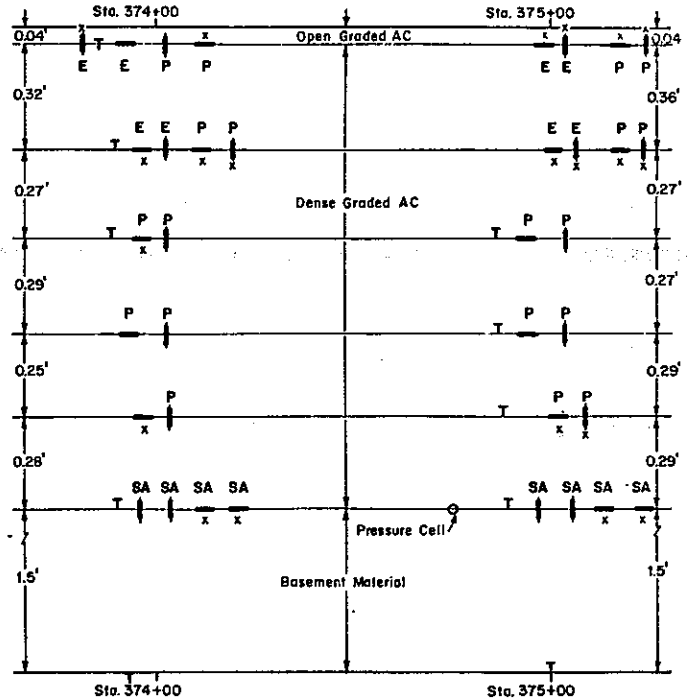

Lift thicknesses shown were determined from cores.
| = Strain gauges placed transversely.
— = Strain gauges placed longitudinally.
T = Thermocouple.
SA = Strain gauge adhered to sand asphalt carriers.
P = Strain gauge adhered to polymide sheets.
E = Strain gauge epoxied to pavement.
x = Inoperative strain gauge

b. Test Section B

Fig. 27 - Blythe pavement sections including instrumentation.

ClibPDF - www.fastio.com

From an analysis of field test data, beam specimens of asphalt concrete were prepared using the Triaxial Institute Kneading Compactor. To obtain an air void content of about 6 percent at an asphalt content of 4.75 percent (i.e., the field conditions) the following procedure was utilized (similar to that reported earlier (1)).

Compaction schedule:	Layer	No. of tamps	Compaction Pressure - psi	(KN/m^2)
	1	20	145	(1,000)
		25	375	(2,700)
	2	20	145	(1,000)
		35	375	(2,700)
	3	20	145	(1,000)
		50	375	(2,700)

Leveling pressure: 375 psi; applied at rate of 0.25 in. min per.

Subgrade. The subgrade was a sandy material. Data for modulus vs. confining stress and modulus vs. the sum of principal stresses are shown in Figs. 29 and 30. There appears to be a slight effect of both water content and dry density on the resilient modulus.

Fatigue Testing

Both controlled-stress and controlled-strain fatigue tests using procedures reported earlier (1) were made on the laboratory prepared beam specimens. Because of the high temperatures encountered at Blythe, it was believed desirable to include the controlled-strain tests since it is possible that this condition might be approached at very low stiffnesses (high temperatures).

Controlled-stress Tests. Controlled-stress tests were performed at 68°F (20°C) at three stress levels -- 75, 100, and 150 psi (520 to 1,040 KN/m^2) Initial strains were determined from flexural stiffnesses using deflections corresponding to 200 stress repetitions. Test results of initial strain vs. stress applications to

ClibPDF - www.fastio.com

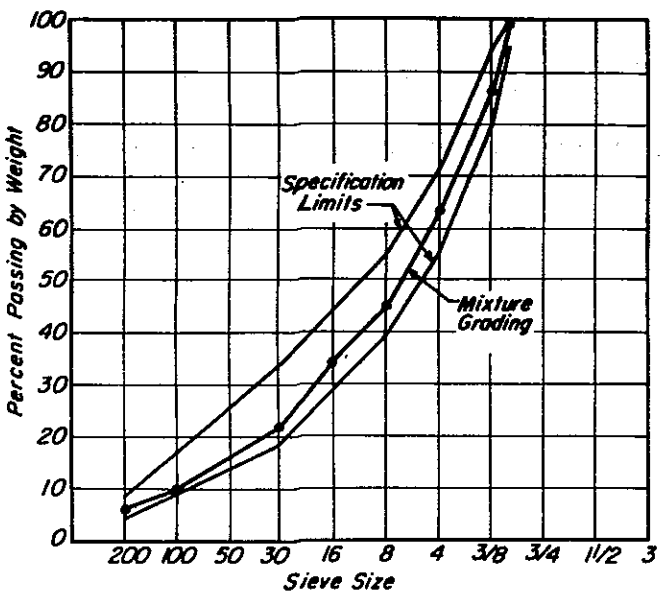

Fig. 28 - Aggregate gradation Blythe asphalt paving mixture.

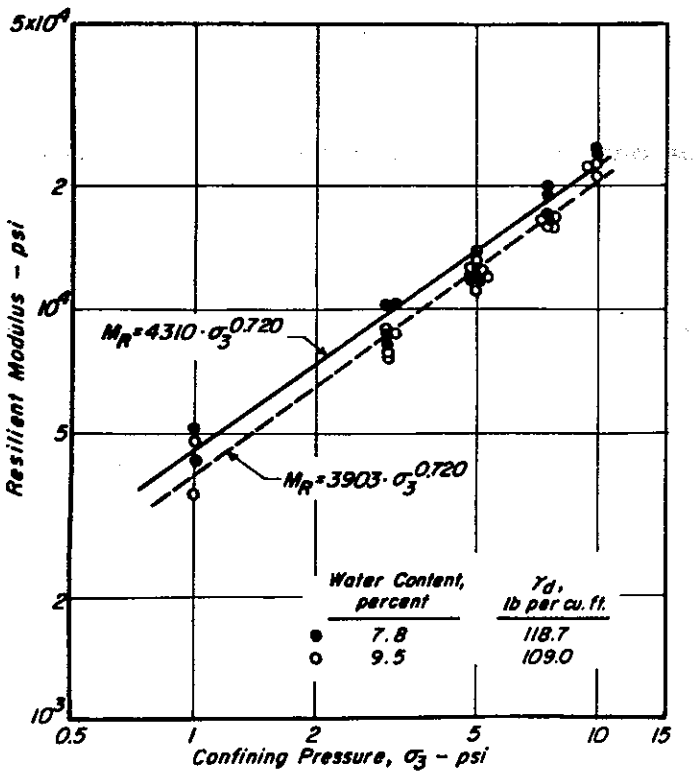

Fig. 29 - Resilient modulus vs. confining pressure relationships, Blythe subgrade.

ClibPDF - www.fastio.com

fracture, N_f, are shown in Fig. 31. The regression equation:

$$N_f = 4.68 \times 10^{-10} \left(\frac{1}{\varepsilon}\right)^{3.73} \tag{6}$$

when compared to that developed in TE 70-5 (1) for a number of mixes designed according to the State of California procedure exhibits a flatter slope and is displaced to the left of the general curve. For the asphalt content and void content for this particular mixture, however, the data appears reasonable. The basis for this comment has been discussed earlier.

Controlled-strain Tests. Controlled-strain tests were performed at both 68° (20°C) and 90°F (32°C). Services lives in these tests were defined as the number of stress applications corresponding to a 50 percent reduction in flexural stiffness. Test results together with the resulting regression equations are shown in Fig. 32; equations for the test results are:

$$\text{At } 68°\text{F:} \quad N_s = 1.83 \times 10^{-6} \left(\frac{1}{\varepsilon}\right)^{2.97} \tag{7}$$

$$\text{At } 90°\text{F:} \quad N_s = 9.8 \times 10^{-8} \left(\frac{1}{\varepsilon}\right)^{3.54} \tag{8}$$

Fig. 33 contains a comparison between the controlled-stress and controlled-strain fatigue data.

Fatigue Life Determination

Both pavement sections have been analyzed according to the flow diagrams of Fig. 1 and results will be presented in that format.

Environment and Traffic Data (Inputs). Climatic data required to estimate pavement temperatures are summarized in Table 5. The temperatures represent a 12-year average for the period 1961-72.

Truck traffic data used in the analysis were furnished by CALTRANS from a 1971 truck traffic count at Lovekin Bl. in Blythe (PM 152.98); the observed average daily truck traffic are summarized in Table 6.

ClibPDF - www.fastio.com

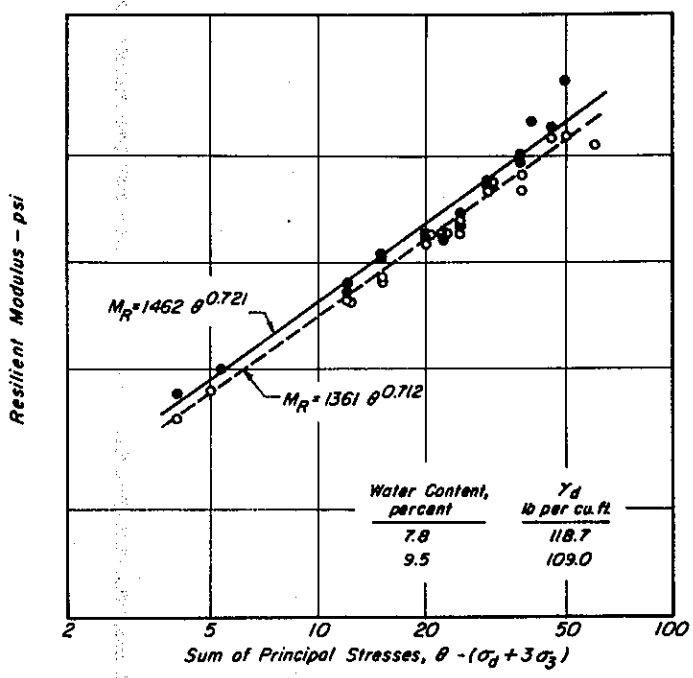

Fig. 30 - Resilient modulus vs. sum of principal stress relationships, Blythe subgrade.

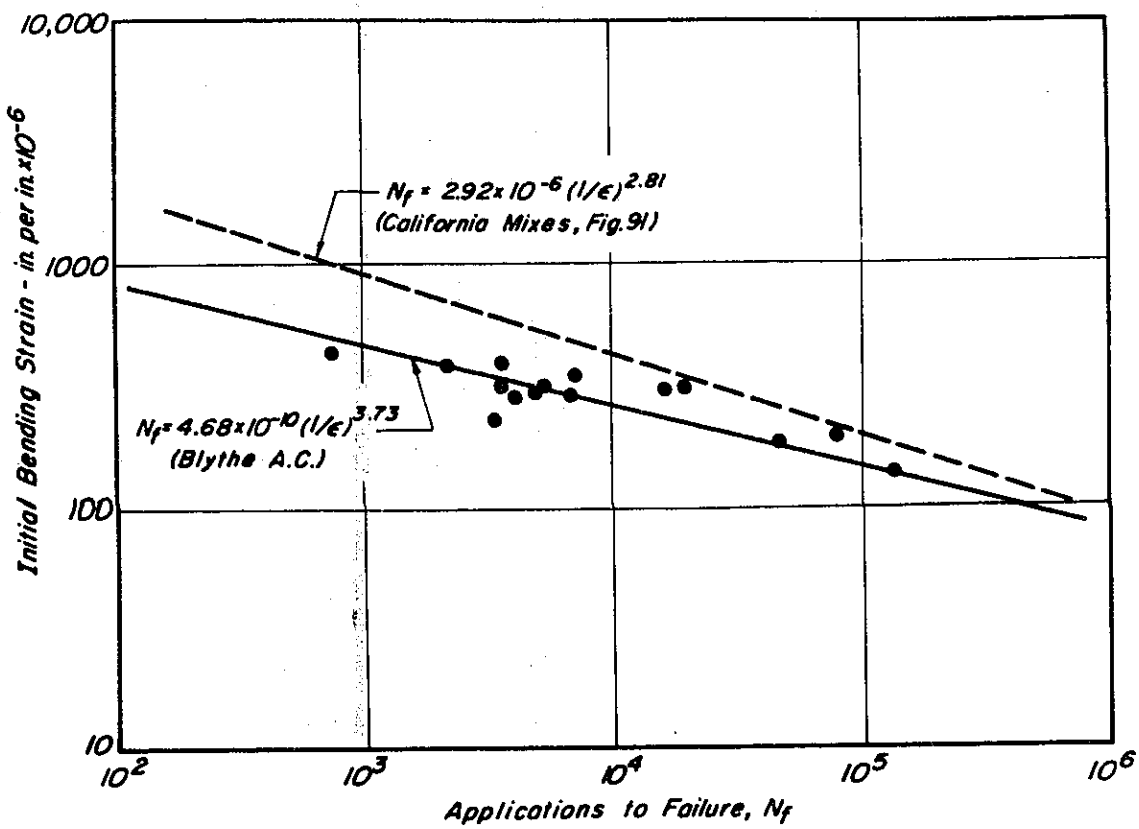

Fig. 31 - Comparison of fatigue response of laboratory prepared specimens with regression analysis for data from all California-type mixes tested.

ClibPDF - www.fastio.com

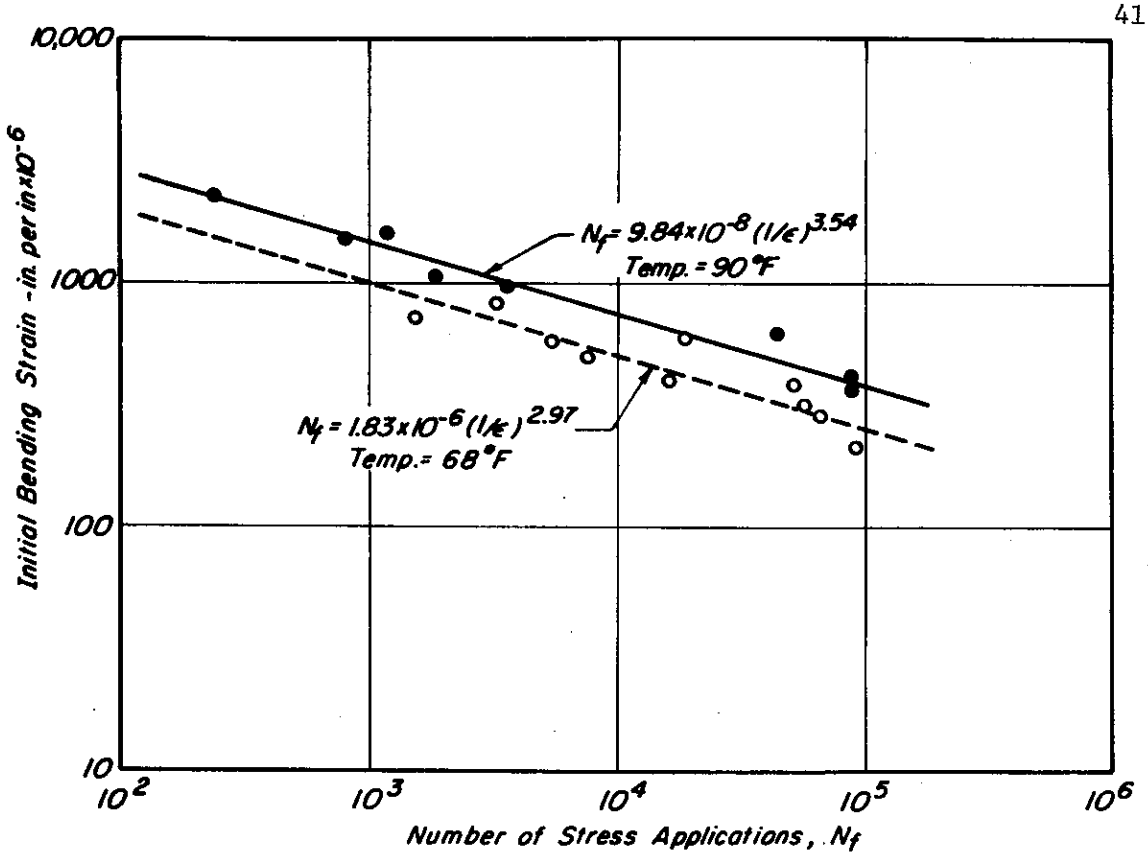

Fig. 32 - Controlled strain fatigue data, 68° and 90°F.

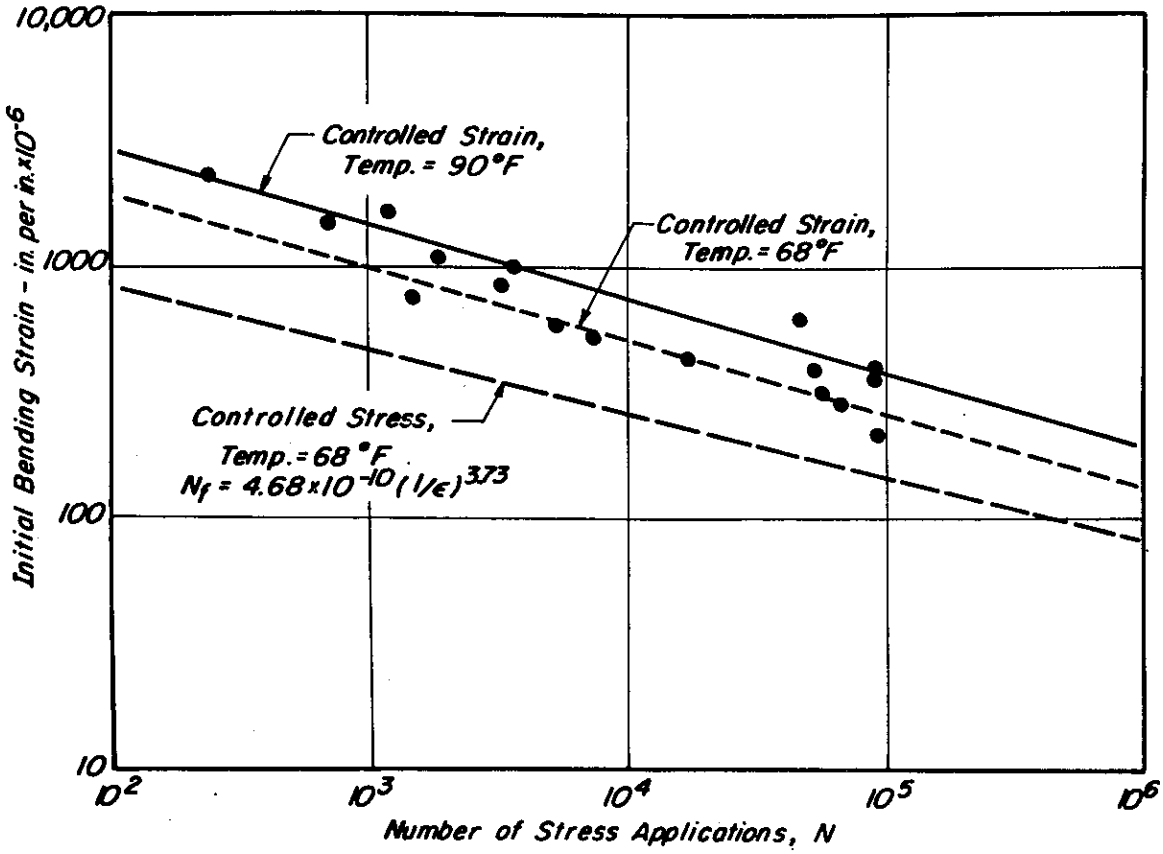

Fig. 33 - Comparison of controlled stress and controlled strain fatigue data, Blythe asphalt paving mixtures.

ClibPDF - www.fastio.com

TABLE 5 - CLIMATIC DATA, BLYTHE, CALIFORNIA

Month	Average* Air Temperature °F	Daily* Air Temperature Range °F	Average Wind Velocity mph	Insolation	Sky Cover
Jan.	52.7	26.2	7.0	305	4.9
Feb.	58.6	27.1	8.0	405	3.4
March	63.6	28.8	8.0	515	3.5
April	70.4	29.8	9.0	610	2.8
May	79.1	30.8	9.0	700	2.3
June	87.5	31.1	9.0	720	1.5
July	95.6	26.7	10.0	670	2.8
Aug.	94.4	24.9	9.0	650	2.5
Sept.	86.7	27.4	7.0	560	1.5
Oct.	74.8	28.1	7.0	430	1.5
Nov.	62.0	25.8	7.0	325	2.8
Dec.	52.5	24.3	6.0	270	3.8

*average - 12 year period, 1961-1972.

TABLE 6 - TRUCK TRAFFIC DATA - BLYTHE, CALIFORNIA, 1971

Classification	ADTT	
	Number	Percent
2 axle	387	35.0
3 axle	107	9.7
4 axle	53	4.8
5 or more axles*	558	50.5
	1,407	100.0

*From TE 70-5 (1) an estimate was obtained for breakdown between 5 and 6 axle vehicles; in this case the 50.5 percent value was distributed 31.5 percent to 5 axle and 19.0 percent to 6 axle vehicles.

ClibPDF - www.fastio.com

The Blythe pavement was opened to traffic in October 1973. To arrive at the ADTT using the facility at this time, the data of Table 6 were increased, assuming the rate of growth for traffic in this area to be 3 percent per year.

Traffic distribution throughout the day was assumed to vary in the manner repeated earlier (1) and as shown in Table 7. To relate the axle load groups to operations in each classification, the data of Table 8 were utilized; these factors were determined from the W-4 loadometer studies by the Transportation Laboratory Staff for the 1969-72 period.

Stiffness Characteristics of Asphalt Concrete. To estimate the stiffness characteristics of the asphalt concrete in the two pavement sections, the Shell procedure was utilized*.

Tests on recovered asphalt from the pavement cores were performed by the staff of the Transportation Laboratory. Table 9 contains a summary of asphalt characteristics as well as other data obtained from tests in the cores.

Average reported thermal characteristics (in English inches) were used for this mix, i.e.:

thermal conductivity = 0.70 (0.12 watt/meter - K)

specific heat capacity = 0.20 (0.8 joule/Kg/K)

surface coefficient = 0.95

to permit solution of the heat conduction equation (1) to in turn estimate temperature profiles for a range in conditions.

A time of loading of 0.02 sec was assumed to be representative for moving traffic at this location.

Using the computer program TEMPS 2 (1) the average stiffnesses for each

*Measured values from the fatigue tests provided comparative values at 0.1 sec loading time and at a temperature of 68°F (20°C).

ClibPDF - www.fastio.com

TABLE 7 - ANNUAL AVERAGE DAILY TRUCK TRAFFIC, STATEWIDE SURVEY-1967

	Hour	Percent Traffic		Hour	Percent Traffic
P.M.	12-1	2.8	P.M.	12-1	5.2
	1-2	2.7		1-2	5.6
	2-3	2.9		2-3	5.7
	3-4	3.1		3-4	5.7
	4-5	3.5		4-5	5.4
	5-6	4.1		5-6	4.5
	6-7	4.2		6-7	3.8
	7-8	4.3		7-8	3.5
	8-9	4.8		8-9	3.3
	9-10	5.0		9-10	3.2
	10-11	5.2		10-11	3.3
	11-12	5.2		11-12	3.0

TABLE 8 - MONTHLY WHEEL LOAD FACTORS BASED ON W-4 LOADOMETER STUDIES
CALIFORNIA - 1969-1972

Axle Load (Kips)	2-Axle	3-Axle	4-Axle	5-Axle	6 or More Axles
Under 3	8.828	0.407	1.140	0.726	1.552
3-6.999	16.029	16.869	20.107	17.222	21.568
7-7.999	1.445	6.613	7.780	5.886	7.168
8-11.999	2.481	13.094	20.994	19.204	32.948
12-15.999	0.879	6.195	7.327	17.525	19.145
16-16.250	0.057	0.415	0.621	2.830	1.423
16.251-17.999	0.169	1.006	1.433	9.093	4.101
18-18.5	0.049	0.232	0.341	1.422	0.516
18.501-19.999	0.048	0.163	0.330	0.593	0.486
20-21.999	0.012	0.049	0.049	0.126	0.661
22-23.999	0.004	0.011	0	0.052	0.685
24-25.99	0.001	0.006	0	0.035	0.338
26-29.999	0.001	0.021	0	0.018	0.081
30 or over	0	0	0	0.005	0

ClibPDF - www.fastio.com

TABLE 9 - IN-SITU CHARACTERISTICS OF ASPHALT CONCRETE IN BLYTHE PAVEMENT

Recovered asphalt penetration, dmm 77°F, 5 sec, 100 gr	41
Ring and Ball Softening Point, °F	122 (50°C)
Unit Weight of Mixture, lb per cu ft	155 (2423 Kg/m^3)
Percent Air Voids	6.0
Volume Concentration of Aggregate, C_v	0.85

ClibPDF - www.fastio.com

hour in a representative day for each month of the year (Table 5) are determined. These values were then grouped to obtain the frequency matrices shown in Table 10 for the 0.8 ft (244 mm) section and in Table 11 for the 1.50 ft (457 mm) section.

Structural Analysis. Using the ELSYM 5 program together with the stiffness moduli shown in Tables 10 and 11, a representative subgrade stiffness (resilient modulus) of 25,000 psi (173 MN/m^2), and a range in axle loads, tensile strains on the undersides of both pavement sections were computed. Results of these computations are summarized in Tables 12 and 13.

As a part of the analyses, mode factors (1) were also determined. While both sections can be considered as relatively thick, because of the low stiffnesses resulting from the high temperatures, it is possible that for a considerable portion of the year, mode-factors intermediate between the controlled-stress and controlled-strain values will be obtained. Moreover, even in the 1.5 ft. (457 mm) section the controlled strain mode might be approach for the condition of low stiffness and heavy load. This point is illustrated in Fig. 34.

An examination of the influence of the magnitude of stiffness reduction on the mode factor was made since this assumption might influence the result of analysis. Stiffness reductions of 20, 25, and 40 percent were used in the computational process. Table 14 summarizes these results for selected axle loads. As noted in this table, for the range of stiffnesses considered, there is little influence of the amount of stiffness reduction on mode factor. For the fatigue analysis reported subsequently, a 40 percent reduction was used.

Fatigue Analysis. In an earlier section it was indicated that the actual number of repetitions associated with cracking will be larger than the number estimated from laboratory controlled-stress tests, in part due to differences in crack propagation in the actual pavement as compared to laboratory specimens.

One alternative is to shift the laboratory determined curves by some factor

ClibPDF - www.fastio.com

TABLE 10 - FREQUENCY OF OCCURRENCE OF PAVEMENT STIFFNESS
10.2 IN BLYTHE PROJECT PAVEMENT ANALYSIS

TIME	STIFFNESS GROUP, psi*							
	$1.2-1.0\times10^6$	$1.0\times10^6-6.0\times10^5$	$6.0-4.0\times10^5$	$4.0-2.0\times10^5$	$2.0\times10^5-8.0\times10^4$	$8.0-4.0\times10^4$	$4.0-3.0\times10^4$	$3.0-2.0\times10^4$
	MIDPOINT STIFFNESS, psi							
	1.1×10^6	8.0×10^5	5.0×10^5	3.0×10^5	1.4×10^5	6.0×10^4	3.5×10^4	2.5×10^4
Morning								
12- 1	1	2	1	1	2	1	1	3
1- 2	1	2	1	1	2	1	1	3
2- 3	2	1	1	1	2	1	2	2
3- 4	2	1	2	0	2	1	2	2
4- 5	2	1	2	1	2	1	1	2
5- 6	2	2	1	1	2	1	1	2
6- 7	2	2	1	1	2	1	1	2
7- 8	2	2	1	1	2	2	1	1
8- 9	2	2	1	1	2	2	1	1
9-10	2	2	1	1	2	2	1	1
10-11	2	2	1	1	2	2	1	1
11-12	2	2	1	1	2	2	1	1
Afternoon								
12- 1	2	2	1	1	2	2	1	1
1- 2	2	2	1	1	2	2	1	1
2- 3	2	2	1	1	2	2	1	1
3- 4	2	2	1	1	2	2	1	1
4- 5	2	2	1	1	2	1	1	2
5- 6	2	2	1	1	2	1	1	2
6- 7	2	2	1	1	2	1	1	2
7- 8	2	1	2	1	1	2	1	2
8- 9	2	1	2	0	2	1	2	2
9-10	2	1	1	1	2	1	2	2
10-11	1	2	1	1	2	1	1	3
11-12	1	2	1	1	2	1	1	3

*8,250 to 170 MN/m^2

ClibPDF - www.fastio.com

TABLE 11 - FREQUENCY OF OCCURRENCE OF PAVEMENT STIFFNESS
18 IN. BLYTHE PROJECT PAVEMENT ANALYSIS

TIME	STIFFNESS GROUP, psi*							
	$1.2-1.0\times10^6$	$1.0\times10^6-6.0\times10^5$	$6.0-4.0\times10^5$	$4.0-2.0\times10^5$	$2.0\times10^5-8.0\times10^4$	$8.0-4.0\times10^4$	$4.0-3.0\times10^4$	$3.0-2.0\times10^4$
	MIDPOINT STIFFNESS, psi							
	1.1×10^6	8.0×10^5	5.0×10^5	3.0×10^5	1.4×10^5	6.0×10^4	3.5×10^4	2.5×10^4
Morning								
12- 1	2	2	1	1	2	1	1	2
1- 2	2	2	1	1	2	1	1	2
2- 3	2	2	1	1	2	1	1	2
3- 4	2	2	1	1	2	1	1	2
4- 5	2	2	1	1	2	1	1	2
5- 6	2	2	1	1	2	1	1	2
6- 7	2	2	1	1	2	1	1	2
7- 8	2	2	1	1	2	1	1	2
8- 9	2	2	1	1	2	1	1	2
9-10	2	2	1	1	2	1	1	2
10-11	2	2	1	1	2	1	1	2
11-12	2	2	1	1	2	1	1	2
Afternoon								
12- 1	2	2	1	1	2	1	1	2
1- 2	2	2	1	1	2	1	1	2
2- 3	2	2	1	1	2	1	1	2
3- 4	2	2	1	1	2	1	1	2
4- 5	2	2	1	1	2	1	1	2
5- 6	2	2	1	1	2	1	1	2
6- 7	2	2	1	1	2	1	1	2
7- 8	2	2	1	1	2	1	1	2
8- 9	2	2	1	1	2	1	1	2
9-10	2	2	1	1	2	1	1	2
10-11	2	2	1	1	2	1	1	2
11-12	2	2	1	1	2	1	1	2

*8,250 to 170 MN/m^2

ClibPDF - www.fastio.com

TABLE 12 - STRAIN ON UNDERSIDE OF ASPHALT CONCRETE AS A FUNCTION OF ASPHALT CONCRETE STIFFNESS - 0.8 FT. (244 MM) PAVEMENT: IN. PER IN. × 10^{-4}

Asphalt Concrete Stiffness - psi* / Wheel load - lbs.	1.1×10^6	8.0×10^5	5.0×10^5	3.0×10^5	1.4×10^5	6.0×10^4	3.5×10^4	2.5×10^4
750	.1094	.1398	.2032	.2997	.5028	.7903	.976	1.081
1,250	.1740	.2260	.3279	.4786	.7868	1.218	1.495	1.652
1,875	.2522	.3263	.4691	.6771	1.098	1.684	2.058	2.267
2,500	.3224	.4145	.5902	.8441	1.356	2.059	2.503	2.749
3,500	.4256	.5435	.7668	1.088	1.729	2.596	3.132	3.425
4,250	.4938	.6279	.8814	1.244	1.963	2.918	3.502	3.818
4,750	.5358	.6798	.9515	1.339	2.102	3.106	3.713	4.041
5,250	.5761	.7295	1.018	1.430	2.233	3.280	3.908	4.245
5,750	.6146	.7770	1.082	1.515	2.355	3.441	4.086	4.431
6,250	.6506	.8211	1.141	1.593	2.465	3.580	4.237	4.586
7,000	.7028	.8853	1.226	1.706	2.621	3.777	4.450	4.818
8,125	.7752	.9737	1.343	1.857	2.825	4.042	4.799	5.208

TABLE 13 - STRAIN ON UNDERSIDE OF ASPHALT CONCRETE AS A FUNCTION OF ASPHALT CONCRETE STIFFNESS - 1.5 FT (457 MM) PAVEMENT; IN. PER IN. × 10^{-4}

Asphalt Concrete Stiffness - psi* / Wheel load - lbs.	1.1×10^6	8.0×10^5	5.0×10^5	3.0×10^5	1.4×10^5	6.0×10^4	3.5×10^4	2.5×10^4
750	.04054	.05079	.07052	.1003	.1661	.2674	.3364	.3761
1,250	.06159	.07824	.1115	.1631	.2759	.4424	.5515	.6130
1,875	.08843	.1137	.1645	.2425	.4093	.6485	.8031	.8903
2,500	.1150	.1490	.2168	.3195	.5342	.8371	1.033	1.143
3,500	.1578	.2049	.2980	.4366	.7215	1.121	1.378	1.523
4,250	.1890	.2454	.3557	.5184	.8504	1.314	1.613	1.781
4,750	.2093	.2715	.3926	.5702	.9316	1.436	1.760	1.941
5,250	.2293	.2971	.4284	.6204	1.010	1.553	1.901	2.096
5,750	.2488	.3220	.4632	.6689	1.086	1.665	2.036	2.243
6,250	.2678	.3460	.4965	.7152	1.158	1.771	2.163	2.381
7,000	.2956	.3812	.5450	.7825	1.262	1.925	2.346	2.580
8,125	.3354	.4311	.6136	.8772	1.408	2.138	2.597	2.852

*To obtain stiffness in MN/m^2 multiply values shown by 6.9×10^{-3}

ClibPDF - www.fastio.com

TABLE 14 - INFLUENCE OF STIFFNESS REDUCTION IN ASPHALT CONCRETE LAYER ON MODE FACTOR*

Axle Load - lb	Mode Factor					
	10.2 in. (259 mm) Pavement % Stiffness Reduction			18.0 in. (457 mm) Pavement % Stiffness Reduction		
	20	25	40	20	25	40
	Asphalt Concrete Stiffness - 500,000 psi (3,450 MN/m^2)					
14,000		-0.390	-0.390	-0.494	-0.500	-0.515
17,000		-0.344	-0.370	-0.478	-0.481	-0.496
19,000		-0.331	-0.358	-0.462	-0.468	-0.484
21,000	-0.31	-0.333	-0.357		-0.452	-0.472
	Asphalt Concrete Stiffness - 25,000 psi (173 MN/m^2)					
14,000		0.883	0.880	0.881	0.897	0.874
17,000	0.91	0.888	0.878	0.888	0.907	0.898
19,000		0.886	0.883	0.888	0.910	0.909
21,000		0.888	0.885	0.854	0.912	0.912

*Computations made for the subgrade modulus of 25,000 psi (173 MN/m^2)

ClibPDF - www.fastio.com

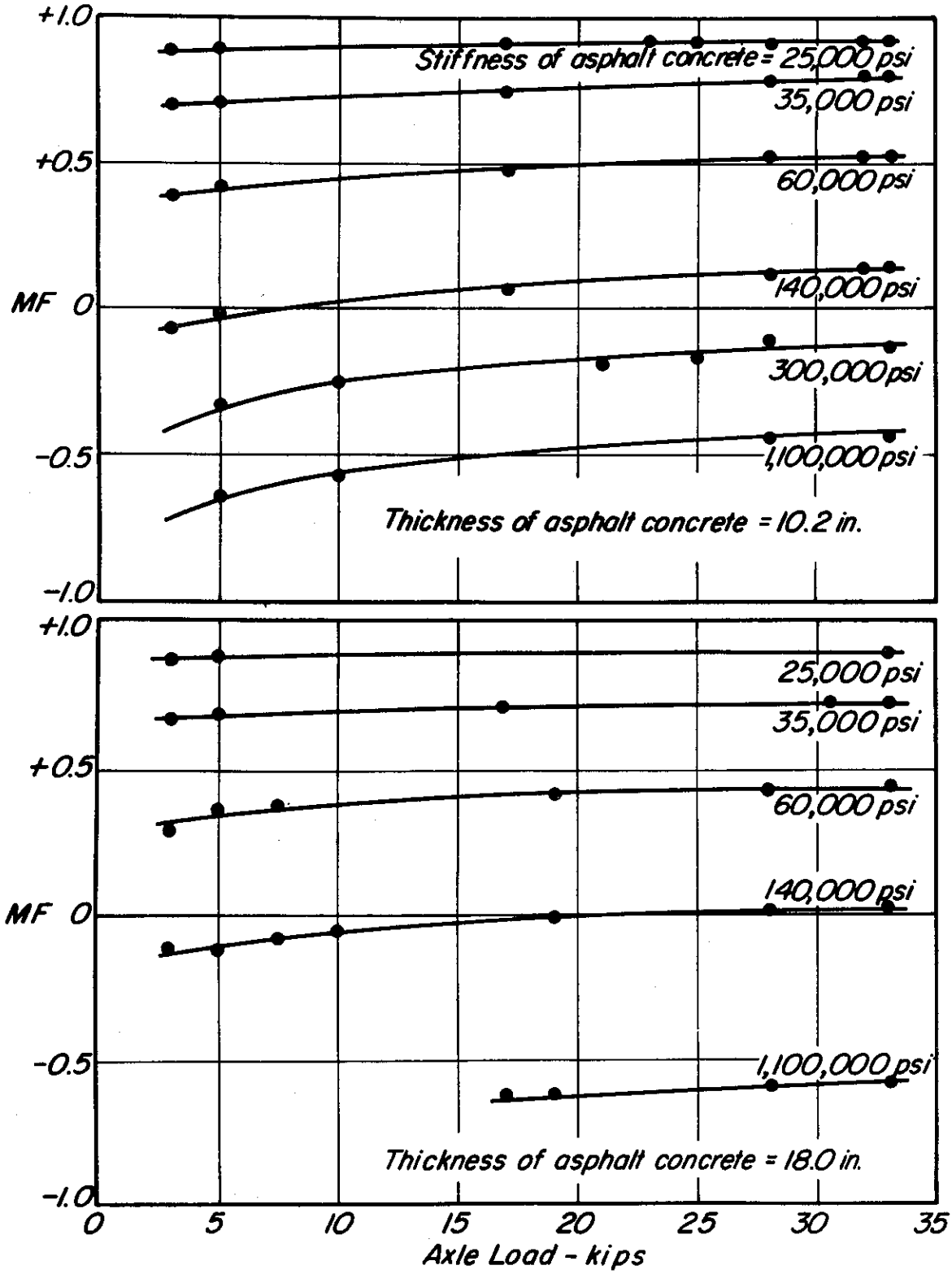

Fig. 34 - Mode factors, Blythe pavement sections.

ClibPDF - www.fastio.com

(e.g. 3, as was done by Santucci (7)). Alternatively both controlled-stress and controlled-strain tests could be performed and use made of the mode factor. This latter was the procedure followed for the Blythe project.

In Fig. 33 some difference in fatigue response between the two modes of loading is observed. At this temperature the mixture stiffness is about 300,000 psi (4,140 MN/m^2). From an examination of Tables 10 and 11 it will be noted stiffnesses as low as 25,000 psi (173 MN/m^2) have been estimated. At such low stiffnesses it is expected that the differences between controlled-stress and controlled-strain tests will be even larger than those occurring at 68°F (20°C). Since it is difficult to test mixes at such low stiffnesses with the equipment used to develop the fatigue data in all of the investigations thus far (1), it was necessary to prepare an estimate of the location of the controlled strain curves relative to the controlled stress curves. Data developed for the Folsom project (1) as well as the data developed in this study were used to prepare the estimates.

A schematic diagram of the procedure is shown in Fig. 35. At high stiffncesses (or 1×10^6 psi (6,900 MN/m^2)) it is assumed that there will be no difference in fatigue response between the two modes of loading. As the stiffness decreases, the difference will increase as seen in Fig. 35.

For a particular stiffness it is possibly using this approach to estimate the controlled-strain curve from the controlled-stress relationship. While controlled-stress tests were only performed at 68°F (20°C), the data presented in earlier reports (1) permitted estimation of the relationships at other temperatures.

With curves so constructed and mode factor estimates like those made for the Indio project, the applications to failure for the various loads and stiffnesses were estimated and are summarized in Tables 15 and 16 . These data provided the necessary input to ascertain when the pavements would exhibit distress using the linear summation of cycle ratios cumulative damage hypothesis (PROGRAM FATIG2).

ClibPDF - www.fastio.com

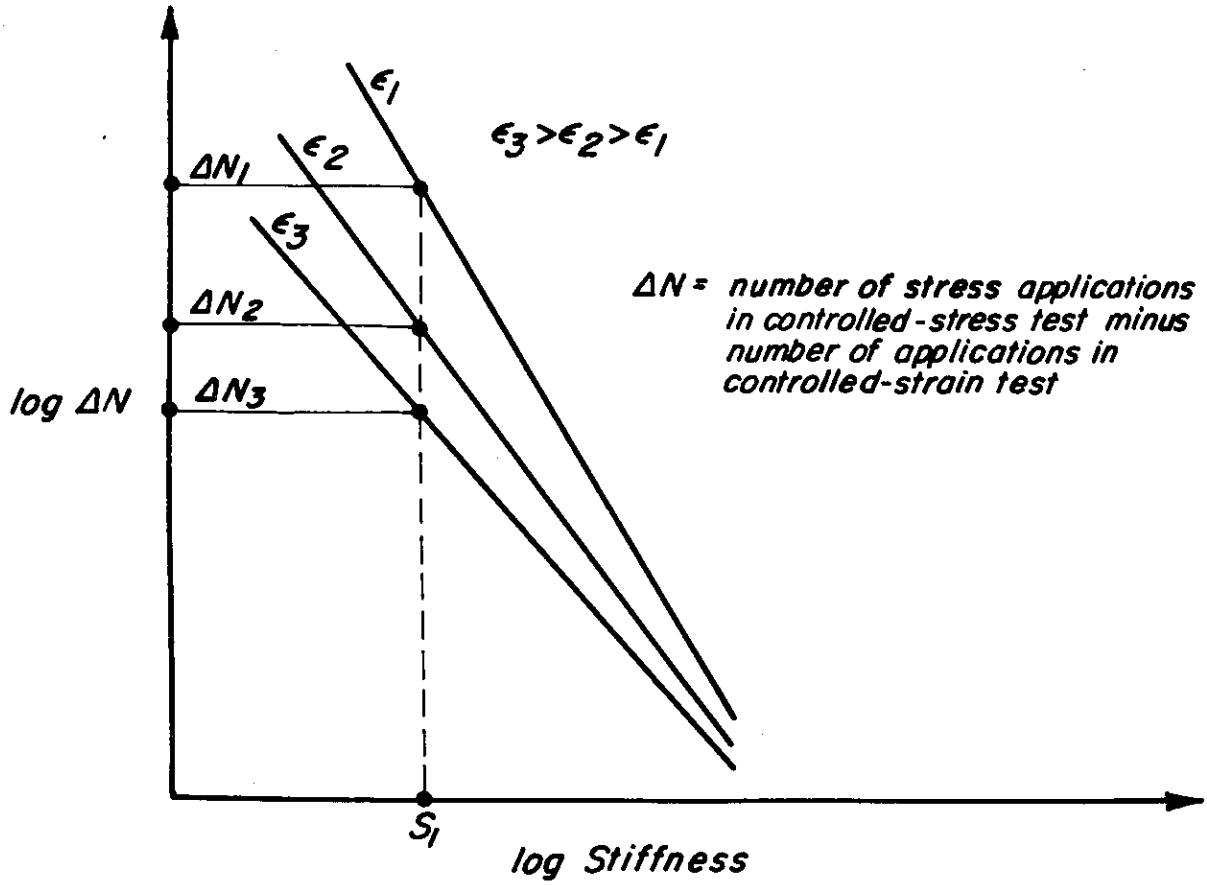

(a) Influence of stiffness on difference between controlled-stress and controlled-strain fatigue curves.

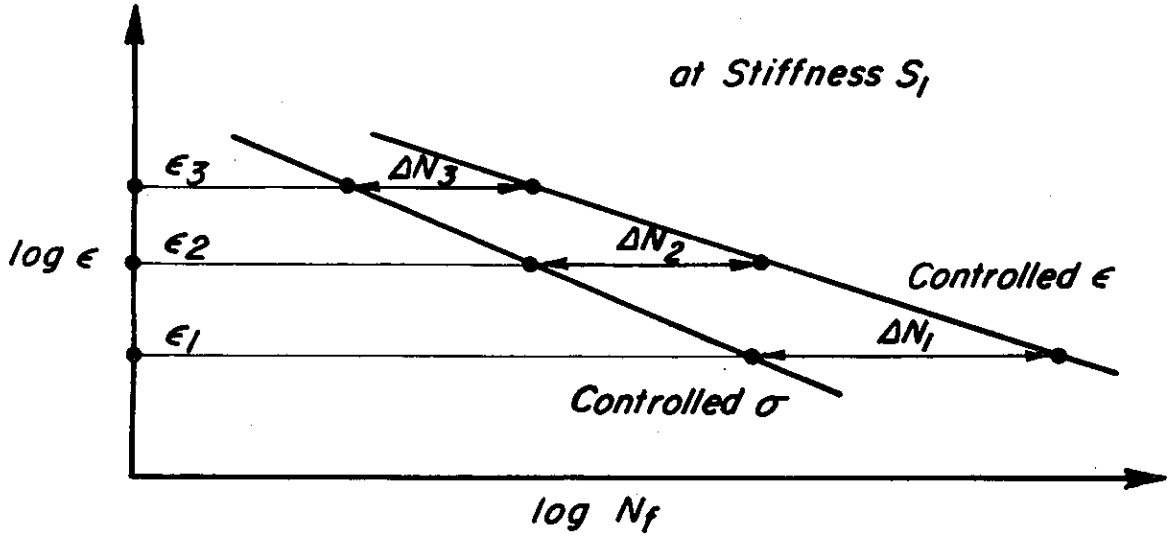

(b) Controlled-strain fatigue curve determined from data in (a), above, and controlled-stress fatigue curve.

Fig. 35 - Schematic representation of estimation of controlled strain to fatigue data at low stiffness values.

ClibPDF - www.fastio.com

TABLE 15 - FATIGUE LIFE ESTIMATE - 0.8 FT. SECTION
BLYTHE PAVEMENT

Wheel Load lbs	APPLICATIONS TO FAILURE - N_f AT STIFFNESSES VARYING FROM 1.1×10^6 to 2.5×10^4 psi*							
	Stiffness Group of Table 10							
750	∞	∞	∞	∞	∞	3.0×10^7	5.2×10^8	2.2×10^9
1,250	∞	∞	∞	∞	∞	5.0×10^6	4.6×10^7	1.6×10^8
1,875	∞	∞	∞	∞	2.4×10^6	1.3×10^6	7.8×10^6	2.0×10^7
2,500	∞	∞	∞	2.3×10^6	1.0×10^6	4.6×10^5	2.3×10^6	5.4×10^6
3,500	∞	∞	∞	9.0×10^5	3.5×10^5	2.0×10^5	6.4×10^5	1.2×10^6
4,250	∞	∞	1.01×10^6	4.8×10^5	2.0×10^5	1.1×10^5	2.9×10^5	4.9×10^5
4,750	∞	∞	8.0×10^5	3.7×10^5	1.5×10^5	8.6×10^4	2.0×10^5	3.3×10^5
5,250	∞	∞	6.0×10^5	2.7×10^5	1.1×10^5	6.4×10^4	1.4×10^5	2.3×10^5
5,750	∞	∞	4.2×10^5	2.1×10^5	8.8×10^4	4.8×10^4	1.0×10^5	1.6×10^5
6,250	∞	1.03×10^6	3.6×10^5	1.6×10^5	7.0×10^4	4.0×10^4	8.0×10^4	1.1×10^5
7,000	∞	8.4×10^5	2.7×10^5	1.1×10^5	5.5×10^4	2.9×10^4	5.4×10^4	7.6×10^4
8,125	∞	5.9×10^5	1.07×10^5	8.2×10^4	3.6×10^4	2.1×10^4	3.6×10^4	4.4×10^4

*$MN/m^2 = 6.9 \times 10^{-3} \times$ (stiffness in psi).

ClibPDF - www.fastio.com

TABLE 16 - FATIGUE LIFE ESTIMATE - 1.5 FT. SECTION
BLYTHE PAVEMENT

Wheel Load lbs	APPLICATIONS TO FAILURE - N_f AT STIFFNESSES VARYING FROM 1.1×10^6 to 2.5×10^4 psi*							
	Stiffness Group of Table 11							
750	∞	∞	∞	∞	∞	∞	∞	∞
1,250	∞	∞	∞	∞	∞	∞	∞	∞
1,875	∞	∞	∞	∞	∞	∞	1.4×10^9	2.5×10^9
2,500	∞	∞	∞	∞	∞	6.6×10^7	3.6×10^8	5.8×10^8
3,500	∞	∞	∞	∞	∞	1.9×10^7	6.6×10^7	1.1×10^8
4,250	∞	∞	∞	∞	7.0×10^6	9.2×10^6	3.0×10^7	5.4×10^7
4,750	∞	∞	∞	∞	5.0×10^6	6.4×10^6	1.8×10^7	3.3×10^7
5,250	∞	∞	∞	∞	3.5×10^6	4.2×10^6	1.1×10^7	2.0×10^7
5,750	∞	∞	∞	∞	2.6×10^6	3.1×10^6	7.6×10^6	1.3×10^7
6,250	∞	∞	∞	∞	2.0×16^6	2.3×10^6	5.4×10^6	8.6×10^6
7,000	∞	∞	∞	∞	1.3×10^6	1.5×10^6	3.6×10^6	5.2×10^6
8,125	∞	∞	∞	2.3×10^6	9.0×10^5	1.0×10^6	2.0×10^6	3.7×10^6

*$MN/m^2 = 6.9 \times 10^{-3} \times$ (stiffness in psi).

ClibPDF - www.fastio.com

According to the analysis both pavements should exhibit fatigue lives greater than 50 years.

From an examination of the controlled-strain curves, however, it would appear that the values so obtained might provide an upper bound. Accordingly, analyses were performed in which the resulting fatigue curves were adjusted by a factor of 10^{-1} and 10^{-2} in fatigue life; this is, the estimated curves were shifted by factors of 10 and 100 to the left (shorter lives)

These adjustments had no measurable effect in the service life of the 1.5 ft. (457 mm) thick section in that its estimated life remained in excess of 50 years.

For the 0.8 ft. (244 mm) thick pavement, on the other hand, the 10^{-1} adjustment reduced the fatigue life to about 21 years while the 10^{-2} adjustment reduced the fatigue life to about three years.

While one cannot provide a definitive recommendation at this as to specific fatigue criteria to use, analysis of the type described in this section should permit the development of design criteria for California conditions. The fatigue tests performed to date provide useful data to assist in the development of such criteria.

WILLITS PROJECT

This project consisted of an instrumented full depth asphalt concrete section as a portion of the widening of U.S. 101 through the city of Willits in Northern California. The 1.0 ft. (305 mm) thick pavement was placed directly on the subgrade as shown in Fig. 36.

Only limited testing was performed on the materials of this project. Tests included resilient moduli determinations on the silty sand subgrade for a range in water contents and repeated load triaxial compression tests on two cores of the asphalt concrete.

Results of repeated load triaxial compression tests in the silty sand subgrade* are shown in Fig. 37. Interestingly, the modulus of this material

---

*R value = 60; liquid limit = 24; plasticity index = 3; percent passing No. 200 sieve = 33 percent.

ClibPDF - www.fastio.com

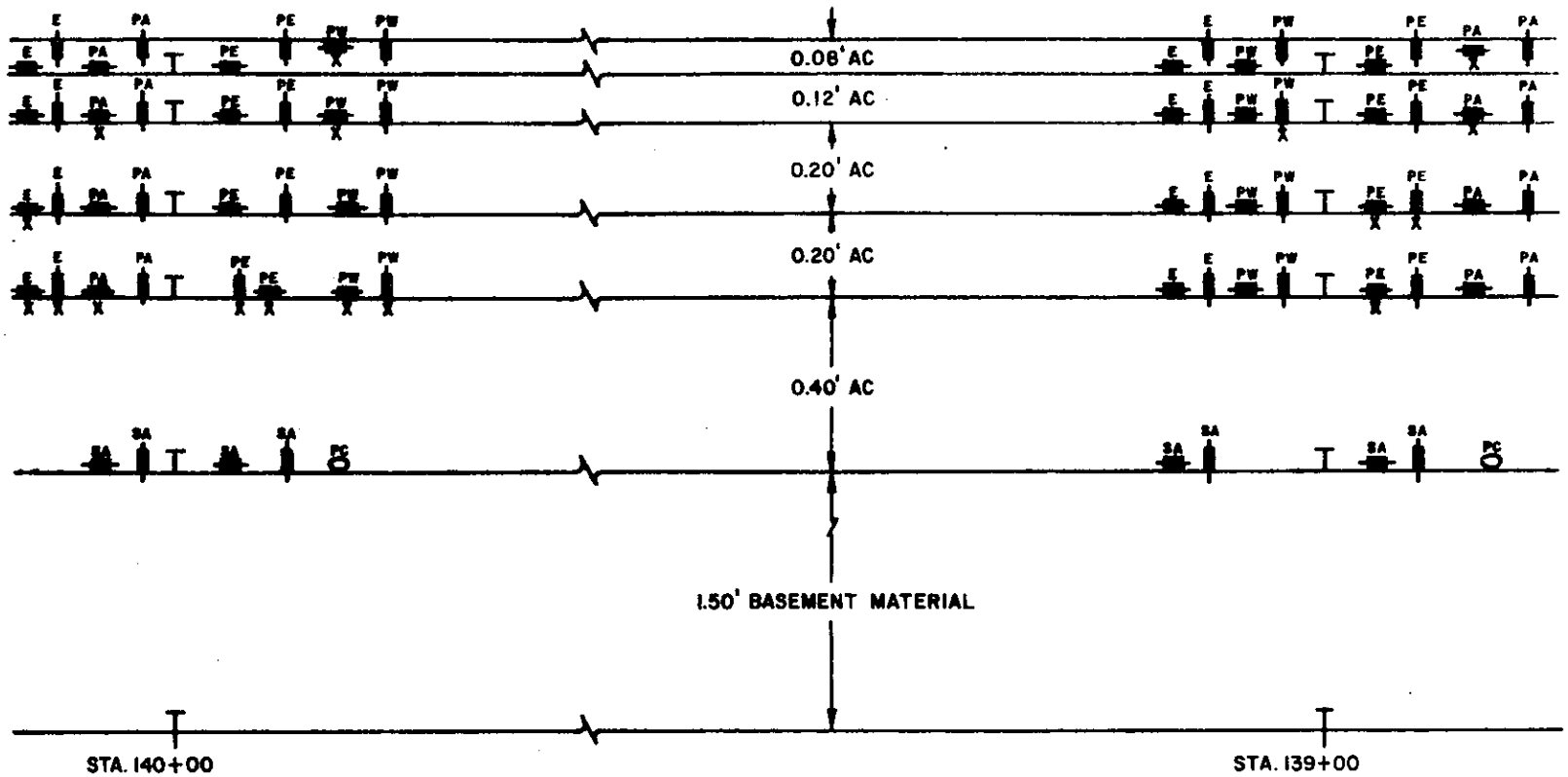

T - THERMOCOUPLE
- STRAIN GAUGE PLACED LONGITUDINALLY TO TRAFFIC
- STRAIN GAUGE PLACED TRANSVERSE TO TRAFFIC
PC - PRESSURE CELL
SA - STRAIN GAUGE ADHERED TO SAND ASPHALT CARRIERS
E - STRAIN GAUGE EPOXIED TO PAVEMENT
PA - POLYMIDE STRAIN GAUGE ADHERED W/ ASPHALT
PW - POLYMIDE STRAIN GAUGE ADHERED W/ WATERPROOFING AGENT
PE - POLYESTER STRAIN GAUGES ADHERED W/ WATERPROOFING AGENT
x - INOPERATIVE STRAIN GAUGE

Fig. 36 - Willits pavement section instrumentation.

ClibPDF - www.fastio.com

appeared to be sensibly independent of stress state, this in contrast to the data reported for the Blythe and Indio projects.

One of the major purposes of this project was to examine the reproducibility of the repeated load triaxial compression test as performed by laboratories with membership in the Triaxial Institute for Structural Pavement Design. The results of this cooperative study are described in the Transportation Laboratory Report.

In addition to comparing the results of the laboratory tests, an estimate of the design of the pavement were made utilizing the laboratory results and a fatigue criterion for the asphalt concrete layer. The Transportation Laboratory Report also summarizes the various estimates.

SUMMARY

In this section of the report, studies associated with three State of California Transportation Laboratory in-situ pavement investigations have been briefly described. These studies suggest the following:

1. Elastic layer theory predicts reasonably well the response of thick asphalt pavement to load using laboratory measured response parameters, e.g., resilient moduli for repeated load triaxial compression tests. Comparison of predicted and measured response of the Indio pavement at high temperatures substantiates this conclusion since the deformation pattern computed within the layer is similar to that as measured by LVDT's so long as appropriate stiffness moduli are used.

2. The analysis of the Indio pavement as well as the results of analyses presented by a number of other investigators (e.g., Witczak and Nunn) suggest that for high temperatures large tensile strains may be developed in the upper part

ClibPDF - www.fastio.com

of the pavement structure contributing in turn to surface cracking.

3. Prediction of the service life of the Blythe pavement demonstrates a procedure whereby fatigue criteria might be evolved for California conditions using the fatigue results developed from the University studies over the years in conjunction with the analysis of the performance of in-situ pavements for which detailed material characteristics, environmental conditions, and traffic loading are known.

ClibPDF - www.fastio.com

PART 3: PERMANENT DEFORMATION CONSIDERATIONS

INTRODUCTION

A part of the investigations has been concerned with the problem of estimation of or minimizing permanent deformation (or distortion) in asphalt concrete pavement systems. Table 17 contains a summary of the various forms of distortion resulting from both traffic and non-traffic causes. In this report only distortion resulting from traffic associated causes will be examined.

As seen in Table 17 traffic-caused permanent deformation can result from: (1) a single or comparatively few excessive loads, (2) a large number of repetitively applied loads, or (3) long term (or static) loads. While all three loading conditions will be discussed, the research effort has been concerned with deformation resulting from comparatively large numbers of repetitively applied loads.

Little attempt has been made to predict the rutting resulting from plastic flow or shear distortion associated with a single or comparatively few excessive loads since the concern of the engineer has been to "design" the material to resist such loads with materials design being predicted on shear strength characteristics, sometimes expressed in terms of the Mohr-Coulomb parameters ϕ and C (e.g., 22, 23). This approach has also been applied to the design of pavements to resist rutting from repetitive traffic loading and tests such as the "R" value (24), the CBR (25), or triaxial compression to determine ϕ and C under specific conditions (e.g., specific time of loading and temperature for asphalt concrete) (26, 27) have been widely utilized. Both TE 71-8 (28) and reference (27) contain recent summaries of such methodology.

The general framework used to either predict or minimize permanent deformation from repeated loading is shown in Fig. 2. As noted earlier, this

ClibPDF - www.fastio.com

TABLE 17 - EXAMPLES OF THE DISTORTION (PERMANENT DEFORMATION) MODE OF DISTRESS FOR ASPHALT PAVEMENTS

General Cause	Specific Causative Factor	Example of Distress
Traffic-load associated	Single or comparatively few excessive loads	Plastic flow (shear distortion)
	Long term (or static) load	Creep (time dependent) deformation
	Repetitive traffic loading (generally large number of repetitions)	Rutting (resulting from accumulation of small permanent deformations associated with passage of wheel loads
Non-traffic associated	Expansive subgrade soil*	Swell or shrinkage
	Compressible material underlying pavement structure	Consolidation settlement
	Frost-susceptible material	Heave (particularly differential amounts)

*Soils in this category exhibit high shrinkage as well as swell characteristics.

ClibPDF - www.fastio.com

has the same format as the system developed for fatigue. Also, as with fatigue, it will be assumed that a pavement section will be available, having been "designed" by a procedure such as the State of California "R" value method.

Two approaches are available to consider rutting from repeated traffic loading; both have been examined as a part of this study. In one method the vertical compressive strain at the subgrade surface is limited to some tolerable amount associated with a specific number of load repetitions (e.g. Shell (15)). By controlling the characteristics of the materials in the pavement section through materials design and proper construction procedures (unit weight or relative compaction requirements) and by insuring that materials of adequate stiffness and sufficient thickness are used so that this strain level is not exceeded, permanent deformation equal to or less than some prescribed amount is thus assured.

The other procedure involves an estimation of the actual amount of rutting which might occur using appropriate materials characterization information together with an analysis procedure assuming the pavement structure to be represented as a layered elastic or viscoelastic system. In this investigation emphasis has been placed on the elastic rather than the viscoelastic methodology, reasons have been detailed in Report TE 73-5 (29).

LIMITING SUBGRADE STRAIN CRITERIA

A number of limiting subgrade strain criteria have been developed for highway pavements. The Shell investigators (15) were the first to suggest this approach and their criteria are summarized in Table 18. These limiting strain values were developed by elastic analyses of pavements designed according to the CBR procedure and pavements in the AASHO Road Test. Considering the performance results of the AASHO Road Test in terms of rut depth, the strain criteria listed in Table 18 are probably associated with ultimate rut depths of the order of 3/4 in. (1.9 cm).

ClibPDF - www.fastio.com

TABLE 18 - ALLOWABLE SUBGRADE COMPRESSIVE STRAIN VALUES CORRESPONDING TO DIFFERENT LOAD APPLICATIONS

Weighted Load Applications	Compressive Strain on Subgrade in. per in.
10^5	1.05×10^{-3}
10^6	6.5×10^{-4}
10^7	4.2×10^{-4}
10^8	2.6×10^{-4}

*From Reference (15).

ClibPDF - www.fastio.com

As a part of this investigation pavement structures designed according to the State of California procedure were analyzed by the procedure described in Report TE 71-8 (28), that is the pavement structure was assumed to behave as a layered elastic solid. While a range in limiting subgrade strain values were obtained depending on the stiffness characteristics assigned to the various components, a specific set of values could be defined for stiffness conditions similar to those used to establish the Shell criteria. These values are shown in Fig. 38. For comparison the values used in the Shell design procedure (Table 18) are also shown.

In Fig. 38 it will be noted that the computed values are less than those suggested by Shell; it is probable that smaller limiting values of permanent deformation occur in pavements designed by the California procedure*.

Hicks and Finn (30) have analyzed the various sections of the San Diego Test Road in the same manner, and the results of their analyses are shown in Fig. 39a. The resulting strain values tend to be more conservative than those shown in Fig. 38 obtained from an analysis of pavements designed according to the California procedure. In this test road, however, relatively small values of permanent deformation were obtained at the time that the criteria were developed, Fig. 39b.

It would appear that the limiting subgrade strain criteria developed as a part of this project are reasonable values to use to minimize permanent surface deformation contributed by the subgrade and are recommended should the State consider pavement design using elastic layer theory. Santucci has already incorporated these criteria in a new design procedure for pavements with asphalt concrete or emulsion-treated bases (7).

---

*While precise values are not available, it should be noted that some engineers who have observed the performance of asphalt pavements in California have stated that ruts were relatively small in the failures which they have observed. Cracking prior to rutting appeared to be the major mode of distress.

ClibPDF - www.fastio.com

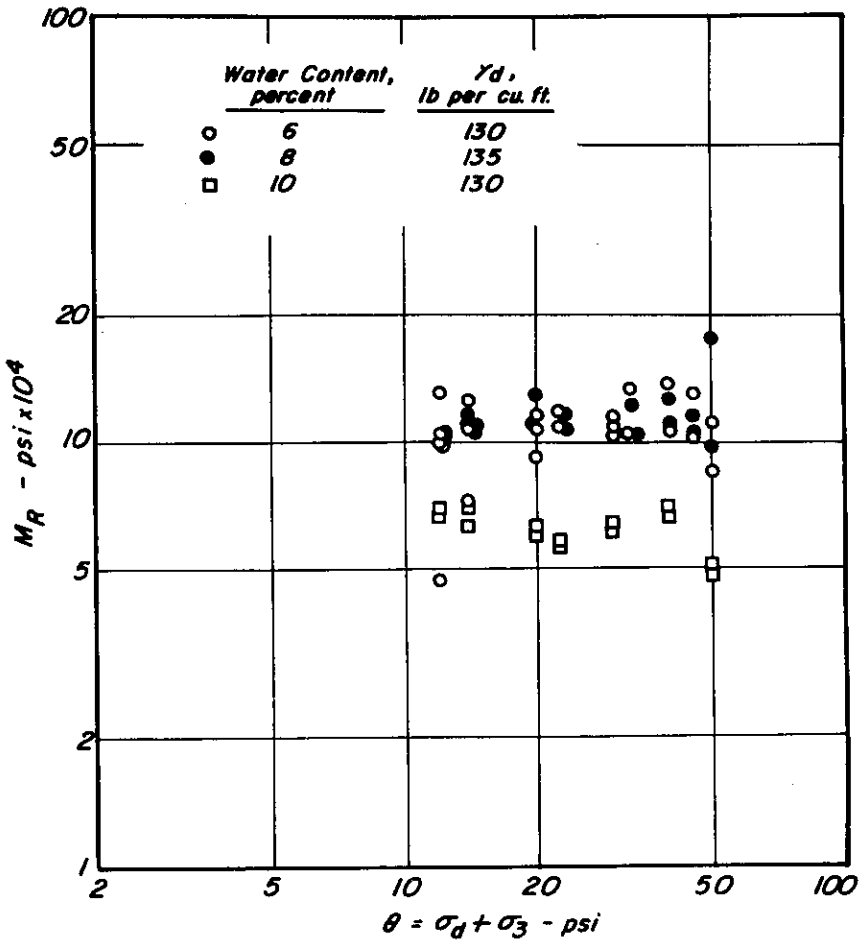

Fig. 37 - Influence of sum of principal stresses on resilient modulus, Willits subgrade material.

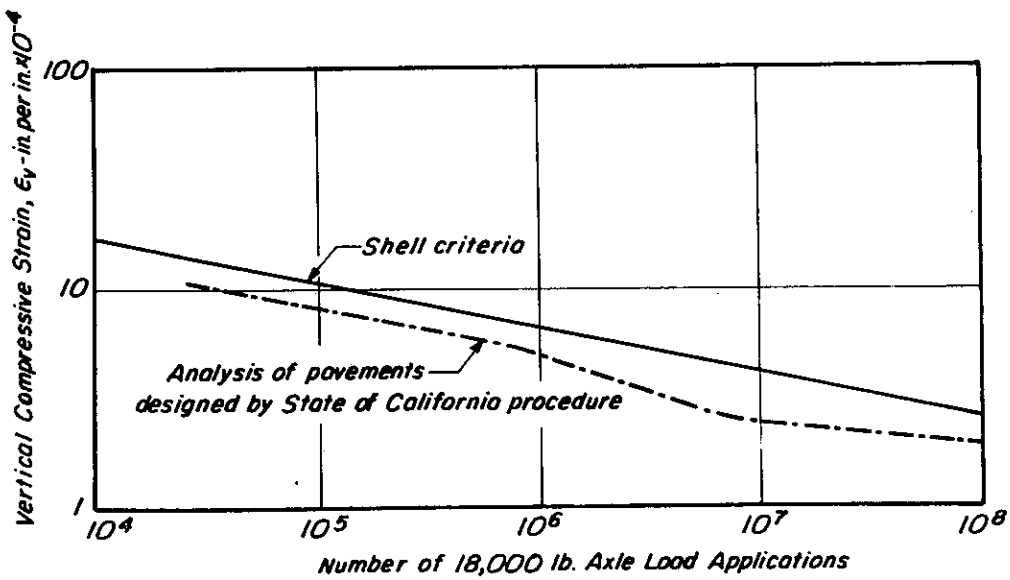

Fig. 38 - Relationships between subgrade strain and axle load applications.

ClibPDF - www.fastio.com

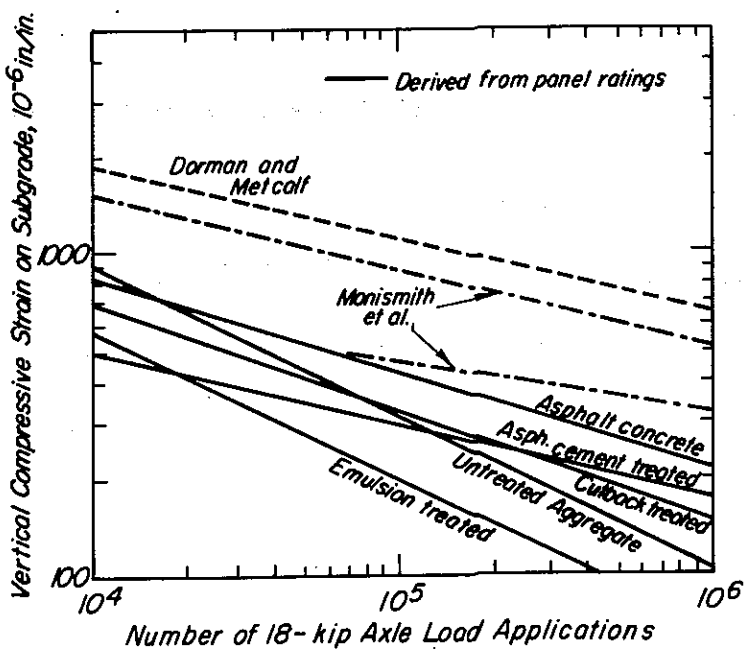

Fig. 39a - ε - N relationship derived from panel ratings for all base types. (after Hicks and Finn (30)).

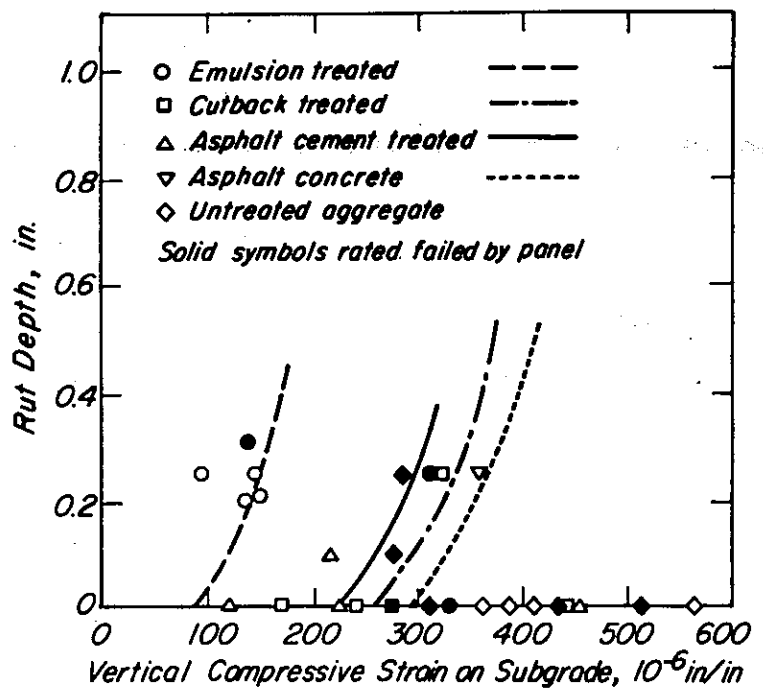

Fig. 39b - Relationship between strain on subgrade and rut depth (EAL_{18}=178,000). (after Hicks and Finn (30)).

ClibPDF - www.fastio.com

RUTTING ESTIMATION FROM REPEATED TRAFFIC LOADING

A number of procedures have been suggested to estimate the amount of rutting from repeated traffic loading. They may be categorized as:

(1) Use of elastic layered system to represent the pavement structure and materials characterization by:

(a) repeated load triaxial compression tests

(b) creep tests (particularly for asphalt-bound layers)

(2) Use of viscoelastic layered system to represent the pavement structure and materials characterization by means of creep tests.

In this investigation efforts have been directed to determination of rutting by method 1(a) above.

Since the inception of this study, a number of investigators have published research results concerned with rutting; these will be briefly summarized also.

Rutting Prediction with Pavement Represented as an Elastic Layered System Based on Laboratory Repeated Load Tests. A number of investigators, including Heukelom and Klomp (31), Barksdale (32) and Romain (33), have suggested that rutting estimates can be obtained by:

(1) assuming the pavement to be represented as a layered elastic system to determine the state of stress and/or strain resulting from surface loading; and

(2) using appropriate constitutive relationships defining permanent strain as a function of stress state to estimate the amount of rutting corresponding to some specified number of load repetitions.

ClibPDF - www.fastio.com

General Procedure. More specifically, relationships between the plastic strain and applied stress must be available for each of the pavement components; i.e.,

$$\varepsilon^p = f\ (\sigma_{ij}) \tag{8}$$

where:

ε^p = plastic or permanent strain

σ_{ij} = stress state

For a particular layer it is then possible to estimate the permanent deformation occurring in that layer. This is done by computing the permanent strain at a number of points within the layer, the number being sufficient to reasonably define the strain variation with depth. Permanent deformation is then determined by summing the products of the average permanent strains and the corresponding difference in depths between the locations at which the strains were determined, Fig. 40, i.e.:

$$\delta_1^p(x\ ,\ y) = \sum_{i=1}^{n} \left(\varepsilon_1^p \Delta z_i\right) \tag{9}$$

where:

$\delta_i^p(x\ ,\ y)$ = rut depth in the ith position at point $(x\ ,y)$ in the horizontal plane.

ε_i^p = average permanent strain at depth $\left(z_i + \frac{\Delta z_i}{2}\right)$

Δz_i = difference in depth.

Total rut depth may be estimated by summing the contributions from each layer.

With the knowledge of plastic strain at various numbers of load repetitions, the development of rutting with increased traffic loading can thus be estimated.

Cumulative Loading Considerations. Normally in the laboratory the constitutive

ClibPDF - www.fastio.com

relationship of equation (8) will be defined for a specific material by application of stresses of a single magnitude, Since the actual stress sequence is not known in the field, it is desirable to have a cumulative loading hypothesis similar to that for fatigue in which the effects of mixed traffic could be predicted from the results of simple loading tests.

In Report TE 73-5 (29) such methodology was suggested and can be briefly summarized as follows:

At least two methods are available to obtain the cumulative permanent strain from the results of simple loading tests: (1) a "time-hardening" procedure, and (2) a "strain-hardening" procedure; both are illustrated schematically in Fig. 41 .

In the "time-hardening" method, if the specimen is loaded for N_1 repetitions of stress state $\bar{\sigma}_1$, the resulting permanent strain will be $\varepsilon_1^p(N)$. The equivalent number of repetitions, N_2' , at stress $\bar{\sigma}_2$ which would have given the same permanent strain is obtained as shown in Fig. 41 . If further N_2 applications of σ_2 are applied, the total strain will following the path as shown in Fig. 41a.

The "strain-hardening" procedure, also illustrated in Fig. 41, requires determination of ε_1^p after N_1 repetitions of stress σ_1 . The number of repetitions at stress $\bar{\sigma}_2$ is then taken equal to N_1, and a further N_2 application is applied. Total permanent strain is the sum ε_1^p and ε_2^p .

While neither method provides a solution which agrees quantitatively with experimental results (for the limited data reported in TE 73-5) it would appear that the time-hardening procedure provides better agreement if the stress levels are successively increased, whereas the strain-hardening method provides closer

ClibPDF - www.fastio.com

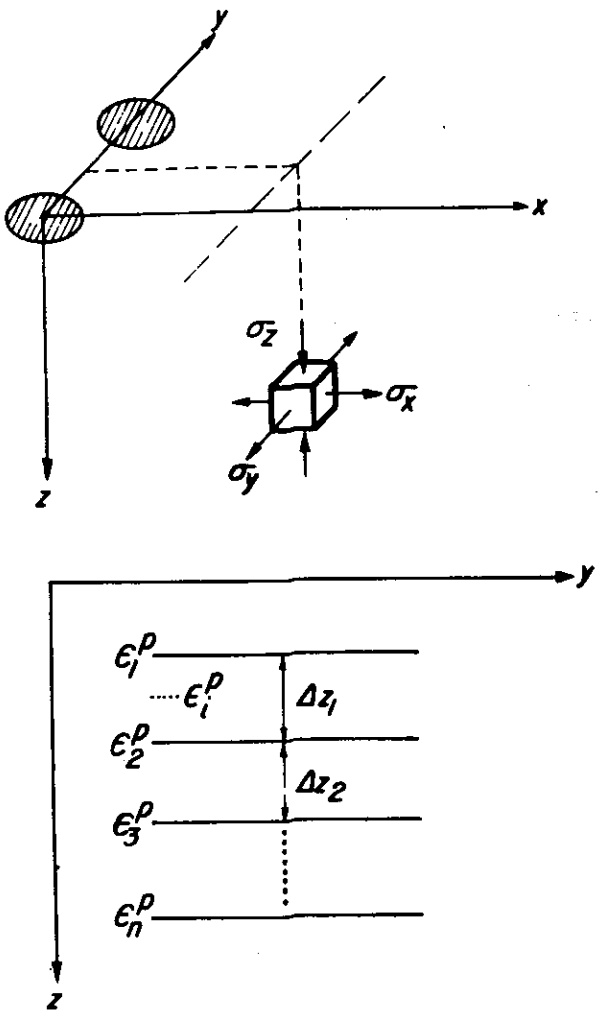

Fig. 40 - Schematic representation of pavement system used to estimate permanent deformation.

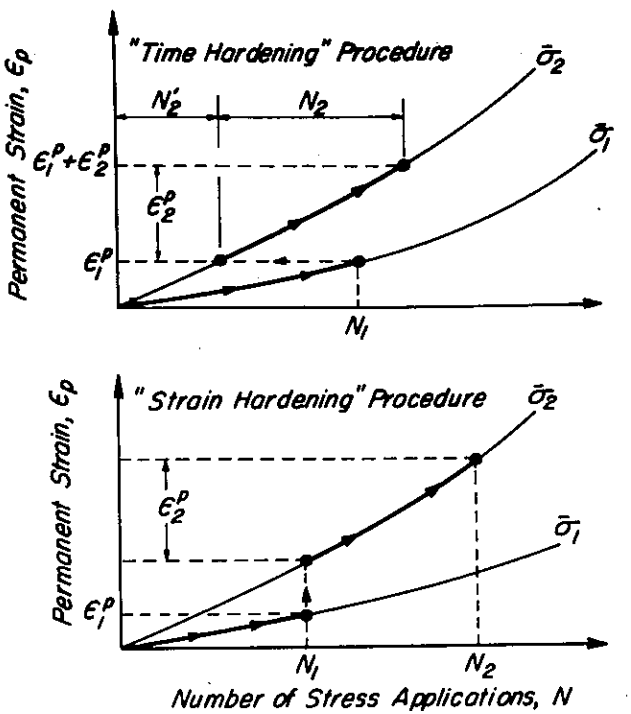

Fig. 41 - Procedures to predict cumulative loading from the results of simple loading tests.

ClibPDF - www.fastio.com

agreement if the loads are successively decreased. Moreover, the procedures appear to provide "bounds" for the amount of permanent deformation to be expected (also as noted in TE 73-5).

The time hardening procedure has also been suggested by van de Loo (34) as a means of developing equivalent wheel loads to simplify rutting estimates. Appendix B contains a summary of this methodology.

Summary of Previous Investigations. A number of investigators have used this approach to predict permanent deformation in either a portion of or in the total pavement structure including Barksdale (32), Morris, et al (35), McLean and Monismith (36), Freeme and Monismith (37), Snaith (38) and Brown and Snaith (39).

Brown, et al (40) and Monismith, et al* (41) have reported the results of repeated load triaxial compression tests on subgrade type materials. Water content, dry density, stress state as well as number of load applications influence the development of permanent strain. Results of repeated load testing can be expressed in equations of the form:

$$\varepsilon^p = AN^b \tag{10}$$

$$\Delta\sigma = \frac{\varepsilon^p}{\ell + m\varepsilon^p} \tag{11}$$

where:

ε^p = permanent strain

$\Delta\sigma$ = applied stress

N = number of stress applications

A, b, ℓ, m = experimentally determined coefficients

---

*Described in detail in Report TE 73-5.

ClibPDF - www.fastio.com

For granular materials, Barksdale (32) has developed considerable data. An equation of the following form appears to represent the test data:

$$\frac{\bar{\varepsilon}^p}{\bar{\sigma}} = \frac{1/K\sigma_3^n}{1 - \dfrac{\bar{\sigma}R_f(1 - \sin\phi)}{2(C\cos\phi + \sigma_3\sin\phi)}} \cdot \left[\frac{N}{N_0}\right]^m \tag{12}$$

where:

$K\sigma_3^n$ = relationship defining the initial tangent modulus as a function of confining pressure

C = cohesion

ϕ = angle of internal friction

R_f = constant relating compressive strength to an asymptotic stress difference; $0.75 \leq R_f \leq 1$

and these parameters are determined at a specific number of stress repetitions, N_0.

For asphalt concrete a number of approaches have been suggested including those developed by Morris, et al (35), McLean and Monismith (36), and Snaith (38).

Morris, et al (35) have developed regression equations for the laboratory test data over a range in temperatures and for a range in stresses, both tensile and compressive. The functional form of their expressions is as follows:

$$\varepsilon^p = f(\sigma_1, \sigma_3, T, N) + E \tag{13}$$

where:

E = estimate of error

Similarly, McLean and Monismith (36) have fitted to their test data a third order polynomial of the form:

$$\log \varepsilon^p = C_0 + C_1(\log N) + C_2(\log N)^2 + C_3(\log N)^3 \tag{14}$$

ClibPDF - www.fastio.com

with the influence of stress state, time of loading and temperature reflected in the coefficients C_0 , C_1 , C_2 , and C_3 .

Snaith (38) has expressed his data by an equation of the form:

$$\log \varepsilon^p = (a + b \log t) \tag{15}$$

In this expression a and b are functions of temperature and applied stress directly estimated from laboratory tests.

Some attempts have been made to predict the accumulation of rutting in various pavement structures using these constitutive relationships together with the process illustrated in Fig. 40 and described earlier.

Morris, et al (35), have prepared an estimate of the rutting occurring in one of the sections of the Brampton Test Road as a function of time. Their estimate is shown in Fig. 42. While the overall results are encouraging, as evidenced by the reasonable correspondence of the measured and predicted values, they suggest that much of the permanent deformation results from accumulations in the lower part of the asphalt bound layer and is a result of the comparatively high tensile stresses occurring near the underside of the section.

McLean and Monismith (36) have compared the form of accumulation of permanent deformation with that reported by Hofstra and Klomp (42) from observations of rutting in a laboratory test track. Comparisons of estimated results with those measured are contained in Fig. 43 *. While the mixtures are different (as noted in the footnote), the shapes of the curves are similar,

---

*It should be noted that the mix tested by Hofstra and Klomp (42) contained a 40-50 penetration asphalt cement and would be considered an over-asphalted mix with less than 2 percent air voids. The mix, used to make the analysis shown in the figure, by comparison contained an 85-100 penetration asphalt cement and had a void content in the range of 4 to 6 percent. At the 86°F (30°C) temperature and time of loading reported by Hofstra and Klomp, this mix exhibited a stiffness of 2.5×10^5 psi (1,725 MN/m^2). Accordingly, it should be kept in mind when comparing the results that the form of the load deformation relationship is more important than the absolute magnitude of the deformations.

ClibPDF - www.fastio.com

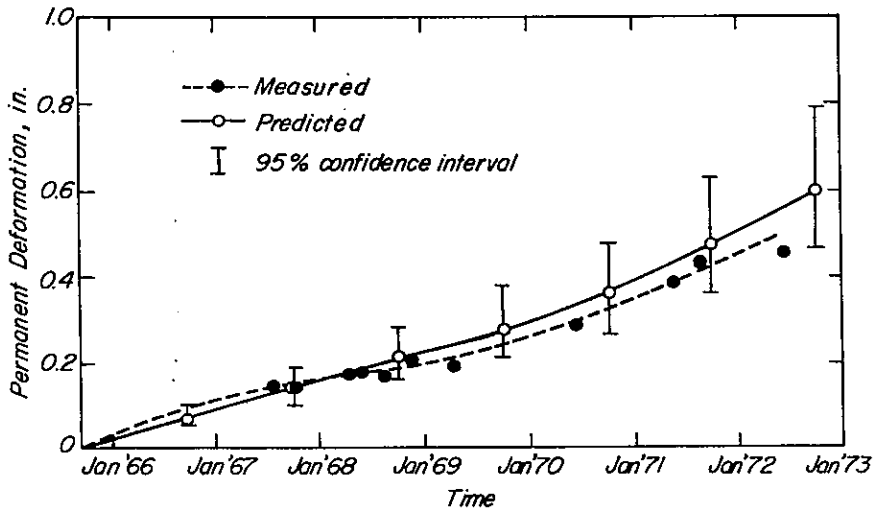

Fig. 42 - Permanent deformation - time relationship Section 3 of Brampton Test Road (11-1/2 in. asphalt concrete). (after Morris et al)

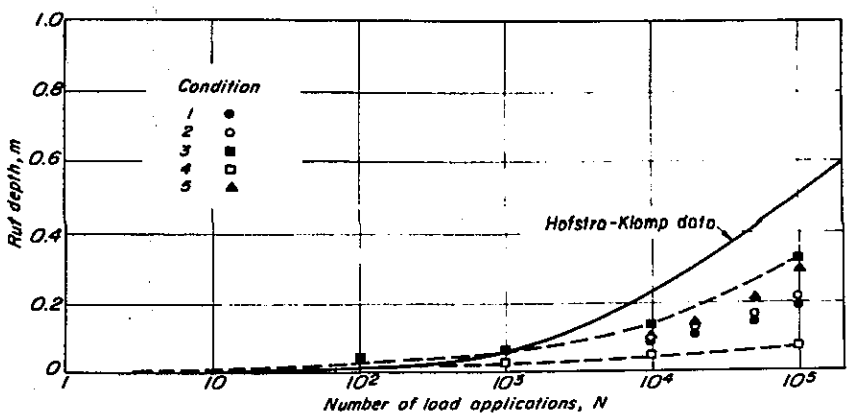

Fig. 43 - Comparison of computed rut depths with those measured by Hofstra and Klomp. (from Ref. (16)

ClibPDF - www.fastio.com

indicating the potential applicability of such a procedure.

Snaith (38), using the same approach and the equations which he developed, predicted accumulation of rutting with load applications of the same form as shown in Fig. 43 .

Barksdale (32) has used this methodology to provide a relative indication of the rutting potential of different granular materials when used in a particular pavement structure. His results are illustrated in Fig. 44 in which the rutting potential is shown in terms of a rut index rather than in terms of actual rutting which might be associated with the different materials.

McLean and Monismith (36) have also used this procedure to examine the influence of certain designer controlled variables on the rutting which might occur in thick asphalt bound layers. Results of these analyses are shown in Figs.45, 46, and 47.

The influence of the stiffness of the asphalt concrete on rut depth is illustrated in Fig. 45. Reducing the stiffness by a factor of two increases the permanent deformation more than proportionally, indicating, at least from the calculations presented, that the influence of stiffness modulus of the asphalt concrete is substantial.

Fig. 46 illustrates, at least for this set of circumstances (h_1 = 12 in.(305 mm)) that the subgrade stiffness has practically no effect on the accumulation of permanent deformation in the asphalt concrete layer. It must be recognized, however, that subgrade stiffness will influence the total permanent deformation at the pavement surface (a factor not considered in this analysis), and for a given thickness, h_1 , total deformation will increase as the stiffness is reduced.

The influence of layer thickness on permanent deformation within the asphalt-bound layer is shown in Fig.47 to be minimal. This same result was reported by Hofstra and Klomp in their laboratory test track study.

ClibPDF - www.fastio.com

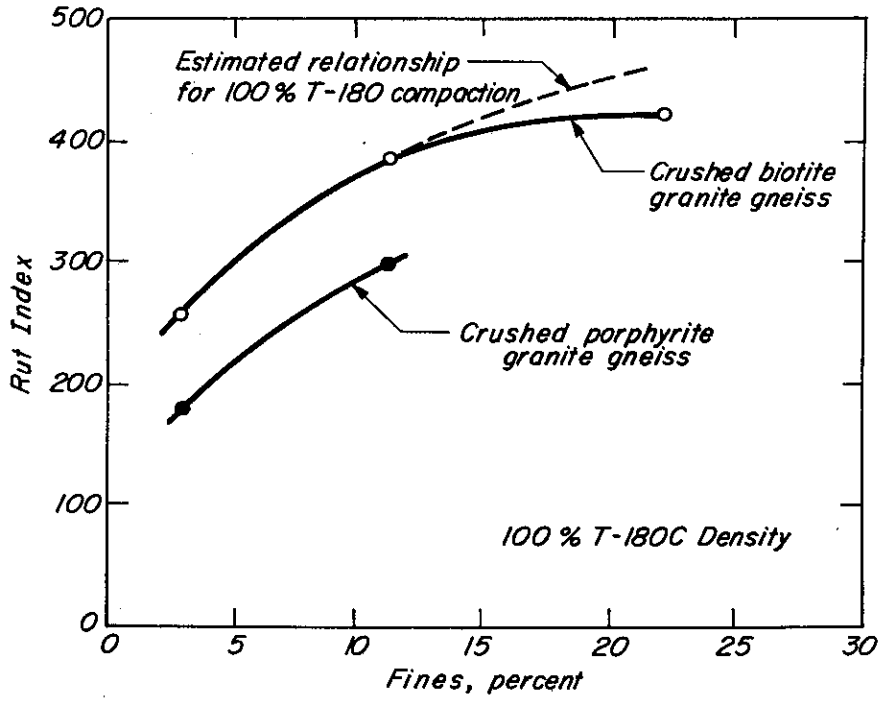

Fig. 44 - Variation of rut index with percent fines for crushed granite gneiss bases after 100,000 load repetitions. (after Barksdale (32)).

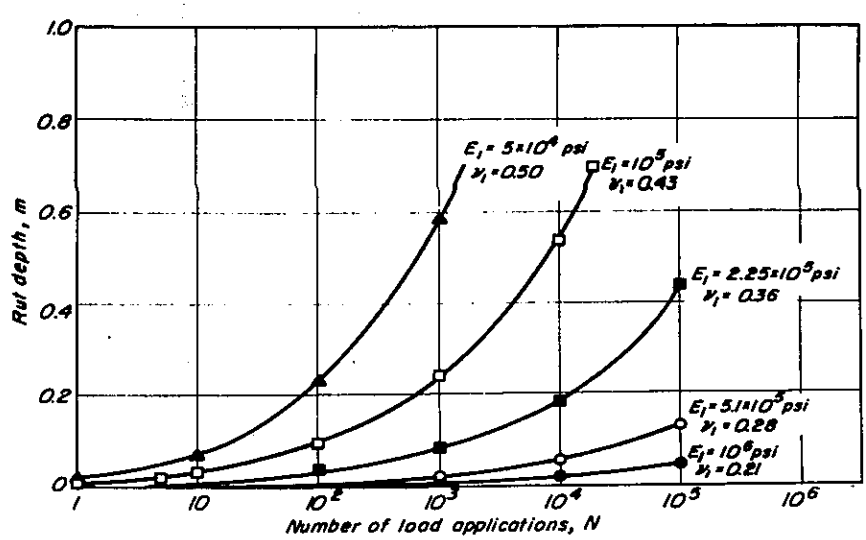

Fig. 45 - Influence of stiffness modulus of asphalt concrete on permanent deformation; E_2=10,000 psi; ν_2=0.45. (from Ref. (36)).

ClibPDF - www.fastio.com

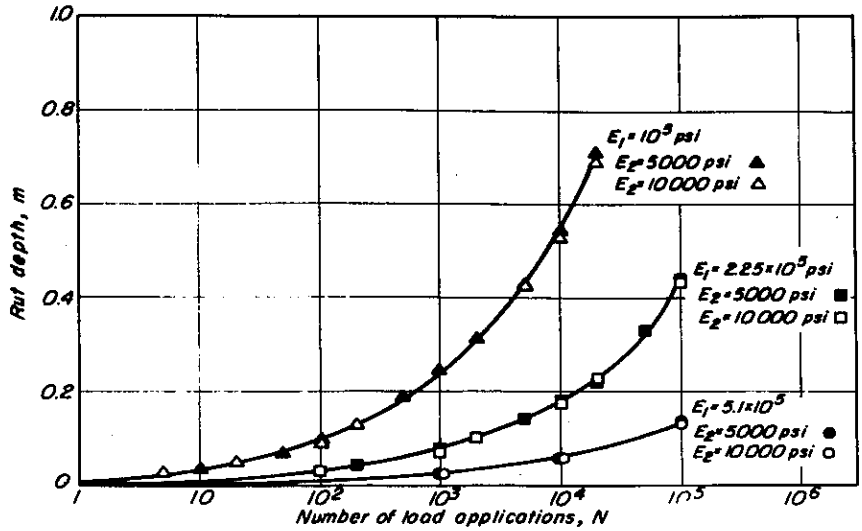

Fig. 46 - Influence of subgrade stiffness on permanent deformation. (from Ref. (36)).

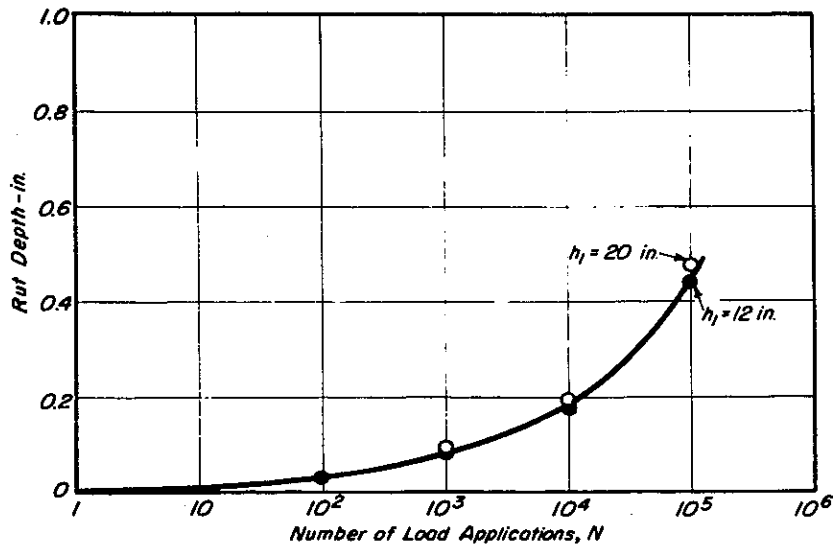

Fig. 47 - Influence of pavement thickness on permanent deformation $E_1 = 2.25 \times 10^5$ psi; $E_2 = 10{,}000$ psi. (from Ref. (36)).

ClibPDF - www.fastio.com

This latter comparison as well as those illustrated earlier indicate that the use of elastic theory for stress and strain distribution together with a constitutive relationship determined from laboratory repeated load tests has the potential to assist in the estimate of permanent deformation accumulation in thick asphalt-bound layers.

Based on Laboratory Creep Tests. The use of creep tests on asphalt concrete together with elastic layer theory to represent the response of the pavement structure to load is an alternative approach proposed by the Hills, et al (43), van de Loo (44, 34), and Chomton and Valayer (45) to estimate the amount of rutting occurring in the asphalt bound layer(s) of a pavement structure.

Observations of the development of rut depth with load repetitions in laboratory test tracks* provide data which, when suitably transformed, exhibit the same shape as test results for laboratory creep tests in uniaxial compression; Fig 48 illustrates such data. In this figure the quantities are estimated as follows:

(1) S_{mix} (laboratory creep) $= \sigma/\varepsilon_{mix}$ (15)

where:

σ = applied creep stress, T (temperature) = constant

ε_{mix} = axial strain at particular time t

S_{mix} = corresponding mix stiffness at specified temperature T , and time, t

(2) S_{bit} (laboratory creep) $= \sigma/\varepsilon_{bit}$ (16)

where:

*Two layer pavements consisting of asphalt concrete resting directly on subgrade.

ClibPDF - www.fastio.com

S_{bit} = asphalt stiffness (estimated using Shell procedure (14)).

(3) S_{mix} (rutting test on field pavement =

$$\frac{Z\sigma_o}{B\frac{r}{H_o}} \tag{17}$$

where:

$$Z = f\left[\frac{\text{radius of loaded area}}{\text{thickness of asphalt bound layer, } H_o}, \frac{E_{subgrade}}{E_{asphalt\ concrete}}\right]$$

σ_o = tire contact pressure

r = total rut depth at pavement surface

B = proportion of total rut depth in asphalt bound layer

(4) S_{bit} (rutting test) -- only the viscous component of S_{bit} is estimated, termed $\left(S_{bit}\right)_v$

$$\text{i.e., } \frac{1}{\left(S_{bit}\right)_v} = \frac{t}{3n} \tag{18}$$

and

$$3\eta = \lim_{t\to\infty} \left(t \cdot S_{bit}\right) \tag{19}$$

For the time of loading in the rutting test

$$t = nt_w$$

where:

n = number of wheel bases

t_w = time of loading for one wheel passage

Recognizing different temperature conditions:

ClibPDF - www.fastio.com

$$\left(S_{bit}\right)_v = \frac{3}{t_w \Sigma \left(\frac{n}{\eta}\right)_T}$$

To use this methodology requires: (1) measuring S_{mix} in the laboratory; (2) estimating S_{bit} by the Shell procedure; (3) estimating $\left(S_{bit}\right)_v$ from a knowledge of traffic and temperature conditions and the nomographic procedure; and thence determining the rut depth, r , from $Z\sigma_o/B\frac{r}{H_o}$ for the specific pavement conditions. Comparisons between estimated and computed values are shown in Fig. 49.

While this procedure is applicable only for asphalt bound materials, that should not be considered a limitation, however, since as suggested by van de Loo (21), the creep test may have been described by Ugé and van de Loo (49).

Rutting Prediction with Pavement Represented as a Layered Viscoelastic System

A number of investigations, e.g., Barksdale and Leonards (47) and Elliott and Moavenzadeh (48, 49) have suggested that rutting can be estimated by assuming the pavement to be represented as a viscoelastic layered system and using creep tests to represent the response characteristics of the various materials in the pavement structure.

Using the procedure terms VESYS II (50), the accumulation of permanent deformation in the same structure for which the results of the elastic analysis were also reported (e.g. TE 73-5) was examined. Compliances were determined both in tension and compression and variations in both time of loading and total time before the next is applied were considered. Fig. 50 contains a summary of these determinations (also individually reported in TE 73-5). In this figure it will be noted that the permanent deformations which have been estimated using this procedure are substantially less than those computed using the elastic analysis for essentially the same conditions. Moreover, the accumulation of permanent deformation with number of load applications by this procedure does not exhibit the same shape as observed in the studies of Hofstra and Klomp (Fig. 43).

ClibPDF - www.fastio.com

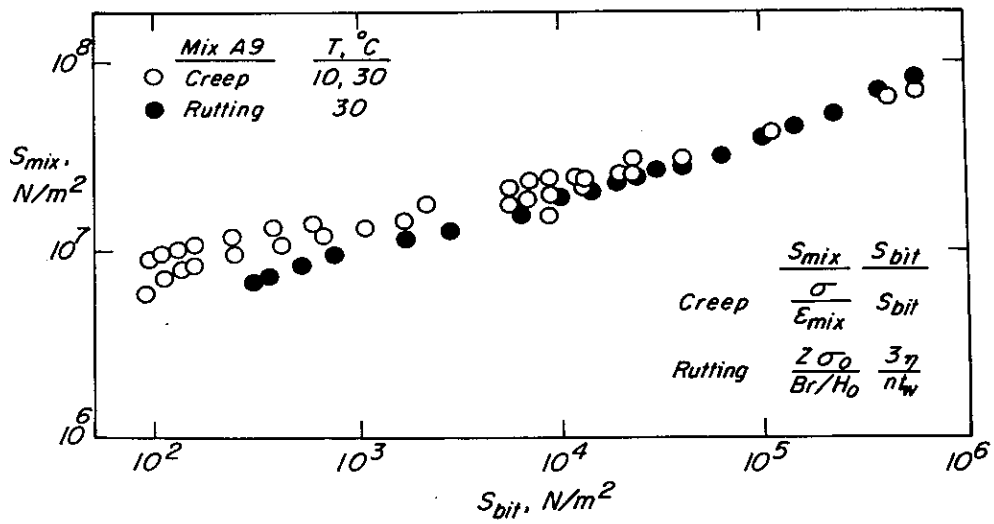

Fig. 48 - Creep and rutting tests (test track) on A9. (after Hills, Brien, and van de Loo).

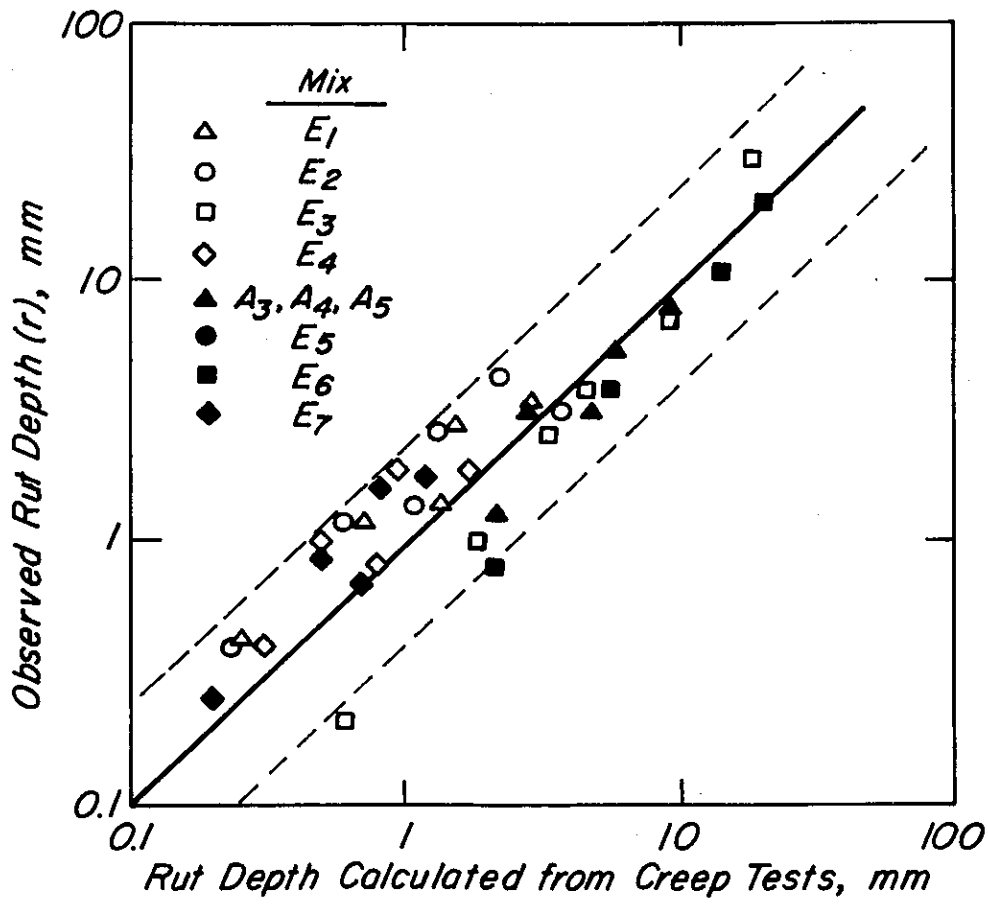

Fig. 49 - Observed rut depth in the tracking machine against rut depth calculated from creep tests. (after Hills, Brien, and van de Loo).

ClibPDF - www.fastio.com

The reasons for these differences are not clear at this time and because of these differences no further studies were directed to the viscoelastic analysis in this investigation.

PROPOSED CHARACTERIZATION FOR PAVING MATERIALS

To provide a convenient form for the constitutive relationships described in the previous section to permit estimate of rutting in the pavement structure, Freeme and Monismith (37) have suggested the use of a determinant for plastic deformation (for the maximum distortion energy yield condition) termed the equivalent stress, $\bar{\sigma}$, and defined as:

$$\bar{\sigma} = \frac{1}{\sqrt{2}}\left[(\sigma_1 - \sigma_2)^2 + (\sigma_2 - \sigma_3)^2 + (\sigma_3 - \sigma_1)^2\right]^{1/2} \tag{20}$$

A relationship, in turn, between this stress and plastic strain which can be utilized is of the form:

$$d\varepsilon_{ij} = \frac{3}{2}\frac{d\bar{\varepsilon}^p}{\bar{\sigma}} S_{ij} \qquad i\ ,\ j = 1,\ 2,\ 3 \tag{21}$$

where:

$d\varepsilon_{ij}$ = the plastic strain corresponding to the deviator stress S_{ij}

$d\bar{\varepsilon}_p$ = an increment of the "effective" or "equivalent" plastic strain defined by

$$d\bar{\varepsilon}_p = \frac{\sqrt{2}}{3}\left[(d\varepsilon_1 - d\varepsilon_2)^2 + (d\varepsilon_2 - d\varepsilon_3)^2 + (d\varepsilon_3 - d\varepsilon_1)^2\right]^{1/2}$$

where $d\varepsilon_1$, $d\varepsilon_2$ and $d\varepsilon_3$ are the principal strain increments.

In this equation it is seen that the plastic strain <u>increments</u> are given and not the plastic strains themselves. In linear-elasticity the current state of stress completely defines the state of strain but the current state of stress cannot define the plastic strains measured from the

ClibPDF - www.fastio.com

virgin condition of the material. Any plastic deformation done before the current stresses were applied would have to be known before the total plastic deformation can be defined.

If there is no unloading, if the principal stress ratios remain fixed, and if the stresses remain in constant ratio throughout the loading history, the strain increments can be integrated to give the total plastic strains. These are referred to as the stress/strain relations of the "deformation theory of plasticity."

In this investigation, an important simplifying assumption has been made, i.e., that the conditions under which the dynamic triaxial tests are carried out in the laboratory simulate the dynamic loading conditions which occur in the pavement. It is then permissible in the case of permanent deformation to use the total strain approach to explain the results of dynamic triaxial tests and to extrapolate these results to the multiaxial conditions in the pavement.

In the pavement structure, the permanent strain in the vertical direction, ε_z^p, occurring under multiaxial conditions is given by*:

$$\varepsilon_z^p = R\left[\sigma_z - 1/2(\sigma_x + \sigma_y)\right] \tag{22}$$

where:

σ_z, σ_y, σ_x = stresses in vertical, radial and tangential directions

$R = \frac{\bar{\varepsilon}^p}{\bar{\sigma}}$, the ratio of <u>total</u> "equivalent" strain to the "equivalent" stress**

---

*Poisson's ratio is assumed equal to 0.5 in equation (22).

**For triaxial conditions the equivalent stress $\bar{\sigma} = (\bar{\sigma}_1 - \bar{\sigma}_3)$ and the total equivalent strain $\bar{\varepsilon}^p = 2/3\ (\varepsilon_1 - \varepsilon_3)$

ClibPDF - www.fastio.com

It is possible that ratio R may be a unique relationship for many materials which will be dependent on $\bar{\sigma}$, number of stress applications, and, in the case of untreated soils and granular materials, water content and dry density.

For fine-grained soils it is possible to recast equation (11) and to incorporate the influence of stress repetitions so that the relationship R will have the form:

$$R_s = \frac{\ell}{1 - m\bar{\sigma}} \left(\frac{N}{N_o}\right)^b \tag{23}$$

where:

N_o = number of repetitions at which coefficients ℓ and m are determined.

Similarly for untreated granular material, the ratio R can be expressed as:

$$R_g = \frac{1/k\sigma_3^n}{\dfrac{1 - \bar{\sigma}R_f(1 - \sin\phi)}{2(C\cos\phi + \sigma_3\sin\phi)}} \cdot \left(\frac{N}{N_o}\right)^b \tag{24}$$

For asphalt concrete an approach is to characterize the material by means of the equation pertaining to time-dependent plastic deformation. The total permanent strain in equation (22) then becomes time dependent as does the relationship for R. From the triaxial compression test data like that reported in TE 73-5, it is possible to formulate an approximate relationship for the rate of change of R, i.e.,

$$\frac{\partial R_B}{\partial t} = \delta(T)N^{\alpha}\bar{\sigma}^{n-1} \tag{25}$$

where:

$\delta(T)$ is a function of temperature, T

α and n are constants

ClibPDF - www.fastio.com

RECOMMENDED DESIGN (ANALYSIS) SUBSYSTEM

Based on the material presented thus far, it is possible to suggest a design (or analysis) subsystem to permit estimates of rutting from repeated traffic loading to be made. The format for this subsystem is shown in Fig. 2. Like the fatigue subsystem (TE 70-5), the procedure involves estimation of the occurrence of distress (in this case the amount of rutting). Having the ability to make such an estimate permits the designer to select a section which will minimize this distress mode. A brief description of the appropriate "blocks" of Fig. 2 are included to illustrate the methodology.

Traffic (Block 1)

Vehicle (truck) characteristics required are: (1) axle and wheel loads; (2) spacing of dual tires; (3) numbers of repetitions of trucks in various categories; and (4) an estimate of lateral distribution.

The procedure is sufficiently general, provided the vehicles characteristics are known, so that it can be applied to airfield pavements, container transfer facilities, and parking areas as well.

Environment (Block 3)

Pavement temperatures are estimated from weather data using an available solution of the heat conduction equation (e.g., procedure developed by Barber (51)).

In addition, the effect of environment as it influences the water contents (or effective stresses) of the untreated materials in the pavement section can be considered. In non-frost areas estimates of the seasonal changes in water contents (or effective stresses) can be incorporated. In conditions where freezing and thawing occur, the work of Bergan (52) provides a means of defining the subgrade characteristics.

Structural Analysis (Block 9)

Stresses and deformations resulting from wheel loadings are estimated

ClibPDF - www.fastio.com

assuming the pavement to be represented as a layered elastic structure and the computer program ELSYM (53) is utilized.

Test Pavement Materials (Blocks 7 and 8)

To estimate the stresses and deformations, the "elastic" or stiffness characteristics of the materials comprising the pavement structures must be ascertained.

For untreated granular and fine-grained materials, resilient moduli determined from repeated load triaxial compression tests can be used (e.g. Ref. (28) contains suggested test procedures.) "Elastic" characteristics estimated by other procedures can also be utilized. For asphalt-bound materials stiffness characteristics, both as a function of time of loading and temperature, should be defined using one of the many availalbe procedures (1).

Distortion Prediction (Block 1)

To estimate the permanent deformation occurring in the pavement structure requires determination of some relationship between plastic (permanent) strain and applied stress, i.e.

$$\varepsilon^p = f(\sigma_{ij}) \tag{8}$$

for each of the components susceptible to rutting.

With such a relationship, the permanent deformation occurring in a particular layer is estimated from

$$\delta_i^p(x\ ,\ y) = \sum_{i=1}^{n} \left(\varepsilon_i^p \cdot \Delta z_i\right) \tag{9}$$

Total rut depth is estimated by summing the contributions from each layer.

Determine Distortion Characteristics (Block 10)

At this time it is recommended that the accumulation of permanent strain with repetitive loading be determined for the respective pavement materials by repeated load triaxial compression tests. Permanent strain at a point in the

ClibPDF - www.fastio.com

pavement structure in the vertical direction is, in turn, estimated using equation (22):

$$\varepsilon_z^p = R\left[\sigma_z - 1/2(\sigma_x + \sigma_y)\right] \tag{22}$$

For fine grained soils:

$$R_s = \frac{\ell}{1 - m\bar{\sigma}} \left(\frac{N}{N_o}\right)^b \tag{23}$$

For untreated granular materials:

$$R_g = \frac{1/K\sigma_3^n}{1 - \dfrac{\bar{\sigma}R_f(1 - \sin\phi)}{2(C \cdot \cos\phi + \sigma_3 \sin\phi)}} \cdot \left(\frac{N}{N_o}\right)^b \tag{24}$$

In the case of asphalt-bound materials, temperature and time of loading effects must also be incorporated as noted earlier, i.e.:

$$\frac{\partial R_b}{\partial t} = \delta(T) \cdot N^\alpha \cdot \bar{\sigma}^{n-1} \tag{25}$$

where:

(T) is a function of temperature T (absolute) with one form as:

$$\delta(T) = Te^{-A/T} \tag{26}$$

α, n, A = experimentally determined coefficients

For short times of loading the permanent vertical strain can be expressed as a linear function of loading time, e.g., Fig. 51 (54) permitting simplification of equation (25)*

---

*Recent data indicate that equation (25) is probably of the form:

$$\frac{\partial R_b}{\partial t} = \delta(T)N^\alpha\sigma^{n-1}t^\beta$$

For the short times of loading considered herein, the linear function is a reasonable approximation.

ClibPDF - www.fastio.com

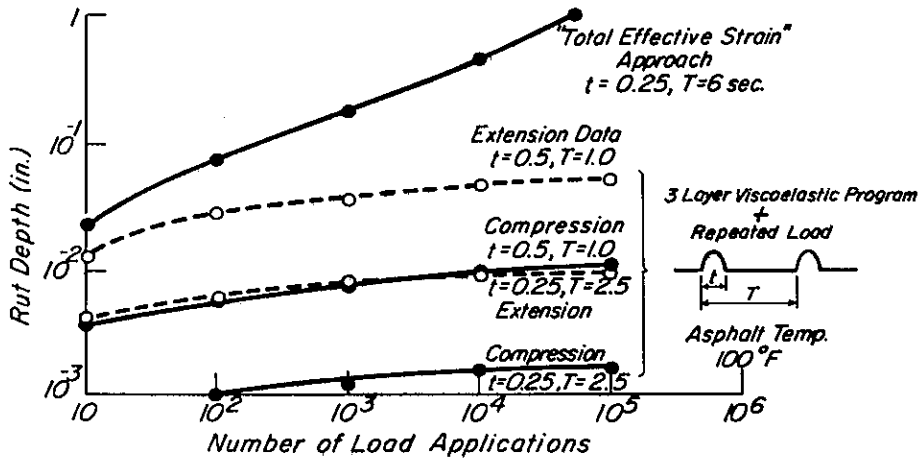

Fig. 50 - Comparison of rut depth predicted using the "total effective strain" approach with those predicted by the "3 layer viscoelastic" approach. (from Ref. (37)).

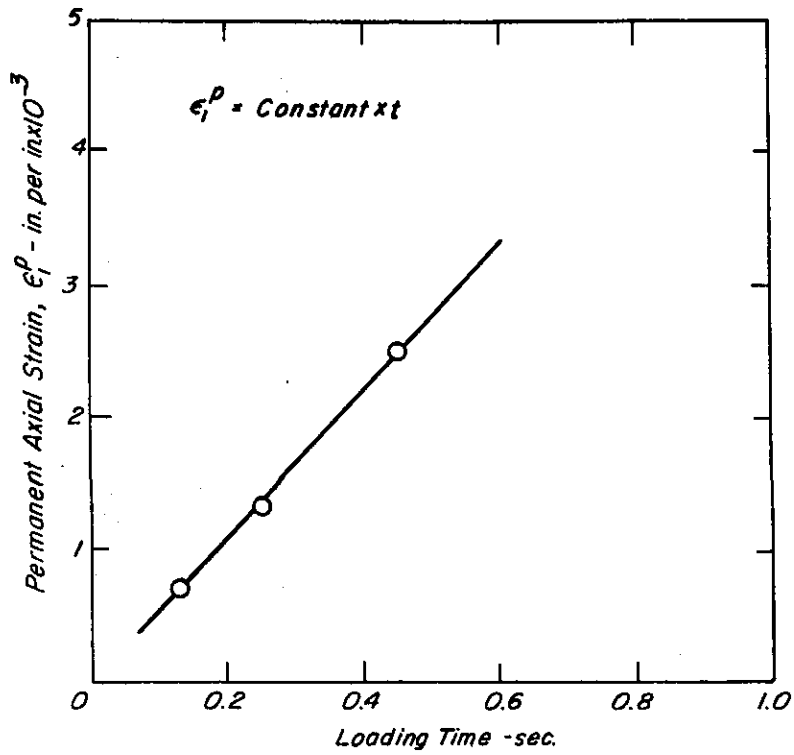

Fig. 51 - Relationship between permanent strain and time of loading; Watsonville aggregate and AR-4000 asphalt cement.

ClibPDF - www.fastio.com

Summary

By following the step by step procedure of Fig. 2 and using the deformation characteristics as well as the measured or estimated stiffness characteristics of the components, an estimate of the surface rutting can be ascertained. If this value is excessive, a second section is evaluated. This process is repeated until a section which produces a tolerable level of permanent deformation is obtained. Appendix C contains a computer program together with a user's guide to make this estimate.

RUTTING ESTIMATE FOR AN IN-SERVICE PAVEMENT

Using the procedure described in the previous section, the amount of rutting was estimated for an in-service pavement north of San Francisco, California, on which some rutting had been observed. This provided an opportunity to assess the potential usefulness of the proposed methodology.

Pavement Section

The pavement section consisted of a layer of asphalt concrete approximately 12 in. (305 mm) in thickness resting on a lime-treated subgrade. From laboratory repeated load tests a value of 10,000 psi (690 MN/m^2) was selected for the subgrade modulus.

For this analysis the asphalt concrete layer was subdivided into three layers. Traffic weighted mean stiffnesses (55) was estimated for each month throughout the year based on pavement temperatures computed from available weather data for the site. Resulting stiffnesses are shown in Table 19.

Loads applied to the pavement were estimated from traffic data supplied by CALTRANS together with wheel load factors based on 1966-68 California loadometer studies.

Distortion Characteristics - Asphalt Concrete

Laboratory repeated load triaxial compression tests were performed on cores taken from the pavement. Only one temperature, 100°F (38°C) was used since only a

ClibPDF - www.fastio.com

TABLE 19 - PAVEMENT STIFFNESS AND TEMPERATURE CONDITIONS

Month	Layer Number	Stiffness -psi*	Poisson's Ratio	Pavement Temperature °F	δ(T)
January	1	2251983.0	0.35	44.5	9.17×10^{-8}
	2	2300399.0	0.35	43.6	8.55×10^{-8}
	3	2314329.0	0.35	43.4	8.42×10^{-8}
	4	10000.0	0.47		
February	1	1896650.0	0.35	50.5	1.45×10^{-7}
	2	1949674.0	0.35	49.3	1.32×10^{-7}
	3	1967260.0	0.35	48.9	1.28×10^{-7}
	4	10000.0	0.47		
March	1	1752677.0	0.35	53.1	1.76×10^{-7}
	2	1822944.0	0.35	51.6	1.57×10^{-7}
	3	1847624.0	0.35	51.1	1.52×10^{-7}
	4	10000.0	0.47		
April	1	1473234.0	0.35	58.1	2.55×10^{-7}
	2	1595049.0	0.35	56.0	2.18×10^{-7}
	3	1631915.0	0.35	55.2	2.06×10^{-7}
	4	10000.0	0.47		
May	1	1123511.0	0.35	65.2	4.25×10^{-7}
	2	1236298.0	0.35	62.7	3.56×10^{-7}
	3	1291455.0	0.35	61.8	3.34×10^{-7}
	4	10000.0	0.47		
June	1	796965.0	0.35	73.0	7.37×10^{-7}
	2	864294.0	0.35	70.0	5.96×10^{-7}
	3	896390.0	0.35	68.9	5.53×10^{-7}
	4	10000.0	0.47		
July	1	436867.0	0.35	85.5	1.71×10^{-6}
	2	481359.0	0.35	80.8	1.25×10^{-6}
	3	520573.0	0.35	79.0	1.11×10^{-6}
	4	10000.0	0.47		
August	1	501140.0	0.35	82.3	1.38×10^{-6}
	2	553306.0	0.35	78.3	1.06×10^{-6}
	3	590288.0	0.35	76.8	9.55×10^{-7}
	4	10000.0	0.47		
September	1	769806.0	0.35	73.9	7.83×10^{-7}
	2	830136.0	0.35	70.9	6.35×10^{-7}
	3	858145.0	0.35	69.8	5.89×10^{-7}
	4	10000.0	0.47		
October	1	1194997.0	0.35	63.6	3.80×10^{-7}
	2	1293172.0	0.35	61.6	3.28×10^{-7}
	3	1340212.0	0.35	60.9	3.13×10^{-7}
	4	10000.0	0.47		
November	1	1766905.0	0.35	52.8	1.72×10^{-7}
	2	1817145.0	0.35	51.7	1.58×10^{-7}
	3	1833969.0	0.35	51.3	1.54×10^{-7}
	4	10000.0	0.47		
December	1	2226274.0	0.35	44.9	9.46×10^{-8}
	2	2263296.0	0.35	44.2	8.97×10^{-8}
	3	2272951.0	0.35	44.0	8.83×10^{-8}
	4	10000.0	0.47		

*Stiffness in $MN/m^2 = 6.9 \times 10^{-3}$ (stiffness in psi)

ClibPDF - www.fastio.com

limited number of cores (four) were obtained. These first results are shown in Fig. 52. The influence of temperature was ascertained from tests on a similar mix, data for which were reported in TE 73-5.

Analysis of the asphalt concrete mixture data reported in TE 73-5 suggested constitutive relationship between permanent strain and stress of the form:

$$\log 3/2\ \bar{\varepsilon}^{p} = \log B + n \operatorname{Log} \bar{\sigma} \tag{27}$$

where

$\bar{\varepsilon}^{p}$, $\bar{\sigma}$ = effective permanent strain and equivalent stress respectively

n = laboratory determined coefficient (0.72 - 0.82 for data in TE 73-5)

B = laboratory determined coefficient dependent on temperature, number of stress applications, N , and mixture structure.

Data obtained at temperatures of 67° (19°C), 85°(39°C), and 100F (39°C) are shown in Figs. 53-55.

At this time it is suggested that the coefficient B might be expressed in terms of the above noted variables as:

$$B = DTN^{\alpha} e^{-A/T} \tag{28}$$

where

T = temperature (absolute)

N = number of stress applications

α, D, A = experimentally determined coefficients

Plotting the data of Figs. 53, 54, and 55 as shown in Figs, 56 and 57 permits estimate of these coefficients:

ClibPDF - www.fastio.com

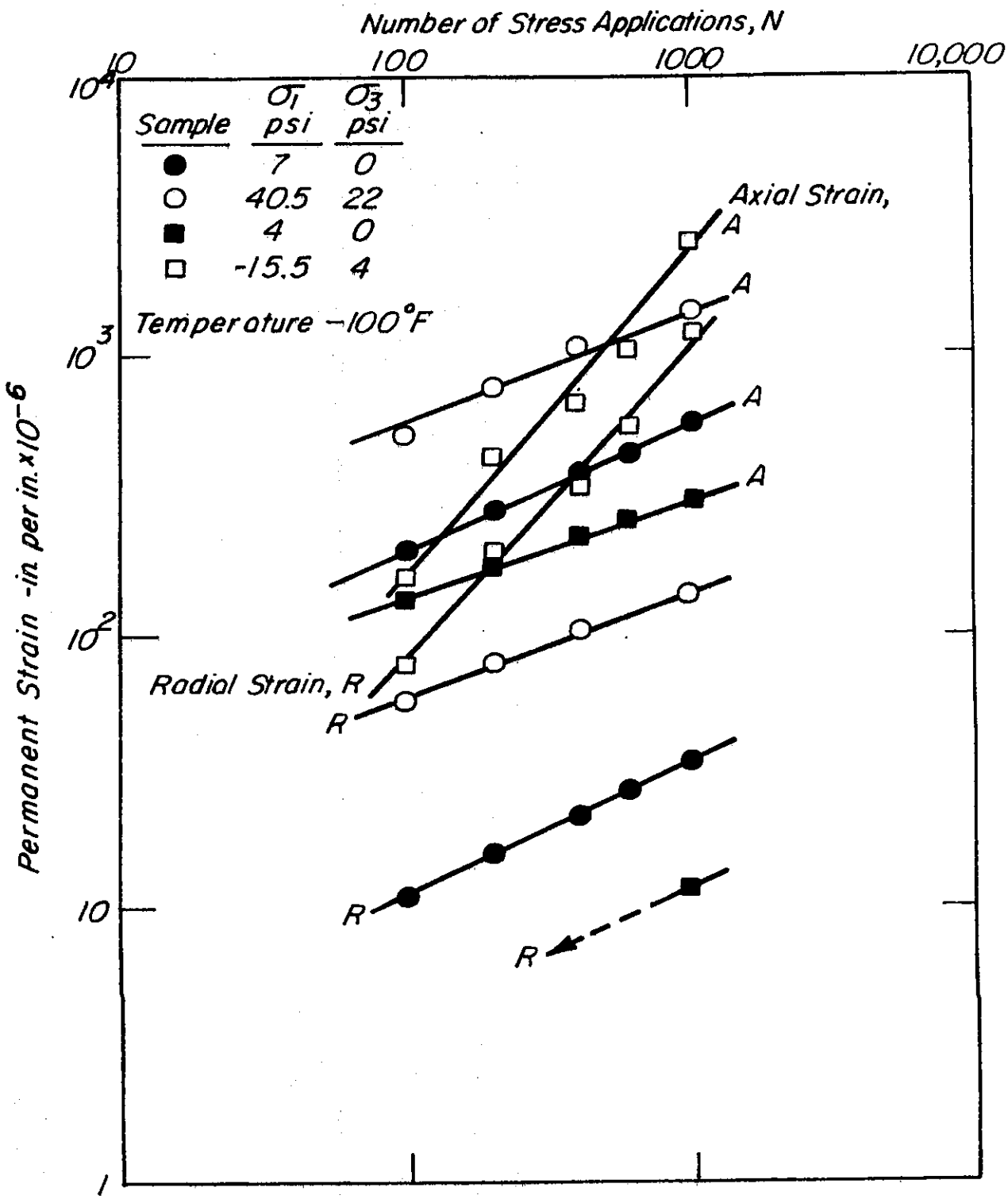

Fig. 52 - Permanent strain vs. stress application data - Cloverdale core specimens.

ClibPDF - www.fastio.com

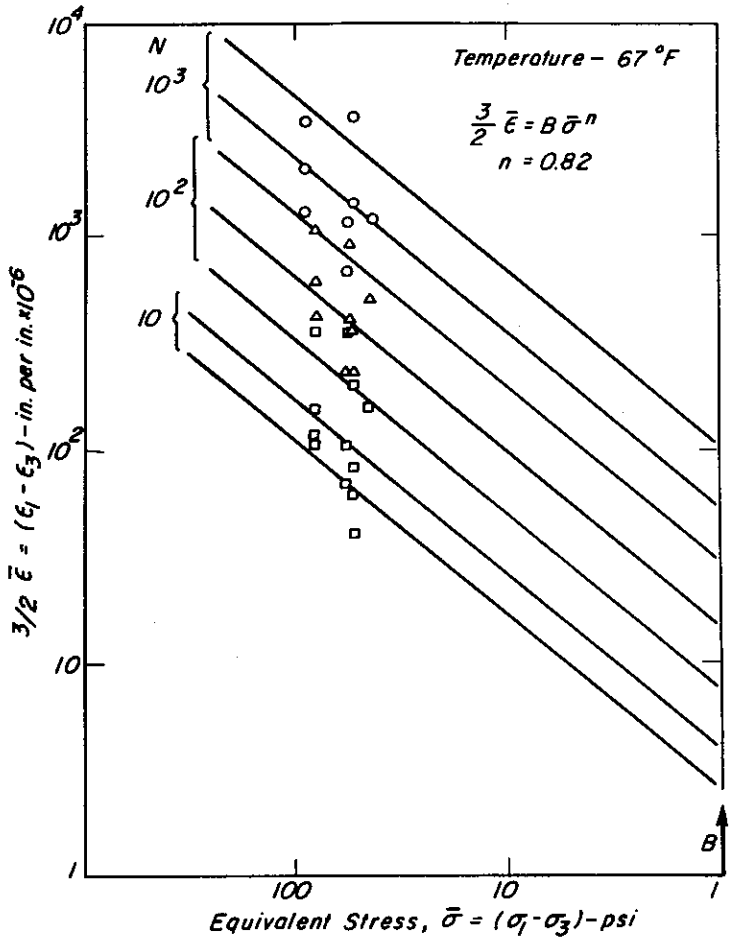

Fig. 53 - Relationship between effective strain and equivalent stress, Watsonville granite and 85/100 pen. asphalt cement; temperature 67°F.

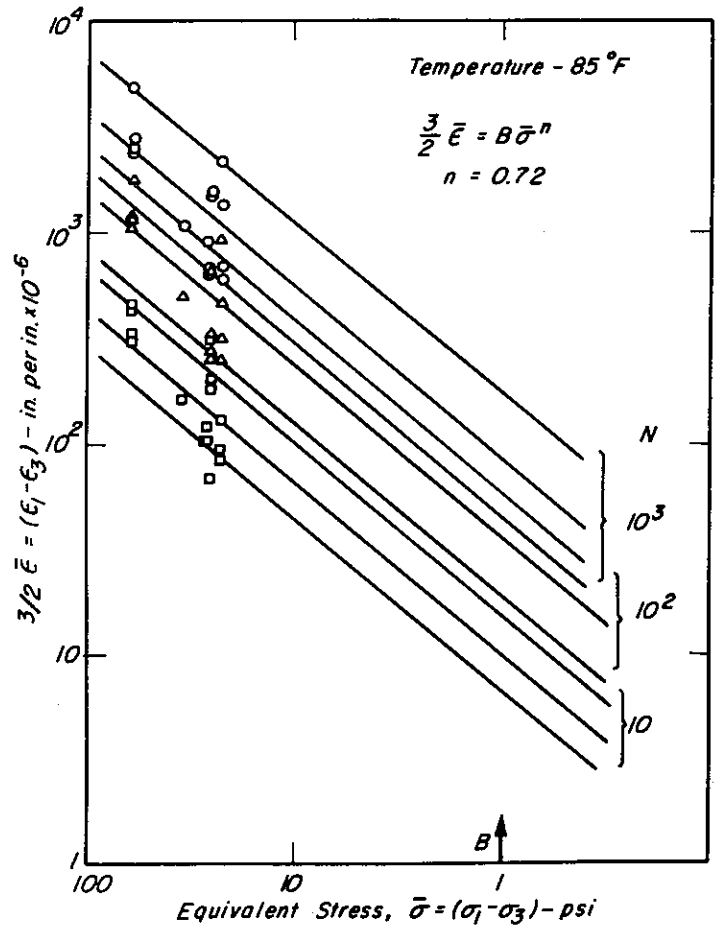

Fig. 54 - Relationship between effective strain and equivalent stress, Watsonville granite and 85/100 pen. asphalt cement; temperature 85°F.

ClibPDF - www.fastio.com

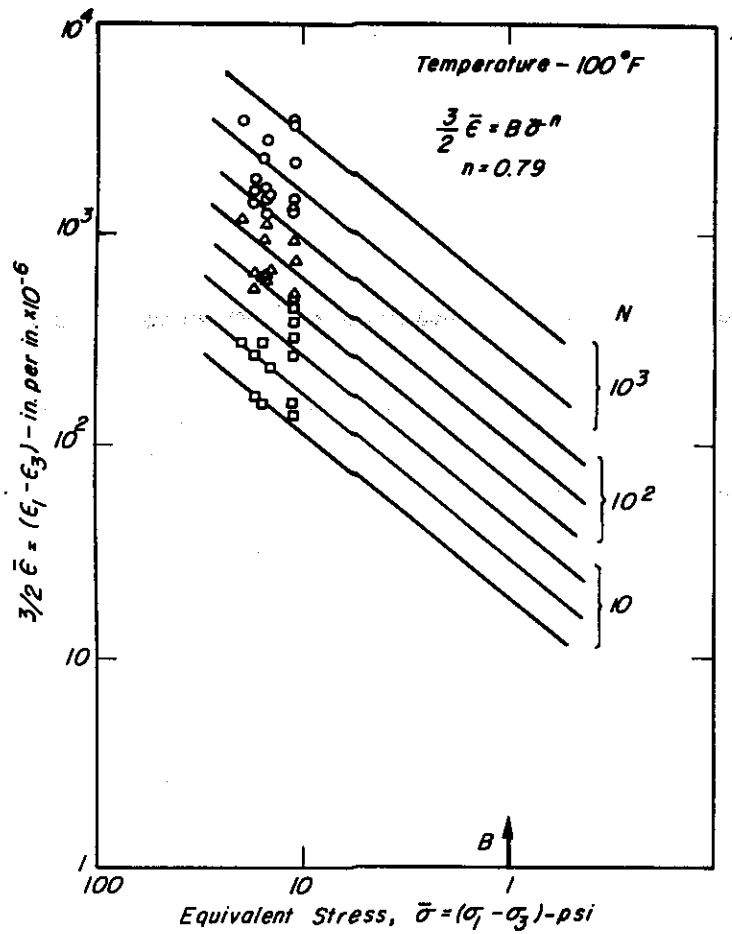

Fig. 55 - Relationship between effective strain and equivalent stress, Watsonville granite and 85/100 pen. asphalt cement; temperature 100°F.

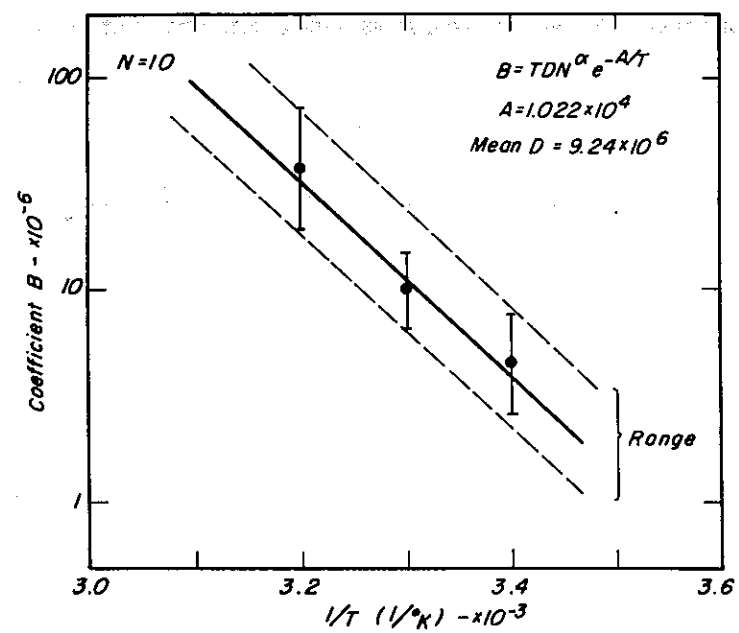

Fig. 56 - Relationship between coefficient B and temperature expressed in term of 1/T; data corresponding to N=10 stress applications.

ClibPDF - www.fastio.com

estimate of these coefficients:

$$D = 9.24 \times 10^6 \text{ (Fig. 56)} ;$$

$$A = 1.02 \times 10^4 \text{ (Fig. 56)} ;$$

$$\alpha = 0.44 \text{ (Fig. 57)}$$

Fig. 58 illustrates the relationship between equivalent stress and strain for the core specimens tested 100°F (39°C) and at a time of loading of 0.07 sec. Similarly: Fig. 59 illustrates the relationship between the coefficient B and the number of stress repetitions. For this mix the values required for equation (25) were determined to be

$n = 0.94$

$\alpha = 0.44$

$A = 1.06 \times 10^4$ (obtained with $D = 9.24 \times 10^6$; i.e., using the value obtained from data presented in Figs. 53 through 55.

Rutting Estimate

Stresses were determined using the ELSYM program assuming the various loads to be applied by dual tires. Permanent strains were estimated from equation (25) assuming a linear dependency on time of loading; this resulted in R having the form:

$$R = \delta(T)N^{\alpha}\bar{\sigma}^{n-1}t \qquad (29)$$

where:

t = time of loading, sec.

Table 20 contains the results of the computations for each month; the values for permanent deformation, corresponding to a time of loading of 0.07 sec., are the maximum occurring in the area between the centerline of the dual tires and the center of one of the tires. The total estimated permanent deformation is 0.93 in. (23.6 mm).

ClibPDF - www.fastio.com

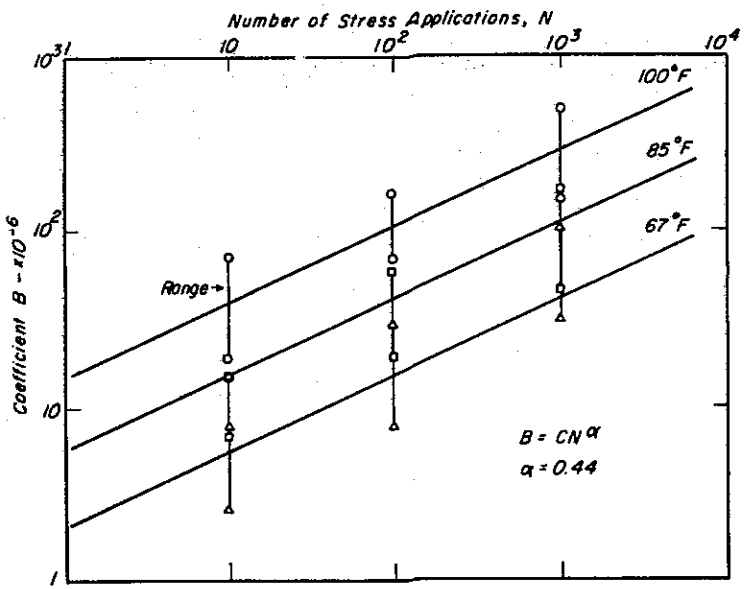

Fig. 57 - Influence of number of stress applications on coefficient B.

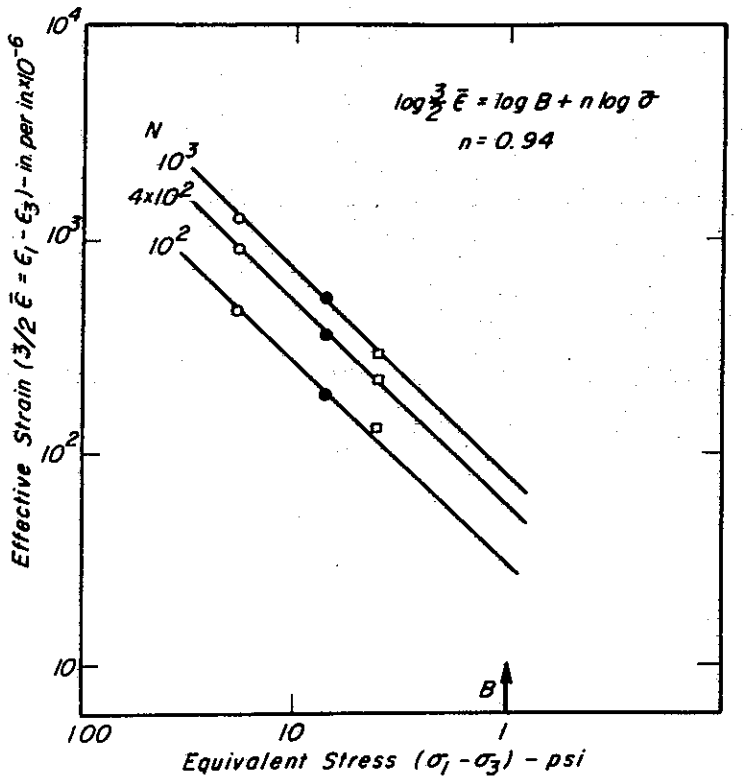

Fig. 58 - Relationship between effective strain and equivalent stress, Cloverdale core specimens; temperature 100°F

ClibPDF - www.fastio.com

TABLE 20 - COMPUTED PERMANENT DEFORMATION

Month	Average Air Temp. °F	Permanent Deformation - in. × 10^{-3} Specific Axle Loads				
		16 - 20^k	8 - 16^k	7 - 8^k	3 - 7^k	< 3^k
January	42.4	.3938	4.98	3.184	5.50	2.15
February	47.2	.4003	5.04	3.21	5.53	2.17
March	48.2	.81	10.14	6.44	11.09	4.35
April	50.6	.81	11.14	7.34	13.19	5.08
May	56.1	1.47	19.09	12.31	21.51	8.38
June	62.4	2.26	33.28	20.85	36.30	14.15
July	66.8	5.79	74.82	46.63	82.40	31.93
August	66.6	4.91	63.15	39.34	69.20	26.86
September	62.9	2.66	34.56	21.81	38.48	14.92
October	57.0	1.26	16.61	10.70	18.94	7.34
November	49.4	.81	3.88	6.44	11.08	4.34
December	43.4	.39	4.98	3.19	5.49	2.15
	Subtotal	22.3	281.6	181.4	318.7	128.8
Σ for all loads = 928 × 10^{-3} in.*						

*To convert deflection in inches to deflection in mm, multiply by 25.2.

ClibPDF - www.fastio.com

For the site under investigation the speed limit is 25 mph and rutting is reported within 100 ft. of a traffic signal. Assuming an average speed of 20 mph, the loading time in the field is estimated to be approximately 0.03 sec. Thus the amount of rutting would be 3/7 of the value shown in Table 2, i.e., about 0.4 in. (10 mm).

Rut depth measured at the site was approximately 0.5 in. (13 mm). It would thus appear that the methodology has the potential to provide rutting estimates so long as appropriate material characteristics and climate and traffic data are available.

EXAMPLE OF RUT DEPTH PREDICTION

The field example used to illustrate the potential applicability of the procedure consisted of a full-depth asphalt concrete pavement section. In this section a brief description is included of the applicable procedure to predict rutting in a pavement with an asphalt concrete surface, a granular base, and a fine-grained soil subgrade. Requisite characteristics of the various materials required for the analysis are shown in Table 21.

Coefficients for the asphalt concrete were estimated from data like that shown in Figs. 53-55. Values for stiffnesses of the various layers are shown in Fig. 60. From the repeated load triaxial compression tests, some reduction in the stiffness was observed with increased number of stress applications; this stiffness decrease was incorporated in the analysis.

While there are no field results for comparison, the example presented illustrate that "reasonable" results are obtainable, i.e., the form of the relationships appear reasonable.

EFFECT OF MIX VARIABLES ON RUTTING

In an earlier investigation (reported in TE 70-5) it was suggested that to improve fatigue resistance in thick asphalt bound layers it would appear worthwhile to increase the asphalt content of the mix in the base above that

ClibPDF - www.fastio.com

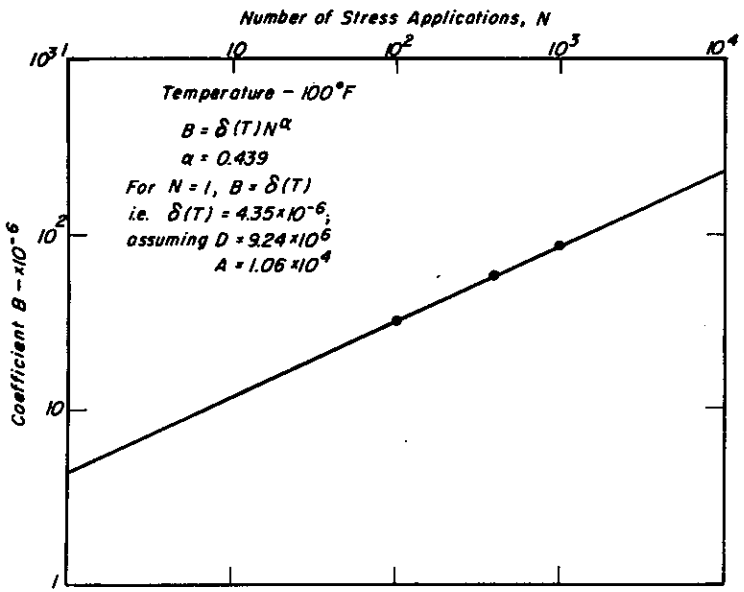

Fig. 59 - Relationship between coefficient B and number of stress applications; Cloverdale specimens.

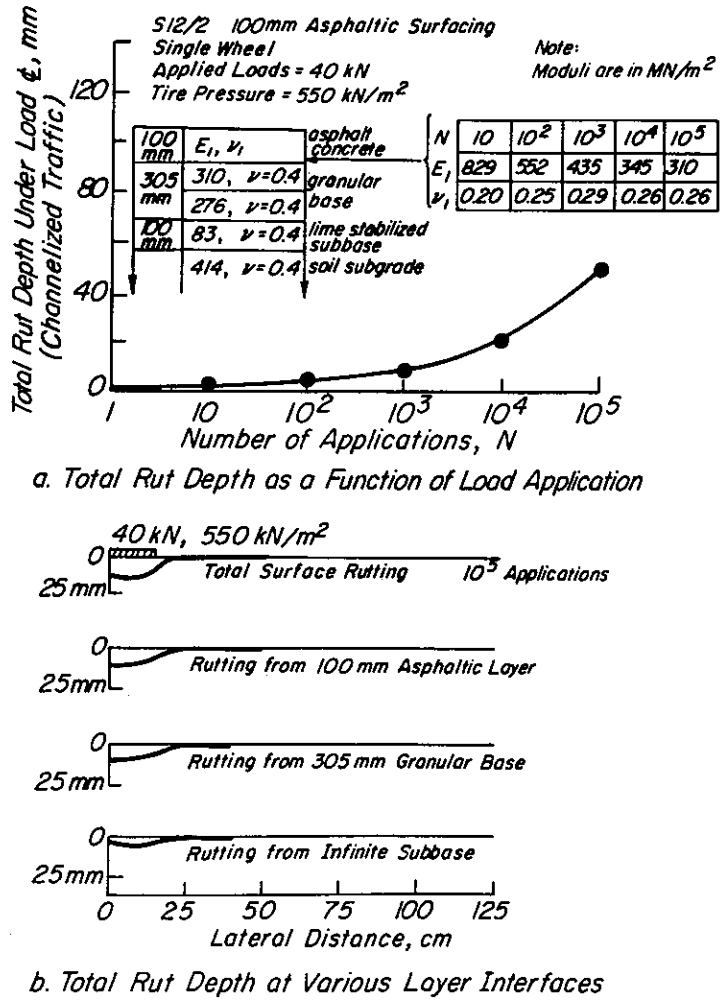

Fig. 60 - Estimated rutting in experimental test road.

ClibPDF - www.fastio.com

in the surface course. This recommendation was based on the observed improved performance of mixes containing asphalt contents slightly in excess of those resulting from the California mix design procedure (up to 1 percent greater).

It was not possible in this investigation to establish the influence of the increased asphalt content on rutting potential due to time limitations. The procedure illustrated in the previous two sections does permit the influence of this variable to be investigated so long as the appropriate laboratory test data have been obtained. An investigation of this type would be a worthwhile additional study.

SUMMARY

From a design standpoint, the procedure for limiting the rutting to some prescribed amount based on limiting subgrade strain criteria would appear to be a procedure which could be used with some confidence at this time since the criteria have been developed from analyses of existing design procedures as well as field trials.

The methodology described to estimate the actual amount of rutting from laboratory repeated load tests together with elastic theory requires field documentation before such methodology can be used with confidence. Nevertheless, while there are some limitations to this approach, e.g., the effects of lateral load placement are not considered; nor are the reversals of shear stress which may take place with load passage and lateral distribution, the methodology does produce results which are "reasonable" in form. Moreover, a limited comparison indicates that the procedure can predict permanent deformations of the right order of magnitude. Accordingly, it is suggested that such methodology can be used for special situations to check whether or not rutting from repeated traffic loading will be of sufficient magnitude to cause concern; if such is the case, the design can be modified to insure that deformations do not exceed some reasonable prescribed amount.

ClibPDF - www.fastio.com

TABLE 21- MATERIAL CONSTANTS USED IN RUT DEPTH CALCULATIONS

Material Type	K Coeff.	n	C psi (R_f = 1)	ϕ	b	N_o	R_f
Subgrade Soil	20,400	0	6.05	0	0.24	1.0×10^4	0.75 → 1.0
Granular Base	8,800	0.108	0	50.1	0.15	1.0×10^5	0.75 → 1.0

K and n in relationship $K\sigma^n$, C = cohesion, ϕ = angle of internal friction.

Material Type	T, °F	δ(T) max	δ(T) min	δ(T) mean	n	α
Asphalt Concrete	100	1×10^{-4}	2×10^{-4}	1.5×10^{-4}	0.335	0.457

Coefficients for equation (25).

ClibPDF - www.fastio.com

ACKNOWLEDGMENTS

The authors wish to acknowledge support provided this project by the Institute of Transportation Studies (formerly ITTE) of the University of California in the form of shop, office, and research facilities.

This report was prepared in cooperation with the State of California Business and Transportation Agency Department of Transportation and the U. S. Department of Transportation Federal Highway Administration.

The contents of this report reflect the views of the author who is responsible for the facts and accuracy of the data presented herein. The contents do not necessarily reflect the official views or policies of the State of California or the Federal Highway Administration. This report does not constitute a standard, specification, or regulation.

ClibPDF - www.fastio.com

REFERENCES

1. Monismith, C.L., et al., "Asphalt Mixture Behavior in Repeated Flexure," Report No. TE 70-5, University of California, Berkeley, California, December 1970.

2. Deacon, J.A., "Fatigue Life Prediction," Structural Design of Asphalt Concrete Pavements to Prevent Fatigue Cracking," Special Report No. 140, Highway Research Board, Washington, D.C., 1973.

3. Finn, F.N., K. Nair, and J. Hilliard, "Minimizing Premature Cracking of Asphalt Concrete Pavements," Final Report, Project 9-4, National Cooperative Highway Research Program, Highway Research Board, Washington, D.C., February 1973.

4. Heukelom, W., and A.J.G. Klomp, "Road Design and Dynamic Loadings," Proceedings, Association of Asphalt Paving Technologists, Vol. 33, 1964, pp. 92-125.

5. Kinghan, R.I., "Failure Criteria Developed from AASHO Road Test Data," Structural Design of Asphalt Concrete Pavements to Prevent Fatigue Cracking, Special Report No. 140, Highway Research Board, Washington, D.C., 1973.

6. Pell, P.S., and S.F. Brown, "The Characteristics of Materials for the Design of Flexible Pavement Structures," Proceedings, Third International Conference on the Structural Design of Asphalt Pavements, London, 1972, Vol. 1, University of Michigan, Ann Arbor, 1972.

7. Santucci, L.E., "Thickness Design Procedure for Asphalt and Emulsified Asphalt Mixes," paper presented at meeting of Committee A2B02 - Flexible Pavement Design, Transportation Research Board, January 1975.

8. van Dijk, W., "Practical Fatigue Characterization of Bituminous Mixes," Proceedings, The Association of Asphalt Paving Technologists, Vol. 44, Minneapolis, Minnesota, 1975, pp. 38-74.

9. Pell, P.S., "Characterization of Fatigue Behavior," in Structural Design of Asphalt Concrete Pavement Systems to Prevent Fatigue Cracking, Highway Research Board, Washington, D.C., 1973, pp. 49-64 (Special Report 140).

10. Verstraeten, J., "Moduli and Critical Strains in Repeated Bending of Bituminous Mixes - Application to Pavement Design," Proceedings, Third International Conference on the Structural Design of Asphalt Pavements, London, 1972, Vol. 1, University of Michigan, Ann Arbor, Michigan, 1972, pp. 729-738.

11. Pell, P.S., and K.E. Cooper, "The Effect of Testing and Mix Variables on the Fatigue Performance of Bituminous Materials," Proceedings, The Association of Asphalt Paving Technologists, Vol. 44, Minneapolis, Minnesota, 1975, pp. 1-37.

12. Epps, J., Influence of Mixture Variables on the Flexural Fatigue and Tensile Properties of Asphalt Concrete, Ph.D. Dissertation, University of California, Berkeley, 1968.

13. Pell, P.S., Discussion of paper by Lister and Powell in Proceedings, The Association of Asphalt Paving Technologists, Vol. 44, Minneapolis, Minnesota, 1975, pp. 111-114.

ClibPDF - www.fastio.com

14. Heukelom, W., "An Improved Method of Characterizing Asphaltic Bitumens with the Aid of their Mechanical Properties," Proceedings, The Association of Asphalt Paving Technologists, Vol. 42, pp. 67-98.

15. Dorman, G.M., and C.T. Metcalf, "Design Curves for Flexible Pavements Based on Layered System Theory," Highway Research Board, Highway Research Record, No. 71, Washington, D.C., 1965.

16. The Asphalt Institute, Full Depth Asphalt Pavements for Air Carrier Reports, College Park, Maryland, 1973 (Manual Series No. 11).

17. Brown, S.F., and P.S. Pell, "A Fundamental Structural Design Procedure for Flexible Pavements," Proceedings, Third International Conference on the Structural Design of Asphalt Pavements, University of Michigan, 1972.

18. Witczak, M.W., Asphalt Pavement Performance at Baltimore-Washington International Airport, The Asphalt Institute, College Park, Maryland, 1974 (Research Report 74-2).

19. Dehlen, G.L., The Effect of Non-Linear Materials Response on the Behavior of Pavements Subjected to Traffic Loads, thesis presented to the University of California, at Berkeley, California, in 1969, in partial fulfillment of the requirements for the degree of Doctor of Philosophy.

20. Nunn, M.E., "Theoretical Evaluation of the Effect of Temperature on the Fatigue Behavior of Bituminous Road-Bases," TRRL Report LR 594, Transport and Road Research Laboratory, Great Britain, 1973.

21. Peutz, M.G.F., H.P.M. van Kempen, and A. Jones, "Layered Systems under Normal Surface Loads," Highway Research Record No. 228, Highway Research Board, Washington, D.C., 1966.

22. Nijboer, L.W., Plasticity as a Factor in the Design of Dense Bituminous Carpets, Elsevier Publishing Co., New York, 1948.

23. Saal, R.N.J., "Mechanics of Technical Applications of Asphalt," Proceedings, Symposium of Fundamental Nature of Asphalt, American Chemical Society, 1960.

24. California Division of Highways, "Test Method No. Calif. 301-F," Materials Manual, Vol. 1, Sacramento, 1964.

25. U.S. Army Corps of Engineers, Flexible Airfield Pavements, Washington, D.C., U.S. GPO, 1957 (Document TM5-824-2).

26. Smith, V.R., "Triaxial Stability Methods for Flexible Pavement Design," Proceedings, The Association of Asphalt Paving Technologists, Vol. 18, 1949, pp. 63-94.

27. Monismith, C.L., and Y.M. Salam, "Distress Characteristics of Asphalt Concrete Mixes," Proceedings, The Association of Asphalt Paving Technologists, Vol. 42, 1973, pp. 320-350.

28. Monismith, C.L., and D.B. McLean, Design Considerations for Asphalt Pavements, Report No. TE 71-8, Berkeley, University of California, Institute of Transportation and Traffic Engineering, 1971.

ClibPDF - www.fastio.com

29. Monismith, C.L., D.B. McLean, and N. Ogawa, Design Considerations for Asphalt Pavements, Report No. TE 73-5, University of California, Institute of Transportation and Traffic Engineering, December 1973.

30. Hicks, R.G., and F.N. Finn, "Prediction of Pavement Performance from Calculated Stresses and Strains at the San Diego Test Road," Proceedings, The Association of Asphalt Paving Technologists, Vol. 43, 1974, pp. 1-40.

31. Heukelom, W., and A.J.G. Klomp, "Consideration of Calculated Strains at Various Depths in Connection with the Stability of Asphalt Pavements," Proceedings, Second International Conference on the Structural Design of Asphalt Pavements, University of Michigan, 1967.

32. Barksdale, R.D., "Laboratory Evaluation of Rutting in Base Course Materials," Proceedings, Third International Conference on the Structural Design of Asphalt Pavements, University of Michigan, 1972.

33. Romain, J.E., "Rut Depth Prediction in Asphalt Pavements," Proceedings, Third International Conference on the Structural Design of Asphalt Pavements, University of Michigan, 1972.

34. van de Loo, P.J., "A Practical Approach to the Prediction of Rutting in Asphalt Pavements, the Shell Method," paper presented at annual meeting of Transportation Research Board, Washington, D.C., January 1976.

35. Morris, J., R.C.G. Hass, P. Reilly, and E.T. Hignell, "Permanent Deformation in Asphalt Pavements can be Predicted," Proceedings, The Association of Asphalt Paving Technologists, Vol. 43, 1974, pp. 41-76.

36. McLean, D.B., and C.L. Monismith, "Estimation of Permanent Deformation in Asphalt Concrete Layers Due to Repeated Traffic Loading," Transportation Research Record No. 510, pp. 14-30, Washington, D.C., Highway Research Board, 1975.

37. Freeme, C.R., and C.L. Monismith, "The Analysis of Permanent Deformation in Asphalt Concrete Pavement Structures," Proceedings, Second Conference on Asphalt Pavements for Southern Africa, 1974.

38. Snaith, M.S., Deformation Characteristics of Dense Bitumen Macadam Subjected to Dynamic Loading, Ph.D. Thesis, University of Nottingham, 1973.

39. Brown, S.F., and M.S. Snaith, "The Permanent Deformation Charactersitics of a Dense Bitumen Macadam Subjected to Repeated Loading," Proceedings, The Association of Asphalt Paving Technologists, Vol. 43, pp. 224-252.

40. Brown, S.F., A.K.F. Lashine, and A.F.L. Hyde, "Repeated Load Triaxial Testing of a Silty Clay," Geotechnique, Vol. 25, No. 1, 1975, pp. 95-114.

41. Monismith, C.L., N. Ogawa, and C.R. Freeme, "Permanent Deformation Characteristics of Subgrade Soils in Repeated Loading," Transportation Research Record No. 537, Transportation Research Board, 1975, pp. 1-17.

ClibPDF - www.fastio.com

42. Hofstra, A., and A.J.G. Klomp, "Permanent Deformation of Flexible Pavements under Simulated Road Traffic Conditions," Proceedings, Third International Conference on the Structural Design of Asphalt Pavements, University of Michigan, 1972.

43. Hills, J.F., D. Brien, and P.J. van de Loo, The Correlation of Rutting and Creep Tests in Asphalt Mixes, Paper IP-74-001, London?, Institute of Petroleum, 1974.

44. van de Loo, P.J., "Creep Testing, a Simple Tool to Judge Asphalt Mix Stability," Proceedings, The Association of Asphalt Paving Technologists, Vol. 43, 1974.

45. Chomton, C., and P.J. Valayer, "Applied Rheology of Asphalt Mixes--Practical Application," Proceedings, Third International Conference on the Sturctural Design of Asphalt Pavements, University of Michigan, 1972, pp. 214-225.

46. Ugé, P., and P.J. van de Loo, "Permanent Deformation of Asphalt Mixes," Proceedings, Canadian Technical Asphalt Association, 1974.

47. Barksdale, R.D., and G.A. Leonards, "Predicting Performance of Bituminous Surface Pavements," Proceedings, Second International Conference on the Structural Design of Asphalt Pavements, University of Michigan, 1967, pp. 321-340.

48. Elliott, J.F., and F. Moavenzadeh, "Moving Load on Viscoelastic Layered System-Phase II, " Cambridge, Massachusetts, M.I.T., Dept. of Civil Engineering, Materials Division, 1969 (Report No. R-69-64).

49. Elliott, J.F., and F. Moavenzadeh, and H. Findakly, "Moving Load on Viscoelastic Layered Systems, Phase II - Addendum," Cambridge, Massachusetts, M.I.T., Dept. of Civil Engineering, April 1970 (Research Report R70-20).

50. Kenis, W.J., and T.F. McMahon, Advance Notice of FHWA Pavement Design System and a Design Check Procedure, prepared for presentation of AASHO Design Committee Meeting, October 1972.

51. Barber, E.S., "Calculation of Maximum Pavement Temperatures from Weather Reports," Bulletin 168, Highway Research Board, Washington, D.C., 1957, pp. 1-8.

52. Bergan, A.T., Some Considerations in the Design of Asphalt Pavements for Cold Regions, Ph.D. Dissertation, University of California, Berkeley, 1972.

53. Ahlborn, G., ELSYM 5, Computer Program for Determining Stresses and Deformation in a Five-Layer Elastic System, University of California, Berkeley.

54. McLean, D.B., Permanent Deformation Characteristics of Asphalt Concrete, Ph.D. Dissertation, University of California, Berkeley, November 1974.

55. Kasianchuk, D.A., Fatigue Considerations in the Design of Asphalt Concrete Pavements, Ph.D. Dissertation, University of California.

56. Monismith, C. L., D. McLean, and R. Yüce, Design Considerations for Asphalt Pavements, Report No. TE 72-4, University of California, Institute of Transportation and Traffic Engineering, 1972.

ClibPDF - www.fastio.com

APPENDIX A

FATIGUE AND STIFFNESS TESTS - INDIO PROJECT

Included is a summary of stiffness and controlled-stress flexural fatigue test results obtained from tests on beams which had been cut from 12 in. (305 mm) diameter cores obtained from the Indio project by the Transportation Laboratory. The cores were obtained in December 1971.

Sample Data

Table A1 shows site number designations attached to the cores as well as the corresponding core locations and sample admission numbers.

Each core was split in the field to separate the surface course layer from the base course. The surface course layer was identified by its sample admission number and the letter A.

As a first step in sawing the cores, the base course was cut in a horizontal plane yielding two cylinders, each approximately three inches in thickness. These cylinders were identified by their sample admission numbers followed by the letter B for the upper section and the letter C for the lower section. The central portion of each cylinder was removed by diamond sawing. These cuts were made in a direction parallel to traffic, identified by arrows on the cores. Beam specimens approximately 1.5 in. (38 mm) square and 12 in. (305 mm) in length were then obtained from the central section two beams from the A portion and four from each of the B and C sections. The remaining portions of each of the cylinders were returned to the Materials and Research Department for extraction and recovery and tests on the extracted asphalt. Table A2 shows the correspondence between the numbers on the extraction samples and those for the beams.

Bulk specific gravity for each beam specimen was determined by weighing it in air and water. Air void contents were determined for each beam using

ClibPDF - www.fastio.com

the measured values of specific gravity and the following information supplied by the Transportation Laboratory:

Pavement Component	Asphalt Content Percent	Specific Gravity of Aggretate
surface course	4.9	2.67
base course	4.4	2.67

To compute section moduli for each beam specimen, average beam dimensions were determined. Because of the comparatively low asphalt contents and the large maximum size of the aggregate relative to the beam dimensions, considerable erosion of fines in some of the specimens resulted during trimming from the action of the cooling water. Accordingly, cross-sections of a number of the beam specimens were not well defined.

Test Programs

A total of 60 beams were obtained from the six cores; twelve from the surface course and 48 from the base course (specimen no. N2-10 broke before testing). Surface course specimens were each tested at three temperatures, 81, 66, and 42°F (27, 19, 5°C) and at three stress levels at each temperature. One load duration (0.1 sec) and one frequency of loading (100 repetitions per minute) were used.

The base course beams were divided into six groups of eight specimens. Each group exhibited approximately the same mean air void content to facilitate comparisons of average test results. Three of the six groups were tested in fatigue at 66°F (19°C) and stress levels of 150, 100, and 75 psi (1,035 to 520 KN/m^2) while the remaining three groups were tested at 81°F (27°C) and stress level of 100, 75, and 50 psi (690 to 350 KN/m^2). Load duration and frequency were 0.1 sec and 100 repetitions per min respectively.

ClibPDF - www.fastio.com

Tests Results

Surface Course. Stiffness measurements are summarized in Table A3. Each stiffness represents the mean value for the three applied stresses. Stiffnesses are also plotted as a function of air void content, Fig. A1; variation in stiffness due to stress level can also be noted in this figure.

Base Course. Results of fatigue tests on the base course are summarized in Table A4. These results have been plotted as bending stress vs. repetitions to failure in Fig. A2 and initial bending vs. repetitions to failure in Fig. A3.

Linear (log-log) least squares regression lines have been fit to the data and are also shown in the figures. In Fig. A3 the fatigue line obtained from the general diagram (TE 70-5) and corresponding to a stiffness of 400,000 psi (2,760 MN/m^2) has been plotted for comparison purposes. Adjustments for void content and asphalt content would shift this relationship to the left somewhat.

Some attempt has also been made to define the influence of void content on fatigue life for the base course mixture. Generally, the results indicate considerable scatter.

Overall, the results indicate more scatter than results obtained for specimens prepared in the laboratory. This is probably due in part to the aggregate size relative to the specimen size and the inherent variability developed during the construction process.

In the future it would appear desirable to test specimens 3 in. (75 mm) by 3 in. (75 mm) in cross-sectional area. This in turn will require a sampling procedure similar to that used for the Gonzales, Morro Bay, and Folsom projects.

ClibPDF - www.fastio.com

TABLE A1- CORE LOCATIONS - INDIO PROJECT

Site No.	Location	Sample Admission No.
1	STA 983 + 10	8062
2	STA 983 + 25	8063
3	STA 983 + 40	8064
4	STA 983 + 60	8065
5	STA 983 + 75	8066
6	STA 983 + 90	8067

ClibPDF - www.fastio.com

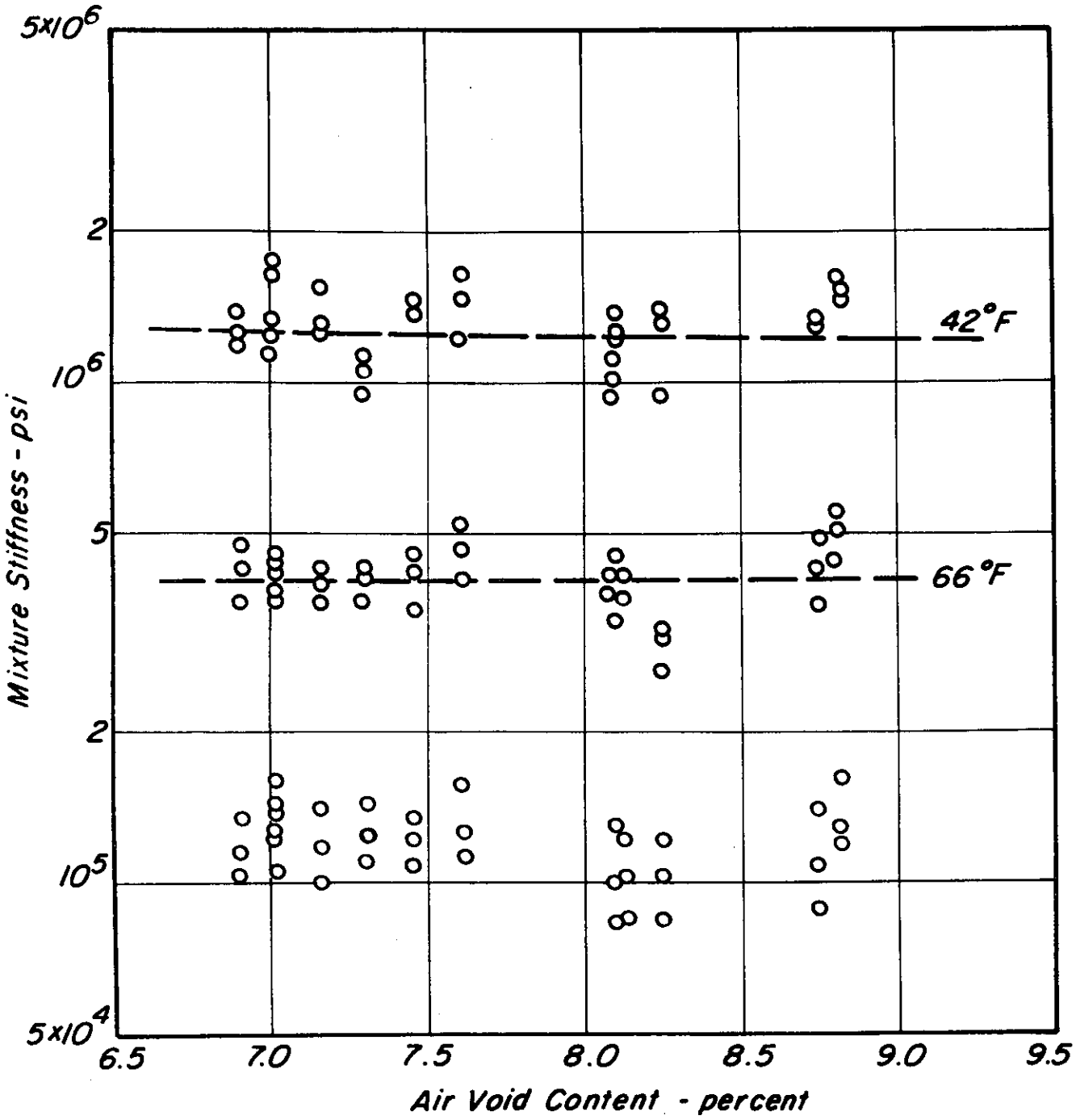

Fig. A-1 - Mixture stiffness vs. air void content for surface course mixture - Indio project.

ClibPDF - www.fastio.com

TABLE A2 - SAMPLE DESIGNATIONS

Site No.	Extraction Sample No.	Beam Sample Designation
1	8062A 8062B 8062C	N - 1 - 1, 2* N - 1 - 3, 4, 5, 6 N - 1 - 7, 8, 9, 10
2	8063A 8063B 8063C	N - 2 - 1, 2 N - 2 - 3, 4, 5, 6 N - 2 - 7, 8, 9, 10
3	8064A 8064B 8064C	N - 3 - 1, 2 N - 3 - 3, 4, 5, 6 N - 3 - 7, 8, 9, 10
4	8065A 8065B 8065C	N - 4 - 1, 2 N - 4 - 3, 4, 5, 6 N - 4 - 7, 8, 9, 10
5	8066A 8066B 8066C	N - 5 - 1, 2 N - 5 - 3, 4, 5, 6 N - 5 - 7, 8, 9, 10
6	8067A 8067B 8067C	N - 6 - 1, 2 N - 6 - 3, 4, 5, 6 N - 6 - 7, 8, 9, 10

*N - 1 - 1 - 10
(Indio) (Site No.) (Sample No.)

ClibPDF - www.fastio.com

TABLE A3 - STIFFNESS TEST RESULTS - INDIO PROJECT SURFACE COURSE

Sample	Temp °F	Stiffness (psi) (Mean Values)	Air Void Content
N1-1	66°F	4.32×10^5	8.75%
N1-2	66°F	5.00×10^5	8.82
N2-1	66°F	4.75×10^5	7.63
N2-2	66°F	4.21×10^5	8.10
N3-1	66°F	3.76×10^5	8.11
N3-2	66°F	2.95×10^5	8.25
N4-1	66°F	3.97×10^5	7.32
N4-2	66°F	4.26×10^5	6.91
N5-1	66°F	4.18×10^5	7.02
N5-2	66°F	3.93×10^5	7.17
N6-1	66°F	4.10×10^5	7.46
N6-2	66°F	4.21×10^5	7.03
N1-1	66°F	1.14×10^5	8.75
N1-2	66°F	1.39×10^5	8.82
N2-1	66°F	1.33×10^5	7.63
N2-2	66°F	1.06×10^5	8.10
N3-1	66°F	1.04×10^5	8.11
N3-2	66°F	1.03×10^5	8.25
N4-1	66°F	1.28×10^5	7.32
N4-2	66°F	1.19×10^5	6.91
N5-1	66°F	1.25×10^5	7.02
N5-2	66°F	1.20×10^5	7.17
N6-1	66°F	1.23×10^5	7.46
N6-2	66°F	1.42×10^5	7.03
N1-1	66°F	13.27×10^5	8.75
N1-2	66°F	15.20×10^5	8.82
N2-1	66°F	14.60×10^5	7.63
N2-2	66°F	10.37×10^5	8.10
N3-1	66°F	12.93×10^5	8.11
N3-2	66°F	12.08×10^5	8.25
N4-1	66°F	10.42×10^5	7.32
N4-2	66°F	13.22×10^5	6.91
N5-1	66°F	17.10×10^5	7.02
N5-2	66°F	13.91×10^5	7.17
N6-1	66°F	14.22×10^5	7.46
N6-2	66°F	12.47×10^5	7.03

ClibPDF - www.fastio.com

TABLE A4 - FATIGUE TEST RESULTS - INDIO PROJECT BASE COURSE

Sample No.	Stiffness p.s.i.	Strain 10^{-6} in./in.	Fatigue Life	Stress p.s.i.	Bulk Sp. Gravity	Air Void Content Percent	Temp °F
N3-8	8.66×10^{4}	1,732	262	150	2.258	9.49	66
N5-8	2.74×10^{5}	547	3,183	150	2.302	7.70	66
N6-5	3.93×10^{5}	382	2,272	150	2.317	7.13	66
N2-6	4.97×10^{5}	302	3,156	150	2.323	6.87	66
N4-10	9.76×10^{5}	166	2,998	150	2.329	6.62	66
N1-10	6.27×10^{5}	239	10,314	150	2.338	6.26	66
N2-4	5.12×10^{5}	293	7,124	150	2.370	5.01	66
N2-3	5.85×10^{5}	171	3,703	150	2.392	4.11	66
N2-8	5.05×10^{5}	198	18,638	100	2.292	8.11	66
N4-6	3.42×10^{5}	292	4,394	100	2.313	7.28	66
N4-7	4.17×10^{5}	240	7,844	100	2.319	7.05	66
N4-5	2.88×10^{5}	347	2,071	100	2.322	6.90	66
N4-9	5.23×10^{5}	191	24,314	100	2.331	6.55	66
N1-6	6.76×10^{5}	148	19,643	100	2.337	6.33	66
N1-4	5.13×10^{5}	148	16,611	100	2.352	5.69	66
N5-3	5.62×10^{5}	178	5,442	100	2.362	5.31	66
N2-7	4.83×10^{5}	155	47,782	75	2.294	8.02	66
N6-8	5.06×10^{5}	148	27,164	75	2.310	7.41	66
N3-9	5.34×10^{5}	141	142,003	75	2.318	7.09	66
N3-10	5.37×10^{5}	140	109,354	75	2.314	7.23	66
N5-10	5.47×10^{5}	137	153,278	75	2.330	6.59	66
N1-9	5.95×10^{5}	126	99,091	75	2.328	6.68	66
N1-3	5.98×10^{5}	125	64,437	75	2.360	5.41	66
N5-4	4.35×10^{5}	172	37,430	75	2.375	4.80	66
N5-6	0.886×10^{5}	1,130	692	100	2.302	7.73	81
N6-9	0.770×10^{5}	1,300	370	100	2.316	7.17	81
N5-5	0.920×10^{5}	1,080	575	100	2.319	7.04	81
N6-10	0.756×10^{5}	1,322	382	100	2.319	7.04	81
N2-9	1.55×10^{5}	645	2,426	100	2.335	6.40	81
N6-6	1.60×10^{5}	625	1,895	100	2.335	6.39	81
N3-5	0.970×10^{5}	1,030	327	100	2.335	6.39	81
N3-3	1.52×10^{5}	658	1,830	100	2.369	5.02	81
N5-7	1.39×10^{5}	540	3,754	75	2.302	7.73	81
N4-3	0.586×10^{5}	-1,280	184	75	2.315	7.21	81
N4-4	0.569×10^{5}	-1,318	169	75	2.325	6.83	81
N5-9	1.58×10^{5}	475	5,368	75	2.335	6.39	81
N1-5	1.74×10^{5}	430	6,210	75	2.334	6.43	81
N6-4	1.21×10^{5}	620	3,153	75	2.345	5.98	81
N6-3	1.52×10^{5}	493	3,435	75	2.345	5.98	81
N2-10	-------	-	-	75	-	-	81
N3-7	0.566×10^{5}	883	777	50	2.260	9.41	81
N6-7	1.59×10^{5}	315	15,013	50	2.325	6.78	81
N3-6	1.60×10^{5}	312	4,926	50	2.326	6.75	81
N1-7	1.89×10^{5}	264	34,331	50	2.335	6.39	81
N4-8	1.92×10^{5}	260	17,870	50	2.326	6.77	81
N2-5	1.75×10^{5}	286	6,860	50	2.338	6.26	81
N1-8	1.72×10^{5}	290	22,182	50	2.330	5.87	81
N3-4	1.99×10^{5}	252	22,226	50	2.371	4.97	81

ClibPDF - www.fastio.com

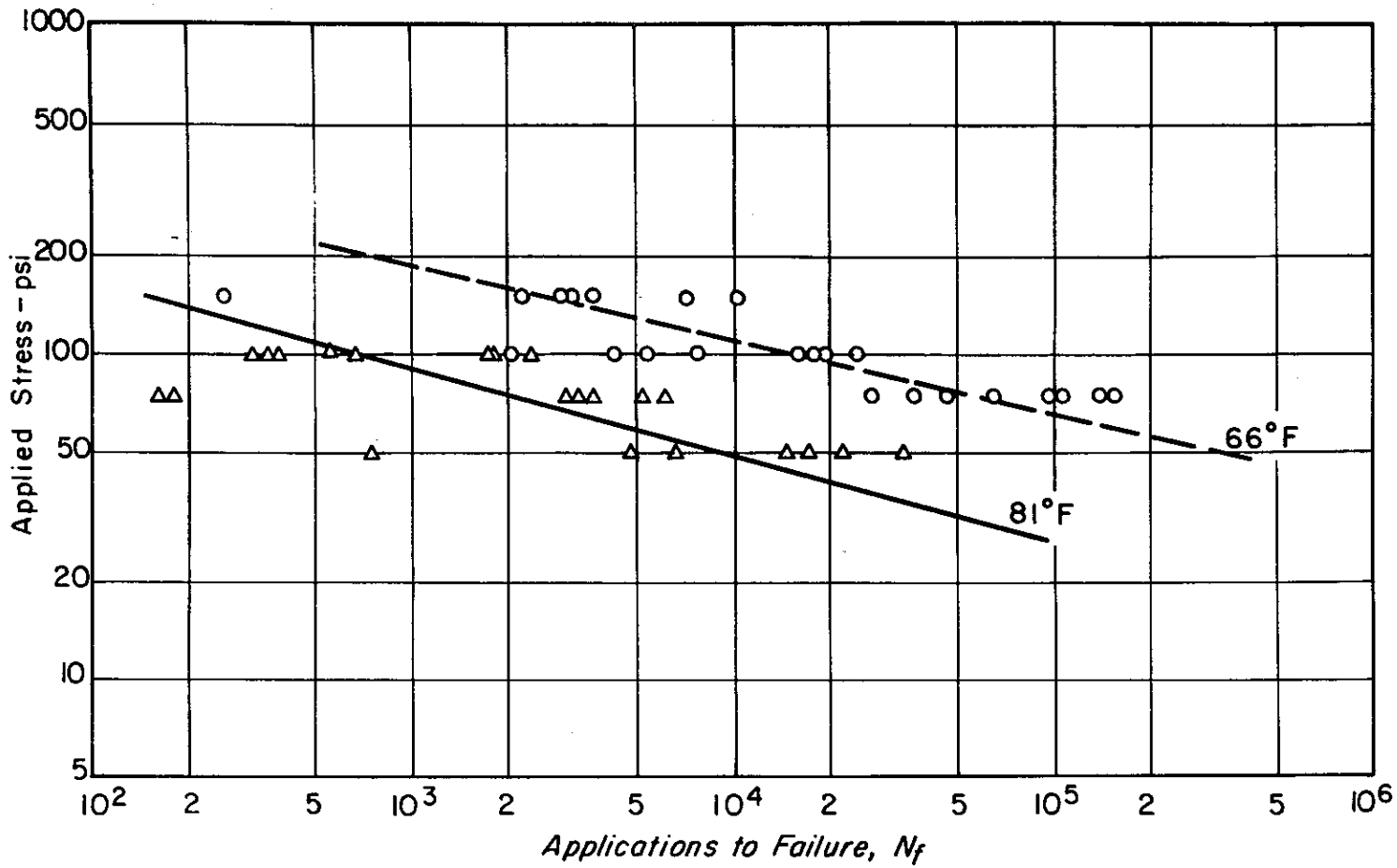

Fig. A-2 - Stress vs. applications to failure, field specimens, Indio base course.

ClibPDF - www.fastio.com

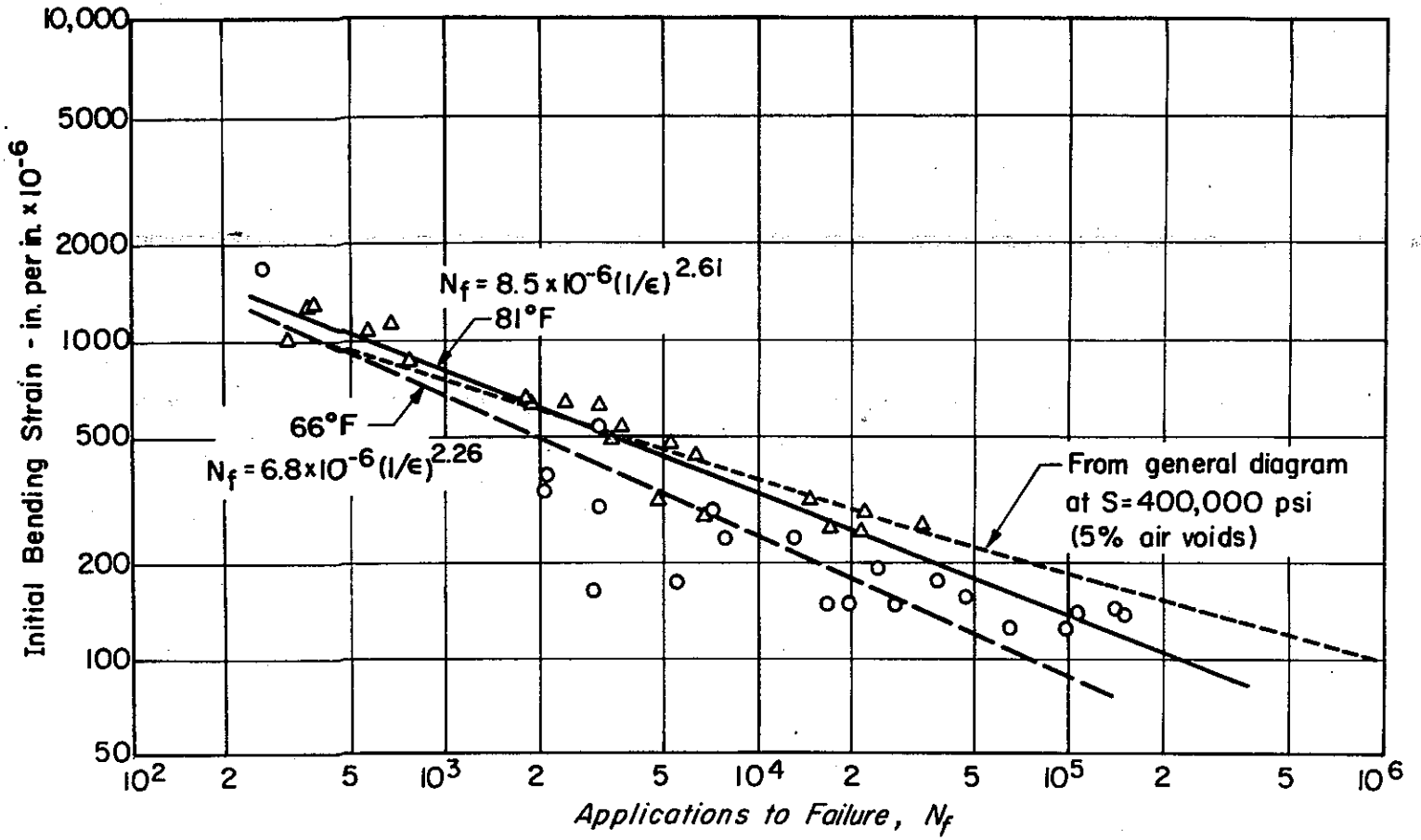

Fig. A-3 - Initial strain vs. applications to failure, field specimens, Indio base course.

ClibPDF - www.fastio.com

APPENDIX B

INFLUENCE OF WHEEL LOAD SPECTRUM ON RUTTING*

In this procedure, the material is characterized by its state of deformation or deformation level regardless of the way in which the state was obtained. This corresponds to the time hardening procedure described earlier.

Van de Loo has suggested that for many asphalt mixes, the accumulation of permanent strain as a function of stress level and number of repetitions can be represented by the equation:

$$\varepsilon = c \cdot \sigma \cdot N^a \tag{B1}$$

This equation is represented schematically in Fig. B1.

The equivalent number of standard loads causing same permanent deformation, ε_p, as N_i repetitions of load σ_i can be derived as follows:

$$N_{st} = \left(\frac{\varepsilon_p}{c\sigma_{st}}\right)^{1/a} \tag{B2}$$

$$N_i = \left(\frac{\varepsilon_p}{c\sigma_i}\right)^{1/a} \tag{B3}$$

$$N_{st} = \left(\frac{\sigma_i}{\sigma_{st}}\right)^{1/a} N_i \tag{B4}$$

Equation (B4) represents the equivalent number of standard loads causing same permanent deformation as the number of loads N_i at stress level σ_i.

It should be noted that at equal values of strain, ε_p, $d\varepsilon/dN$ differs for the different applied stress relationships and is a function of N.

---

*After P.J. van de Loo in paper presented to the Symposium on Predicting Rutting in Asphalt Concrete Pavements, Transportation Research Board, January 1976.

ClibPDF - www.fastio.com

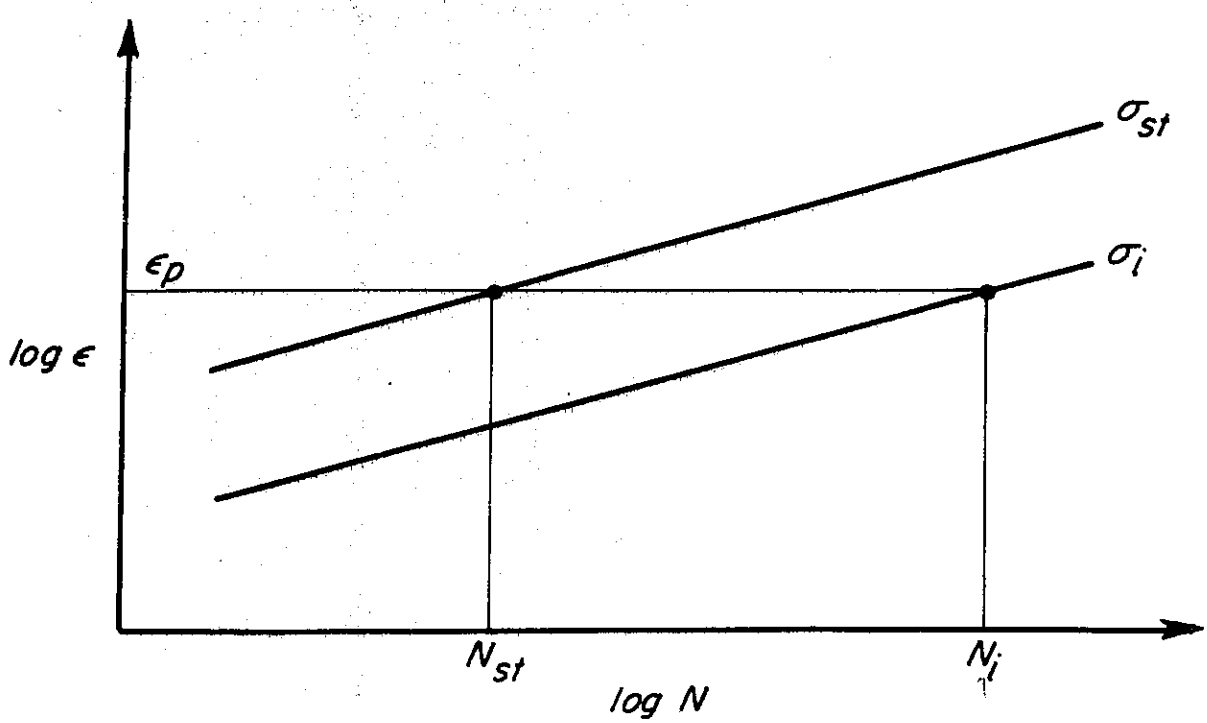

Fig. B-1 - Influence of stress level and numbers of load repetitions on accumulation of permanent strain.

ClibPDF - www.fastio.com

$$\frac{d\varepsilon}{dN} = c\ \sigma\ a\ N^{a-1} \tag{B5}$$

or

$$\frac{d\varepsilon}{dN} = \varepsilon_p \cdot \frac{a}{N} \tag{B6}$$

For the standard load:

$$d\varepsilon_{st} = \varepsilon_p \frac{a}{N_{st}} \cdot dN_{st} \tag{B7}$$

and for any other load, σ_i:

$$d\varepsilon_i = \varepsilon_p \cdot \frac{a}{N_i} \cdot dN_i \tag{B8}$$

Letting $n_i = dN_i$ and determining $dN_{st} = n_{st}$ for the situation where increases in deformation along both curves are equal, it can be shown that:

$$n_{st} = \frac{N_{st}}{N_i} n_i \tag{B9}$$

Substituting equations (B2) and (B3) results in the following:

$$n_{st} = \left(\frac{\sigma_i}{\sigma_{st}}\right)^{1/a} n_i \tag{B10}$$

Equation (B10) is similar to equation (B4) indicating that for any load pattern, the equivalent number of standard loads can be determined for both a specific deformation level and incremental deformations, the latter regardless of the fact that $d\varepsilon/dN$ differs for the various stress curves at equal values of ε_p.

Finally, considering a wheel load spectrum which can be divided into classes of different stresses:

$$N\ \text{equiv.} = N_{st} \sum_{i=1}^{k} \left(\frac{\sigma_i}{\sigma_{st}}\right)^{1/a} \frac{n_i}{n_{st}} \tag{B11}$$

ClibPDF - www.fastio.com

ClibPDF - www.fastio.com

APPENDIX C

USER'S GUIDE: RUT DEPTH PREDICTION PROGRAM

The program is an extension of the 3-dimensional elastic layered system program ELSYM5; the stress output of ELSYM5 is used in the calculation of plastic strains.

Limitations of the program are similar to that of ELSYM5; i.e.

1. Minimum of one system maximum of five.
2. Minimum of one elastic layer maximum of five.
3. Minimum of one uniform circular load maximum of five (all identical)
4. Minimum of one point where output is required maximum of 100 (10xy + 10z)
5. For rigid base maximum Z value must be less than depth to rigid base.
6. All input values must be positive except xy positions.
7. Poisson ratio must not have a value of one and for a bottom elastic layer on a rigid base it must not be in the range 0.748 to 0.752.
8. The integration process (truncated series) leads to some approximation of the results at and near the surface and at points out at some distance from the load.

It is therefore advisable to specify that results be computed at control points where a check can be conducted; e.g., directly beneath the load at the surface where the pressure is known.

If more than one system is analyzed, the second and subsequent system results are modified according to the time or strain hardening concepts for repeated loading, using the results from the preceding system, i.e., if there

ClibPDF - www.fastio.com

is more than one system the program assumes that the second system is merely the same as the first being subjected to a further number of load repetitions.

PERMANENT STRAIN COMPUTATION

Plastic Strain

Plastic strains are calculated by both the effective stress and Barksdale equations:

1. Effective Stress

Effective stress $\bar{\sigma} = \frac{1}{\sqrt{2}} \left[(\sigma_1 - \sigma_2)^2 + (\sigma_2 - \sigma_3)^2 + (\sigma_3 - \sigma_1)^2 \right]^{1/2}$

where σ_1 , σ_2 , σ_3 are principal stresses determined by elastic theory - ELSYM 5.

The permanent strain in the vertical direction is given by

$$\varepsilon_{p_{(z)}} = \frac{\bar{\varepsilon}_p}{\bar{\sigma}} \left[\sigma_2 - \frac{1}{2} (\sigma_x + \sigma_y) \right] \qquad (1)$$

σ_x , σ_y , σ_z are normal stresses at location where computation is required.

$\bar{\varepsilon}_p$ = total effective strain

The ratio $\frac{\bar{\varepsilon}_p}{\bar{\sigma}}$ is determined from the relationship: $\frac{\bar{\varepsilon}_p}{\bar{\sigma}} = \frac{a}{1 - b\bar{\sigma}}$

where a is an input parameter ($a = \frac{1}{k}$ from equation $\varepsilon_p = k\sigma^n$ or $a = \frac{1}{E_i}$; E_i = initial tangent modulus.

$$b = \frac{1}{\bar{\sigma}_{ultimate}}$$

$$\bar{\sigma}_{ultimate} = \frac{\bar{\sigma}_{failure}}{R_f} \qquad R_f = \text{Reduction Factor } 0.75 \leq R_f \leq 1.0$$

and

$$\bar{\sigma}_{failure} = \frac{2c \cos \phi + 2\sigma_3 \sin \phi}{1 - \sin \phi}$$

ClibPDF - www.fastio.com

ϕ = angle of internal friction

c = cohesion value

For a required number of repetitions (N) of load the permanent strain $\varepsilon_{p(z)}$ in equation 1 is modified according to the following

$$\varepsilon_{p(z)} = \varepsilon_{p(z)} \left(\frac{N}{N_{RB}}\right)^A$$

where

N_{RB} = number of load repetitions at which constants a and b were determined

A is the slope of the straight line portion on a log-log plot of ε vrs N for the repeated load triaxial test.

2. Barksdale equation

This is a relationship between permanent strain and deviator stress for unbound aggregates:

$$\bar{\varepsilon}_p = \frac{\bar{\sigma} \cdot a \cdot \sigma_3^{-n}}{1 - \dfrac{\bar{\sigma} R_f (1 - \sin\phi)}{2(c \cos\phi + \sigma_3 \sin\phi)}}$$

where $\bar{\sigma} = \sigma_1 - \sigma_3$

n, a, c, ϕ, R_f as defined above.

Elastic Strains

By definition, $\varepsilon_p = 0$; the program DEFORM sets the same value

Visco-elastic Strains

The material is characterized as a time dependent plastic material and the following equation is used:

ClibPDF - www.fastio.com

$$\varepsilon_p = \frac{\dot{\bar{\varepsilon}}}{\bar{\sigma}} [\sigma_2 - \frac{1}{2} (\sigma_x + \sigma_y)]$$

$$\frac{\dot{\bar{\varepsilon}}}{\bar{\sigma}} = \frac{k}{1,5\bar{\sigma}^n} \quad \text{k, n as defined above}$$

INPUT CARDS

The notation CC refers to card columns with the range of columns being inclusive. All 'real' values (REAL) are punched with a decimal point as part of the value and all "integer" values (INTEGER) are to be punched without a decimal point and right justified in the data field.

1.	CC 1-5	(INTEGER)	Number of systems to be run (NSYM)
2.	CC 1-3	(INTEGER)	Punch the number 999
	5-60	(ALPHA)	any combination of alphanumeric characters may be used to identify the system i,e. title
3.	CC 1-5	(INTEGER)	Number of elastic layers in the system (NEL)
	CC 6-10	(INTEGER)	Number of uniform circular loads to be applied normal to the surface of the system (NLD)
	CC 11-15	(INTEGER)	Number of XY locations where results are desired (NXY)
	CC 16-20	(INTEGER)	Number of Z locations where results are desired (NZ)
	CC 21-25	(INTEGER)	Indication whether or not computation of deformation is required (NDEF)
			NDEF = 0 No deformation computation
			= 1 Deformation computation desired
	CC 26-35	(E10.3)	Desired number of load repetitions (REPIT)
4.	CC 1-5	(INTEGER)	Layer number (LN)
	CC 6-10	(REAL)	thickness of layer in inches (TH)
	CC 11-15	(REAL)	Poisson's ratio of layer (V)

ClibPDF - www.fastio.com

	CC 16-25	(REAL)	Modulus of elasticity for layer (E)
	*CC 30-31	(ALPHA)	Base interface condition

*Note: This is for only rigid base. Leave blank for other layer interface. Punch FF for full friction rigid base interface or NF for no friction rigid base interface. One card is required for each elastic layer in the system. Leave thickness blank for bottom elastic layer when layer is to be semi-infinite in thickness.

5.	CC 1-10	(REAL)	Load force in pounds
	CC 11-20	(REAL)	Load pressure in pounds per square inch
	CC 21-30	(REAL)	Load radius in inches. Any two of the above items can be input, program determined for the third. Only one card required.
6.	CC 1-10	(REAL)	X position of a load
	CC 11-20	(REAL)	Y position of a load
			one card per load
7.	CC 1-10	(REAL)	X position for evaluation
	CC 11-20	(REAL)	Y position for evaluation
			one card for each XY position
8.	CC 1-5	(REAL)	first Z value for evaluation
	CC 6-10	(REAL)	second Z value for evaluation
	CC 11-15	(REAL)	third Z value for evaluation, etc.
			only one card required, maximum of ten values
9.	CC 1	(INTEGER)	layer number
	CC 2	(INTEGER)	Material type (Elastic = 1, Plastic = 2, Viscoelastic = 3)

ClibPDF - www.fastio.com

	CC 3-10	(REAL)	Coefficient K from Rel. $\varepsilon_p = K\sigma^n$ (PLK)
	CC 11-20	(REAL)	Exponent in Rel. $\varepsilon_p = K\sigma^n$ (PLS)
	CC 21-30	(REAL)	Cohesion (COH)
	CC 31-40	(REAL)	Angle of internal friction (Deg.) ϕ
	CC 41-50	(REAL)	Reduction factor R_f $0.75 \leq R_f \leq 1.0$ from $\bar{\sigma}_f = R_f \bar{\sigma}_{ULT}$
	CC 51-60	(REAL)	Density of layer (lb/ft^3) (SGG)
	CC 61-70	(REAL)	Water content of layer (%)
			one card for each layer
			If type of material (IYP) = 1 put PLK = 0.0
			Leave other parameters blank except SGG
10.	CC 1	(INTEGER)	Layer number
	CC 2-11	(E10.3)	Exponent F(K) in relation $\varepsilon_p = BN^{F(K)}$
	CC 12-21	(E10.3)	Number of repetitions N_{RB} at which hyperbolic parameters PLK, etc., are specified
			one card for each layer

To evaluate a second system, follow card type 10 by card types 2-10 for the second system, etc.

COMPUTER
LISTING
WILL
ALSO BE INCLUDED.

ClibPDF - www.fastio.com

```
                SUBROUTINE DEFORM
          C
          C
          C
000002          COMMON E(5),V(5),DI(5),R(100),Z(10),EX(32),
               1        CDAB(5,736),AJ1(184),RJ1(184),RJ0(184),
               2        VSE,SSE,RDP,VDP,RSE,TSE,ST1,ST2,ST3,ST4,
               3        WR,WZ,WRL,RL,PRES,RLP,TST1,TST2,TST3,TST4,
               4        NSYM,NSY,NLSW,NBZ,NGQP,NX,NEX,NR,NRC,NZ,NZC,MSW,
               5        NEL,NEI,NI,NBLL,LAY,NTEST,NTSI,ITS,IND,NAB,NBZC,
               6        KSW1,KSW2,KSW3,KSW4,KSW5,KSW6,KSW7,KSW8,KSW9
000002          COMMON XL(10),YL(10),XP(10),YP(10),LAYZ(10),
               1  ANS(6,100,10),AS(9,3,10),TITLE(14),IXR(100),NLD,NXY
          C
000002          COMMON NDEF,IYP(5),PLK(5),PLS(5),COH(5),FRI(5),RF(5),SGG(5),
               1REPIT,NSYMM,EDE(5,10,100),EDER(5,10,100),F(5),RB(5),RES(5),
               2WATER(5)
000002          DIMENSION LAB1(3,9),LAB2(3,9)
          C
000002          DATA (LAB1(I),I=1,27)/10HNORMAL STR,5HESSES,1H ,10HSHEAR STRE,
               1 4HSSES,1H ,10HPRINCIPAL ,8HSTRESSES,1H ,10HPRINCIPAL ,
               2 10HSHEAR STRE,4HSSES,10HDISPLACEME,3HNTS,1H ,10HNORMAL STR,
               3 4HAINS,1H ,10HSHEAR STRA,3HINS,1H ,10HPRINCIPAL ,7HSTRAINS,
               4 1H ,10HPRINCIPAL ,10HSHEAR STRA,3HINS/
000002          DATA (LAB2(I),I=1,27)/3HSXX,3HSYY,3HSZZ,3HSXY,3HSXZ,3HSYZ,
               1 4HPS 1,4HPS 2,4HPS 3,5HPSS 1,5HPSS 2,5HPSS 3,2HUX,2HUY,
               2 2HUZ,3HEXX,3HEYY,3HEZZ,3HEXY,3HEXZ,3HEYZ,4HPE 1,4HPE 2,
               3 4HPE 3,5HPSE 1,5HPSE 2,5HPSE 3/
          C
000002          DIMENSION PB(100),EOS(100)
000002          RES(NSYMM)=REPIT
000004          N=IYP(LAY)
000006          DO 20 K2=1,NXY
000010          AS(1,1,K2)=-1.0*AS(1,1,K2)
000014          AS(1,2,K2)=-1.0*AS(1,2,K2)
000017       20 AS(1,3,K2)=-1.0*AS(1,3,K2)
000024          IF(N-2)30,50,51
000027       50 DO 9 K2=1,NXY
000031          P1=-1.0*AS(3,1,K2)
000035          P2=-1.0*AS(3,2,K2)
000040          P3=-1.0*AS(3,3,K2)
000043          PX=AS(1,1,K2)
000046          PY=AS(1,2,K2)
000051          PZ=AS(1,3,K2)
000054          PB(K2)=SQRT((P1-P2)**2+(P2-P3)**2+(P1-P3)**2)
000070          AA=1.0/PLK(LAY)
000073          IF(COH(LAY)-0.1)36,35,35
000075       36 BB=RF(LAY)/(PX+PY)*(1./SIN(FRI(LAY))-1.)
000105          GO TO 37
000106       35 BB=2.0*COH(LAY)*1.414/RF(LAY)
000112       37 IF(PB(K2)-BB)10,11,11
000115       11 PRINT 1002,XP(K2),YP(K2)
000125     1002 FORMAT(1H0,5X,*EFFECTIVE STRESS AT POSITION X=*,F10.2,2X,*Y=*,
```

```
                SUBROUTINE RUTDEP
          C
          C     SUBROUTINE TO COMPUTE THE RUT DEPTHS
          C
          C
000002          COMMON E(5),V(5),DI(5),R(100),Z(10),EX(32),
               1        CDAB(5,736),AJ1(184),RJ1(184),RJ0(184),
               2        VSE,SSE,RDP,VDP,RSE,TSE,ST1,ST2,ST3,ST4,
               3        WR,WZ,WRL,RL,PRES,RLP,TST1,TST2,TST3,TST4,
               4        NSYM,NSY,NLSW,NBZ,NGQP,NX,NEX,NR,NRC,NZ,NZC,MSW,
               5        NEL,NEI,NI,NBLL,LAY,NTEST,NTSI,ITS,IND,NAB,NBZC,
               6        KSW1,KSW2,KSW3,KSW4,KSW5,KSW6,KSW7,KSW8,KSW9
000002          COMMON XL(10),YL(10),XP(10),YP(10),LAYZ(10),
               1  ANS(6,100,10),AS(9,3,10),TITLE(14),IXP(100),NLD,NXY
          C
000002          COMMON NDEF,IYP(5),PLK(5),PLS(5),COH(5),FRI(5),RF(5),SGG(5),
               1REPIT,NSYMM,EDE(5,10,100),EDEB(5,10,100),F(5),RB(5),RES(5),
               2WATER(5)
          C
000002          DIMENSION RED(10,100),REDB(10,100),EDES(5,10,100),EDEBS(5,10,100),
               1TOT(100),TOTB(100),TOTS(100),TOTBS(100)
000002          IF(NSYMM-1)1,1,2
000005        1 N=NSYMM
000007          RE=REPIT
000010          DO 3 K1=1,NZ
000012          NK=NEL-1
000014          DO 4 J=1,NK
000016          IF(Z(K1)-DI(J))5,5,6
000021        5 LAY=J
000023          GO TO 8
000023        6 IF(Z(K1)-DI(NK))4,4,7
000027        7 LAY=NEL
000031          GO TO 8
000031        4 CONTINUE
000034        8 IF(IYP(LAY)-2)80,80,81
000037       81 DO 82 K2=1,NXY
000041          EEE=EDE(N,K1,K2)*RB(LAY)*RE**F(LAY)
000053          EDE(N,K1,K2)=EEE
000061          EDEB(N,K1,K2)=EEE
000065          EDES(N,K1,K2)=EEE
000071       82 EDEBS(N,K1,K2)=EEE
000077          GO TO 3
000100       80 DO 3 K2=1,NXY
000102          EDE(N,K1,K2)=(RE/RB(LAY))**F(LAY)*EDE(N,K1,K2)
000114          EDEB(N,K1,K2)=(RE/RB(LAY))**F(LAY)*EDEB(N,K1,K2)
000126          EDES(N,K1,K2)=EDE(N,K1,K2)
000137          EDEBS(N,K1,K2)=EDEB(N,K1,K2)
000141          RED(K1,K2)=0.0
000144        3 REDB(K1,K2)=0.0
000154          GO TO 10
000155        2 N=NSYMM
000157          RE=REPIT
000160          TRE=0.0
```

ClibPDF - www.fastio.com

```
000161          DO 70 I=1,N
000162       70 TRE=TRE+RES(I)
000166          TREL=TRE-RE
000170          DO 11 K1=1,NZ
000171          NK=NEL-1
000173          DO 12 J=1,NK
000175          IF(Z(K1)-DI(J))13,13,14
000200       13 LAY=J
000202          GO TO 16
000202       14 IF(Z(K1)-DI(NK))12,12,15
000206       15 LAY=NEL
000210          GO TO 16
000210       12 CONTINUE
000213       16 IF(IYP(LAY)-2)83,83,81
000216       83 BB=1.0/(RB(LAY)**F(LAY))
000223          DO 11 K2=1,NXY
000224          RED(K1,K2)=(EDE((N-1),K1,K2)/(EDE(N,K1,K2)*BB))**(1.0/F(LAY))
000250          REDB(K1,K2)=(EDEB((N-1),K1,K2)/(EDEB(N,K1,K2)*BB))**(1.0/F(LAY))
000274          X1=EDE((N-1),K1,K2)
000303          X2=EDEB((N-1),K1,K2)
000312          X3=EDES((N-1),K1,K2)
000321          X4=EDEBS((N-1),K1,K2)
000330          REM=BB*(TRE**F(LAY)-TREL**F(LAY))
000342          EDES(N,K1,K2)=EDE(N,K1,K2)*REM+X3
000354          EDEBS(N,K1,K2)=EDEB(N,K1,K2)*REM+X4
000361          REDD=RED(K1,K2)+RE
000366          REBB=REDB(K1,K2)+RE
000371          EDE(N,K1,K2)=EDE(N,K1,K2)*BB*REDD**F(LAY)
000400       11 EDEB(N,K1,K2)=EDEB(N,K1,K2)*BB*REBB**F(LAY)
000415       10 PRINT 1000,NSYMM
000423     1000 FORMAT(1H ,120(1H*)//10X,≠PERMANENT STRAINS≠/10X,17(1H-)//
             120X,≠SYSTEM NUMBER ≠,I2/)
000423          DO 1100 K=1,NEL
000425          PRINT 1101,K,IYP(K),PLK(K),PLS(K),COH(K),FRI(K),RF(K),SGG(K),
             1WATER(K),F(K),RB(K)
000456     1101 FORMAT(1H ,≠LAYER NO ≠,I2,≠ MATERIAL TYPE ≠,I2/10X,≠ K COEFF ≠,
             1F10.2,≠ N COEFF ≠,F10.2,≠ COHESION ≠,F10.2,≠FRICTION-RADIANS-≠,
             2F10.2/10X,≠ RF ≠,F10.2,≠ DENSITY ≠,F10.2,≠ WATER CONTENT ≠,F10.2/
             3≠ EXPONENT IN B*N**F(K)≠,1PE10.3,≠ SPECIIFED REPITITIONS≠,1PE10.3)
000456     1100 CONTINUE
000461          FOR=PRES*RL**2/0.31830987
000464          PRINT 1102,REPIT,FOR,PRES
000475     1102 FORMAT(1H ,10X,100(1H-)/10X,1PE10.3,≠ REPITITIONS OF THE LOAD OF≠,
             10PF10.1,≠ ARE APPLIED AT A TYRE PRESSURE OF ≠,0PF10.1)
000475          DO 41 K1=1,NZ
000477          NK=NEL-1
000501          DO 21 J=1,NK
000503          IF(Z(K1)-DI(J))22,22,23
000506       22 LAY=J
000510          GO TO 24
000510       23 IF(Z(K1)-DI(NK))21,24,25
000514       25 LAY=NEL
000516          GO TO 24
000516       21 CONTINUE
```

ClibPDF - www.fastio.com

```
                 1F10.2,≠ GREATER THAN ASYMTOTIC STRESS DIFFERENCE TIMES RF≠/
                 210X,≠EFFECTIVE STRESS PUT EQUAL TO 2*COHESION*0.99≠)
000125             PB(K2)=COH(LAY)*1.414
000130          10 EOS(K2)=AA/(1.0-PB(K2)/BB)
000135           9 EDE(NSYMM,NZC,K2)=EOS(K2)*(PZ-0.5*(PX+PY))
          C        BARKSDALE FORMULA
000151             DO 12 K2=1,NXY
000152             PX=0.5*(AS(1,1,K2)+AS(1,2,K2))
000160             PZ=AS(1,3,K2)
000161             IF(PZ-PX)13,13,14
000164          13 PRINT 1003,XP(K2),YP(K2)
000174        1003 FORMAT(1H0,5X,≠VERTICAL STRESS AT POSITION X=≠,F10.2,2X,≠Y=≠,
                 1F10.2,≠ LESS THAN HORIZONTAL STRESS≠)
000174          14 DEN=(PZ-PX)*RF(LAY)*(1.0-SIN(FRI(LAY)))
000204             DEN1=2.0*(COH(LAY)*COS(FRI(LAY))+PX*SIN(FRI(LAY)))
000217             DEN2=1.0-DEN/DEN1
000222             IF(DEN2)15,15,16
000223          15 PRINT 1004,XP(K2),YP(K2)
000233        1004 FORMAT(1H0,5X,≠DENOMINATOR OF BARKSDALE FORMULA LESS THAN ZERO≠,
                 1≠AT POSITION X=≠,F10.2,≠ Y=≠,F10.2,≠DENOM PUT EQUAL TO 1-0.99≠)
000233             DEN2=1.0-RF(LAY)/2.0
000237          16 DEN3=PLK(LAY)*ABS(PX)**PLS(LAY)*DEN2
000246          12 EDEB(NSYMM,NZC,K2)=(PZ-PX)/DEN3
000260             RETURN
000260          51 DO 52 K2=1,NXY
000262             P1=-1*AS(3,1,K2)
000266             P2=-1*AS(3,2,K2)
000272             P3=-1*AS(3,3,K2)
000276             PX=AS(1,1,K2)
000301             PY=AS(1,2,K2)
000304             PZ=AS(1,3,K2)
000307             PB(K2)=SQRT((P1-P2)**2+(P2-P3)**2+(P1-P3)**2)/1.414
000324             EOS(K2)=PLK(LAY)/(1.5*PB(K2)**PLS(LAY))
000333             EDE(NSYMM,NZC,K2)=EOS(K2)*(PZ-0.5*(PX+PY))
000345          52 EDEB(NSYMM,NZC,K2)=EDE(NSYMM,NZC,K2)
000357             RETURN
000357          30 DO 31 K2=1,NXY
000361             EDE(NSYMM,NZC,K2)=0.0
000366          31 EDEB(NSYMM,NZC,K2)=0.0
000375             RETURN
000375             END
```

ClibPDF - www.fastio.com

ClibPDF - www.fastio.com

DEFORM

SUBPROGRAM LENGTH
001150

FUNCTION ASSIGNMENTS

STATEMENT ASSIGNMENTS

10	-	000130	11	-	000115	13	-	000164	14	-	000174
15	-	000223	16	-	000237	30	-	000357	35	-	000106
36	-	000075	37	-	000112	50	-	000027	51	-	000260
1002	-	000406	1003	-	000433	1004	-	000446			

BLOCK NAMES AND LENGTHS
- 050707

VARIABLE ASSIGNMENTS

AA	-	001142	AJ1	-	007375C01	ANS	-	010513C01	AS	-	024373C01
BB	-	001143	CDAB	-	000235C01	COH	-	025215C01	DEN	-	001144
DEN1	-	001145	DEN2	-	001146	DEN3	-	001147	DI	-	000012C01
E	-	000000C01	EDE	-	025243C01	EDEB	-	037053C01	EOS	-	000766
EX	-	000175C01	F	-	050663C01	FRI	-	025222C01	IXR	-	025027C01
IYP	-	025176C01	K2	-	001133	LAB1	-	000534	LAB2	-	000567
LAY	-	010511C01	LAYZ	-	010601C01	N	-	001132	NSYMM	-	025242C01
NXY	-	025174C01	NZC	-	010503C01	PB	-	000622	PLK	-	025203C01
PLS	-	025210C01	PX	-	001137	PY	-	001140	PZ	-	001141
P1	-	001134	P2	-	001135	P3	-	001136	R	-	000017C01
RB	-	050670C01	REPIT	-	025241C01	RES	-	050675C01	RF	-	025227C01
RJ0	-	010155C01	RJ1	-	007665C01	SGG	-	025234C01	TITLE	-	025011C01
V	-	000005C01	WATER	-	050702C01	XL	-	010531C01	XP	-	010555C01
YL	-	010543C01	YP	-	010567C01	Z	-	000163C01			

START OF CONSTANTS
000377

START OF TEMPORARIES
000466

START OF INDIRECTS
000515

UNUSED COMPILER SPACE
060500

```
000521      24 PRINT 1001,LAY
000527    1001 FORMAT(1H0,6X,≠LAYER≠,I3)
000527         PRINT 1002,(XP(J),J=1,NXY)
000542    1002 FORMAT(1H0,6X,≠X=≠,10F11.2)
000542         PRINT 1003,(YP(J),J=1,NXY)
000555    1003 FORMAT(1H0,6X,≠Y=≠,10F11.2)
000555         PRINT 1004,Z(K1),(EDE(N,K1,K2),K2=1,NXY)
000575    1004 FORMAT(1H ,F6.0,1P10E11.3)
000575         PRINT 1005,(EDEB(N,K1,K2),K2=1,NXY)
000613    1005 FORMAT(1H ,6X,1P10E11.3)
000613         PRINT 1005,(EDES(N,K1,K2),K2=1,NXY)
000631         PRINT 1005,(EDEBS(N,K1,K2),K2=1,NXY)
000647      41 CONTINUE
000652         DO 38 K2=1,NXY
000653         TOT(K2)=0.0
000654         TOTB(K2)=0.0
000655         TOTS(K2)=0.0
000656      38 TOTBS(K2)=0.0
000661         NXX=1
000662         NX=0
000663         DO 26 K1=1,NZ
000665         NK=NEL-1
000667         DO 27 J=1,NK
000671         IF(Z(K1)-DI(J))28,28,29
000674      28 LAY=J
000676         GO TO 30
000676      29 IF(Z(K1)-DI(NK))27,27,32
000702      32 LAY=NEL
000704         GO TO 30
000704      27 CONTINUE
000707      30 NX=NX+1
000711         IF(NX-1)26,26,36
000712      36 DO 40 K2=1,NXY
000714         X1=(Z(K1)-Z(K1-1))*0.5
000720         TOT(K2)=TOT(K2)+X1*(EDE(N,K1,K2)+EDE(N,(K1-1),K2))
000734         TOTB(K2)=TOTB(K2)+X1*(EDEB(N,K1,K2)+EDEB(N,(K1-1),K2))
000747         TOTS(K2)=TOTS(K2)+X1*(EDES(N,K1,K2)+EDES(N,(K1-1),K2))
000762      40 TOTBS(K2)=TOTBS(K2)+X1*(EDEBS(N,K1,K2)+EDEBS(N,(K1-1),K2))
001000         IF(LAY-NXX)60,60,61
001002      61 PRINT 1006,NSYMM
001010         PRINT 1007,(TOT(K2),K2=1,NXY)
001023         PRINT 1007,(TOTB(K2),K2=1,NXY)
001036         PRINT 1007,(TOTS(K2),K2=1,NXY)
001051         PRINT 1007,(TOTBS(K2),K2=1,NXY)
001064      60 NXX=LAY
001066      26 CONTINUE
001071         PRINT 1006,NSYMM
001076    1006 FORMAT(1H ,10X,≠RUT DEPTHS PREDICTED BY≠/20X,≠ONE -EFFECTIVE STRES
            1S APPROACH AND TIME HARDENING≠/20X,≠TWO -BARKSDALE FORMULA AND TIM
            2E HARDENING APPROACH≠/20X,≠THREE -EFFECTIVE STRESS AND STRAIN HARD
            3ENING APPROACH≠/20X,≠FOUR -BARKSDALE FORMULA AND STRAIN HARDENING
            4APPROACH≠//10X,≠SYSTEM NO≠,I3)
001076         PRINT 1007,(TOT(K2),K2=1,NXY)
001111    1007 FORMAT(1H ,6X,1P10E11.3)
```

ClibPDF - www.fastio.com

ClibPDF - www.fastio.com

ClibPDF - www.fastio.com